PHYSICAL REVIEW C **96**, 064908 (2017)

Femtoscopy with identified charged pions in proton-lead collisions at $\sqrt{s_{NN}} = 5.02$ TeV with ATLAS

M. Aaboud *et al.**
(ATLAS Collaboration)

(Received 7 April 2017; published 28 December 2017)

Bose-Einstein correlations between identified charged pions are measured for p+Pb collisions at $\sqrt{s_{NN}} =$ 5.02 TeV using data recorded by the ATLAS detector at the CERN Large Hadron Collider corresponding to a total integrated luminosity of 28 nb^{-1}. Pions are identified using ionization energy loss measured in the pixel detector. Two-particle correlation functions and the extracted source radii are presented as a function of collision centrality as well as the average transverse momentum (k_{T}) and rapidity ($y^{\star}_{\pi\pi}$) of the pair. Pairs are selected with a rapidity $-2 < y^{\star}_{\pi\pi} < 1$ and with an average transverse momentum $0.1 < k_{\mathrm{T}} < 0.8$ GeV. The effect of jet fragmentation on the two-particle correlation function is studied, and a method using opposite-charge pair data to constrain its contributions to the measured correlations is described. The measured source sizes are substantially larger in more central collisions and are observed to decrease with increasing pair k_{T}. A correlation of the radii with the local charged-particle density is demonstrated. The scaling of the extracted radii with the mean number of participating nucleons is also used to compare a selection of initial-geometry models. The cross term R_{ol} is measured as a function of rapidity, and a nonzero value is observed with 5.1σ combined significance for $-1 < y^{\star}_{\pi\pi} < 1$ in the most central events.

DOI: 10.1103/PhysRevC.96.064908

I. INTRODUCTION

Studies of multiparticle correlations in proton-lead (p+Pb) [1–5] and proton-proton (pp) [6] collisions at the CERN Large Hadron Collider (LHC) and in deuteron-gold (d+Au) [7–9] and helium-3–gold (^{3}He+Au) [10] collisions at the BNL Relativistic Heavy Ion Collider (RHIC) have shown that these correlation functions exhibit features similar to those observed in nucleus-nucleus collisions [11–16] that are attributed to collective dynamics of the strongly coupled quark-gluon plasma. In particular, two-particle angular correlations studied in high multiplicity p+Pb [1,4,17] and pp [6,18] collisions at the LHC show a "ridge"—an enhancement in the correlation function at small relative azimuthal angle ($\Delta\phi$) that extends over a range of relative pseudorapidity ($\Delta\eta$). The ridge in both systems is generally understood to result from a combination of sinusoidal modulations of the two-particle correlation function of different harmonics [1–5]. Hydrodynamic calculations show that such a modulation can arise from initial-state spatial anisotropies that, through the collective expansion of the medium, are imprinted on the azimuthal-angle distributions of the final-state particles (see, e.g., Refs. [19–21] and references therein). Such hydrodynamic models can also reproduce the modulation observed in p+Pb, d+Au, and ^{3}He+Au collisions [22–25], but the suitability of hydrodynamics in "small" systems remains a topic of active debate. Alternatively, the observed modulation in these collisions has been explained by so-called "glasma" models that invoke saturation of the nuclear parton distributions [26–30]. To disentangle these competing explanations and, more specifically, to test whether collective phenomena are present in p+Pb collisions at the LHC, additional measurements are required to constrain the source geometry.

Hanbury Brown and Twiss (HBT) correlations, which probe the space-time extent of a particle-emitting source (see Ref. [31] and references therein), may provide valuable insight into the problems described above. The HBT method originated in astronomy [32,33], where space-time correlations of photons due to wave function symmetrization are used to measure the size of distant stars. The procedure can be adapted to the extremely small sources encountered in hadronic collisions if identical-particle Bose-Einstein correlations are instead studied in relative momentum space [34]. The two-particle correlation function $C(\mathbf{q})$, parametrized as a function of relative momentum, is sensitive to the two-particle source density function $S(\mathbf{r})$ through the two-particle final-state wave function [31]:

$$C_{\mathbf{k}}(\mathbf{q}) - 1 = \int d^3r\, S_{\mathbf{k}}(\mathbf{r})(|\langle\mathbf{q}|\mathbf{r}\rangle|^2 - 1), \qquad (1)$$

where $\mathbf{q}$ and $\mathbf{k}$ are, respectively, the relative and average momentum of a pair of particles, $\mathbf{r}$ is the distance between the origin points of the two particles, and the two-particle source function $S_{\mathbf{k}}$ is normalized so that $\int d^3r\, S_{\mathbf{k}}(\mathbf{r}) = 1$. In the case of a noninteracting identical boson wave-function, the term within the parentheses of Eq. (1) is a cosine and the correlation function is enhanced by the Fourier transform of the source function. Thus, the Bose-Einstein modification of the relative momentum distributions produces an enhancement at small $\mathbf{q}$ whose range in $\mathbf{q}$ is inversely related to the size of the source.

In a typical HBT analysis, the correlation functions are fit to a function of relative momentum that is often a Gaussian or exponential function, or a stretched exponential function that can interpolate between these two. The parameters of

*Full author list given at the end of the article.

the fits that relate to the space-time extent of the source function are referred to as the "HBT radii." Measurements of Bose-Einstein correlations in pp collisions at center-of-mass energies $\sqrt{s} = 0.9$ TeV and $\sqrt{s} = 7$ TeV have been made by the ATLAS [35], CMS [36], and ALICE [37] experiments. At both energies the source radii are observed to decrease with rising transverse momentum. It is also observed that the extracted radii increase with particle multiplicity but saturate at the highest multiplicities.

Although Bose-Einstein correlations are the most straightforward to measure experimentally, any final-state interaction can in principle be used to image the source density. The term "femtoscopy" is often used to refer to any measurement that provides spatio-temporal information about a hadronic source [38]. The measured source radii are interpreted as the dimensions of the region of homogeneity of the source at freeze-out, after all interactions between final-state particles and the bulk have ceased; thus, they are sensitive to the space-time evolution of the event. In particular, an increase in radii at low average transverse momentum k_{T} indicates radial expansion since higher-momentum particles are more likely to be produced earlier in the event [39]. The k_{T} scaling of HBT radii in p+Pb systems is of significant interest when studied as a function of centrality, an experimental proxy for the impact parameter. Thus, these measurements can provide insight into the conditions necessary for hydrodynamic behavior in small systems.

In many HBT measurements, the correlation functions are evaluated in one dimension using the invariant relative momentum $q_{\mathrm{inv}} \equiv \sqrt{-q_\mu q^\mu}$, where $q = p^a - p^b$ for a pair of particles a and b with four-momenta p^a and p^b. In three dimensions, HBT correlations are studied using the "out-side-long" convention [40–43]. In this system, q_{out}, the outwards component, is the projection along $\mathbf{k}_{\mathrm{T}}$; q_{side}, the sideways component, is the projection along $\hat{\mathbf{z}} \times \mathbf{k}_{\mathrm{T}}$ (with the z axis along the beamline); and q_{long} is the longitudinal component. The relative momentum of the pair is evaluated in the longitudinally comoving frame (LCMF), i.e., the frame boosted such that $k_z = 0$. This formulation of the HBT analysis has the advantage that it decomposes the correlation function into components that emphasize distinct physical effects. In particular, the spatial extent of the source in the longitudinal and transverse directions is likely to be different. The out and side radii are also expected to differ due to the effects of the Lorentz boost in the out direction and, if the system exhibits collectivity, due to space-momentum correlations. In a fully boost-invariant system, observables evaluated in the LCMF should be independent of k_z (or rapidity). The inherent asymmetry of p+Pb collisions seen, for example, in the charged-particle pseudorapidity distributions [44,45], provides a unique opportunity to study the correlations between source sizes and the pair's rapidity, collision centrality, or the local (in rapidity) charged-particle density. The results of such a study may provide insight into or constrain theoretical models of the underlying dynamics responsible for producing the final-state particles.

To address the topics and questions discussed above, this paper presents measurements of correlations between identified charged pions in 5.02 TeV p+Pb collisions which were performed by the ATLAS experiment at the LHC. While femtoscopic methods have already been applied to p+Pb systems at the LHC [46,47], this paper presents a new data-driven technique to constrain the significant background contribution from jet fragmentation, referred to in this paper as the "hard process" background. It also provides new measurements of the dependence of the source radii on the pair's rapidity $y^\star_{\pi\pi}$, calculated assuming both particles have the mass of the pion, over the range $-2 < y^\star_{\pi\pi} < 1$. Results are presented for one- and three-dimensional source radii as a function of the pair's average transverse momentum, k_{T}, over the range $0.1 < k_{\mathrm{T}} < 0.8$ GeV and for several p+Pb centrality intervals with the most central case being 0–1%. The p+Pb collision centrality is characterized using $\Sigma E_{\mathrm{T}}^{\mathrm{Pb}}$, the total transverse energy measured in the Pb-going forward calorimeter (FCal) [45]. It is defined such that central events, with large $\Sigma E_{\mathrm{T}}^{\mathrm{Pb}}$, have a low centrality percentage, and peripheral events, with a small $\Sigma E_{\mathrm{T}}^{\mathrm{Pb}}$, have a high centrality percentage. Using the measured centrality dependence of the source radii, the scaling of the system size with the number of nucleon participants N_{part} is also investigated, using a generalization of the Glauber model [48].

II. ATLAS DETECTOR

The ATLAS detector is described in detail in Ref. [49]. The measurements presented in this paper have been performed using the inner detector, minimum-bias trigger scintillators (MBTS), FCal, zero-degree calorimeter (ZDC), and the trigger and data acquisition systems. The inner detector [50], which is immersed in a 2 T axial magnetic field, is used to reconstruct charged particles within $|\eta| < 2.5$.[1] It consists of a silicon pixel detector, a semiconductor tracker (SCT) made of double-sided silicon microstrips, and a transition radiation tracker made of straw tubes. All three detectors consist of a barrel and two symmetrically placed endcap sections. A particle traveling from the interaction point (IP) with $|\eta| < 2$ crosses at least 3 pixel layers, 4 double-sided microstrip layers and typically 36 straw tubes. In addition to hit information, the pixel detector provides time over threshold for each hit pixel which is proportional to the deposited energy and which is used to provide measurements of specific energy loss (dE/dx) for particle identification.

The FCal covers a pseudorapidity region of $3.1 < |\eta| < 4.9$ and is used to estimate the centrality of each collision. The FCal uses liquid argon as the active medium with tungsten and copper absorbers. The MBTS, consisting of two arrays of scintillation counters, are positioned at $z = \pm 3.6$ m and cover $2.1 < |\eta| < 3.9$. The ZDCs, situated approximately 140 m from the nominal IP, detect neutral particles, mostly neutrons and photons, that have $|\eta| > 8.3$. They are used to distinguish pileup events (bunch crossings involving more than

[1] ATLAS uses a right-handed coordinate system with its origin at the nominal interaction point (IP) in the center of the detector and the z axis along the beam pipe. The x axis points from the IP to the center of the LHC ring, and the y axis points upward. Cylindrical coordinates (r,ϕ) are used in the transverse plane, ϕ being the azimuthal angle around the beam pipe. The pseudorapidity is defined in terms of the polar angle θ as $\eta = -\ln\tan(\theta/2)$.

one collision) from central collisions by detecting spectator nucleons that did not participate in the interaction. The calorimeters use tungsten plates as absorbers and quartz rods sandwiched between the tungsten plates as the active medium.

Events used for the analysis presented in this paper were primarily obtained from a combination of minimum-bias (MinBias) triggers that required either at least two hit scintillators in the MBTS or at least one hit on each side of the MBTS. An additional requirement on the number of hits in the SCT was imposed on both of these minimum-bias triggers to remove false triggers. To increase the number of events available in the highest $\Sigma E_{\mathrm{T}}^{\mathrm{Pb}}$ interval, the analysis includes a separate sample of events selected by a trigger (HighET) that required a total transverse energy in both sides of the FCal of at least 65 GeV.

III. DATA SETS

A. LHC data

This analysis uses data from the LHC 2013 p+Pb run at $\sqrt{s_{NN}} = 5.02$ TeV with an integrated luminosity of 28 nb^{-1}. The Pb ions had an energy per nucleon of 1.57 TeV and collided with the 4 TeV proton beam to yield a center-of-mass energy $\sqrt{s_{NN}} = 5.02$ TeV with a longitudinal boost of $y_{\mathrm{CM}} = 0.465$ in the proton direction relative to the ATLAS laboratory frame. The p+Pb run was divided into two periods between which the directions of the proton and lead beams were reversed. The data in this paper are presented using the convention that the proton beam travels in the forward ($+z$) direction and the lead beam travels in the backward ($-z$) direction. When the data from these two periods are combined, the MinBias triggers sampled a total luminosity, after prescale, of 24.5 μb^{-1} and yielded a total of 44 million events; the HighET trigger sampled a total luminosity of 41.4 μb^{-1} after prescale and yielded 700 thousand events.

B. Monte Carlo event generators

The effects of charged-particle reconstruction and selection are studied in a p+Pb sample generated using HIJING [51] and simulated with the GEANT4 package [52]. Five million events are generated at a center-of-mass energy per nucleon-nucleon pair of $\sqrt{s_{NN}} = 5.02$ TeV with a longitudinal boost of $y_{\mathrm{CM}} = 0.465$ in the proton direction. The sample is fully reconstructed with the same conditions as the data [53].

Four additional Monte Carlo generator samples are used to study the background from hard processes, as described in Sec. IV B. No detector simulation is performed on these samples, as the net effects of the simulation and reconstruction were studied using the fully reconstructed p+Pb simulation events and found to be negligible. The two-particle reconstruction effects occur only at very low $\mathbf{q}$ (as discussed in Sec. V A), but these generated samples are used only to study correlations from jet fragmentation which span a much broader range of $\mathbf{q}$. In each of the following samples, 50 million (250 million for PYTHIA 8) minimum-bias events are generated at a center-of-mass energy per nucleon-nucleon pair of $\sqrt{s_{NN}} = 5.02$ TeV:

(1) HIJING p+Pb. The energy and boost settings are the same as in the nominal p+Pb reconstructed simulation, except that the minimum hard-scattering transverse momentum is adjusted as described in Sec. IV B. This boost is applied only in the p+Pb sample.
(2) HIJING pp. The generator is run with all settings the same as in the p+Pb sample, except that both incoming particles are protons.
(3) PYTHIA 8 pp [54]. The set of generator parameters from ATLAS "UE AU2-CTEQ6L1" [55] is used with PYTHIA 8.209, which utilizes the CTEQ 6L1 [56] parton distribution function (PDF) from LHAPDF6 [57].
(4) Herwig ++ pp [58]. The NNLO MRST PDF [59] is used with Herwig ++ 2.7.1.

C. Event selection and centrality

In the offline analysis, charged-particle tracks and collision vertices are reconstructed using the same algorithms and methods applied in previous minimum-bias pp and p+Pb measurements [45,60]. Events included in this analysis are required to pass either of the two MinBias triggers or the HighET trigger, to have a hit on each side of the MBTS with a difference in average particle arrival times measured on the two sides of the MBTS which is less than 10 ns, a reconstructed primary vertex (PV), and at least two tracks satisfying the selection criteria listed in Sec. III D. Events that have more than one reconstructed vertex (including secondary vertices) with either more than ten tracks or a sum of track transverse momentum (p_{T}) greater than 6 GeV are rejected. An upper limit is placed on the activity measured in the Pb-going ZDC to further reject pileup events.

The centralities of the p+Pb events are characterized following the procedures described in Ref. [45], using $\Sigma E_{\mathrm{T}}^{\mathrm{Pb}}$, the total transverse energy in the Pb-going side of the FCal. The use of the FCal for measuring centrality has the advantage that it is not sensitive to multiplicity fluctuations in the kinematic region covered by the inner detector, where the measurements are performed. Measurements are presented in this paper for the centrality intervals listed in Table I. The events selected using the HighET trigger are used only in the 0–1% centrality interval. Figure 1 shows the distribution of $\Sigma E_{\mathrm{T}}^{\mathrm{Pb}}$ values obtained from events included in this measurement. The discontinuity in the spectrum occurs at the low edge of the 0–1% centrality interval, above which the HighET events are included.

For each centrality interval, the average multiplicity of charged particles with $p_{\mathrm{T}} > 100$ MeV and $|\eta| < 1.5$, $\langle dN_{\mathrm{ch}}/d\eta \rangle$, and the corresponding average number of participating nucleons, $\langle N_{\mathrm{part}} \rangle$, are obtained from a previous publication [45]. Since this analysis uses finer centrality intervals (no wider than 10% of the total centrality range) than those used in Ref. [45], a linear interpolation over the Glauber $\langle N_{\mathrm{part}} \rangle$ is used to construct additional values for $\langle dN_{\mathrm{ch}}/d\eta \rangle$ based on the published results. This interpolation is justified by the result in Ref. [45] that charged-particle multiplicity is proportional to $\langle N_{\mathrm{part}} \rangle$ in the peripheral region. The values and uncertainties from this procedure are listed in Table I.

TABLE I. The average number of nucleon participants $\langle N_{\text{part}}\rangle$ [45] for each centrality interval in the Glauber model as well as the two choices for the Glauber-Gribov model with color fluctuations (GGCF) [61] (and references therein), along with the average multiplicity with $p_T > 100$ MeV and $|\eta| < 1.5$ also obtained from Ref. [45]. The parameter ω_σ represents the size of fluctuations in the nucleon-nucleon cross section. Asymmetric systematic uncertainties are shown for $\langle N_{\text{part}}\rangle$. The uncertainties in $\langle dN_{\text{ch}}/d\eta\rangle$ are given in the order of statistical followed by systematic.

Centrality	$\langle N_{\text{part}}\rangle$			$\langle dN_{\text{ch}}/d\eta\rangle$
	Glauber	GGCF $\omega_\sigma = 0.11$	GGCF $\omega_\sigma = 0.2$	
0–1%	$18.2^{+2.6}_{-1.0}$	$24.2^{+1.5}_{-2.1}$	$27.4^{+1.6}_{-4.5}$	$58.1 \pm 0.1 \pm 1.9$
1–5%	$16.10^{+1.66}_{-0.91}$	$19.5^{+1.2}_{-1.3}$	$21.4^{+1.5}_{-2.0}$	$45.8 \pm 0.1 \pm 1.3$
5–10%	$14.61^{+1.21}_{-0.82}$	$16.5^{+1.0}_{-1.0}$	$17.5^{+1.1}_{-1.1}$	$38.5 \pm 0.1 \pm 1.1$
10–20%	$13.05^{+0.82}_{-0.73}$	$13.77^{+0.79}_{-0.81}$	$14.11^{+0.86}_{-0.79}$	$32.34 \pm 0.05 \pm 0.97$
20–30%	$11.37^{+0.65}_{-0.63}$	$11.23^{+0.62}_{-0.67}$	$11.17^{+0.68}_{-0.62}$	$26.74 \pm 0.04 \pm 0.80$
30–40%	$9.81^{+0.56}_{-0.57}$	$9.22^{+0.50}_{-0.54}$	$8.97^{+0.60}_{-0.49}$	$22.48 \pm 0.03 \pm 0.75$
40–50%	$8.23^{+0.48}_{-0.55}$	$7.46^{+0.41}_{-0.43}$	$7.15^{+0.54}_{-0.39}$	$18.79 \pm 0.02 \pm 0.69$
50–60%	$6.64^{+0.41}_{-0.52}$	$5.90^{+0.36}_{-0.34}$	$5.60^{+0.47}_{-0.30}$	$15.02 \pm 0.02 \pm 0.62$
60–70%	$5.14^{+0.35}_{-0.43}$	$4.56^{+0.32}_{-0.26}$	$4.32^{+0.41}_{-0.23}$	$11.45 \pm 0.01 \pm 0.56$
70–80%	$3.90^{+0.24}_{-0.30}$	$3.50^{+0.22}_{-0.18}$	$3.34^{+0.29}_{-0.16}$	$8.49 \pm 0.02 \pm 0.51$

D. Charged-particle selection and pion identification

Reconstructed tracks used in the HBT analysis are required to have $|\eta| < 2.5$ and $p_T > 0.1$ GeV and to satisfy a standard set of selection criteria [60]: a minimum of one pixel hit is required, and if the track crosses an active module in the innermost layer, a hit in that layer is required; for a track with p_T greater than 0.1, 0.2, or 0.3 GeV there must be at least two, four, or six hits respectively in the SCT; the transverse impact parameter with respect to the primary vertex, d_0^{PV}, must be such that $|d_0^{\text{PV}}| < 1.5$ mm; and the corresponding longitudinal impact parameter must satisfy $|z_0^{\text{PV}} \sin\theta| < 1.5$ mm. To reduce contributions from secondary decays, a stronger constraint on the pointing of the track to the primary vertex is applied. Namely, neither $|d_0^{\text{PV}}|$ nor $|z_0^{\text{PV}} \sin\theta|$ can be larger than three times its uncertainty as derived from the covariance matrix of the track fit.

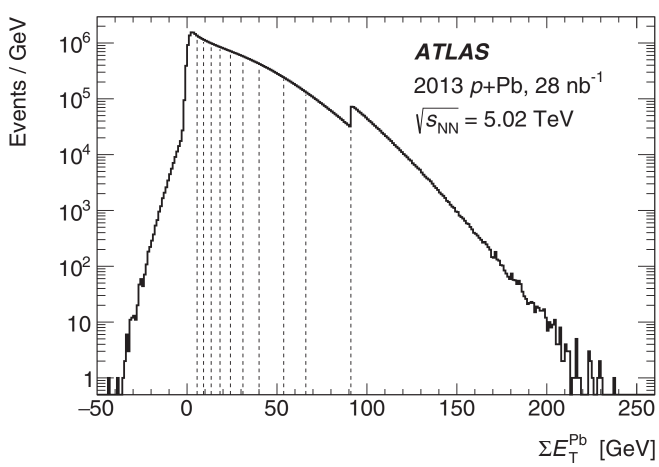

FIG. 1. The distribution of the total transverse energy in the forward calorimeter in the Pb-going direction (ΣE_T^{Pb}) for the events used in this analysis. Dashed lines are shown at the boundaries of the centrality intervals, and the discontinuity at $\Sigma E_T^{\text{Pb}} = 91.08$ GeV corresponds to the lower ΣE_T^{Pb} boundary of the 0–1% centrality interval.

Particle identification (PID) is performed through measurements of the specific energy loss dE/dx derived from the ionization charge deposited in the pixel clusters associated with a track. The dE/dx of a track is calculated as a truncated mean of the dE/dx in individual pixel clusters as described in Ref. [62], since the truncated mean gives a better resolution than the mean. Relative likelihoods that the track is a π, K, and p are formed by fitting the dE/dx distributions to $\sqrt{s} =$ 7 TeV pp data in several momentum intervals as explained in Ref. [63]. Three PID selection levels are defined: one designed to have a high efficiency for pions, one designed to result in high pion purity, and one in between that was chosen as the nominal selection level and is used throughout the analysis if other PID selections are not explicitly mentioned. The efficiency and purity of these selections are studied in the fully reconstructed simulated sample. The resulting purity of track pairs in the nominal selection is shown in Fig. 2 as a function of pair's k_T and $y^{\star}_{\pi\pi}$. The results are also evaluated at the looser and tighter PID definitions (also in Fig. 2), and the differences are incorporated into the systematic uncertainty (see Sec. V).

E. Pair selection

Track pairs are required to have $|\Delta\phi| < \pi/2$ to avoid an enhancement in the correlation function arising primarily from dijets. This enhancement does not directly affect the signal region but can influence the results by affecting the overall normalization factor in the fits. The pair's rapidity $y^{\star}_{\pi\pi}$, measured with respect to the nucleon-nucleon center of mass, must lie in the range $-2 < y^{\star}_{\pi\pi} < 1$. This requirement is more stringent than the single-track requirement $|\eta| < 2.5$. When analyzing track pairs of opposite charge, common particle resonances are removed via requirements on the invariant mass so that $|m_{\pi\pi} - m_{\rho^0}| > 150$ MeV, $|m_{\pi\pi} - m_{K^0_S}| > 20$ MeV, and $|m_{KK} - m_{\phi(1020)}| > 20$ MeV, where m_{ab} is the pair's invariant mass calculated with particle masses m_a and m_b. The

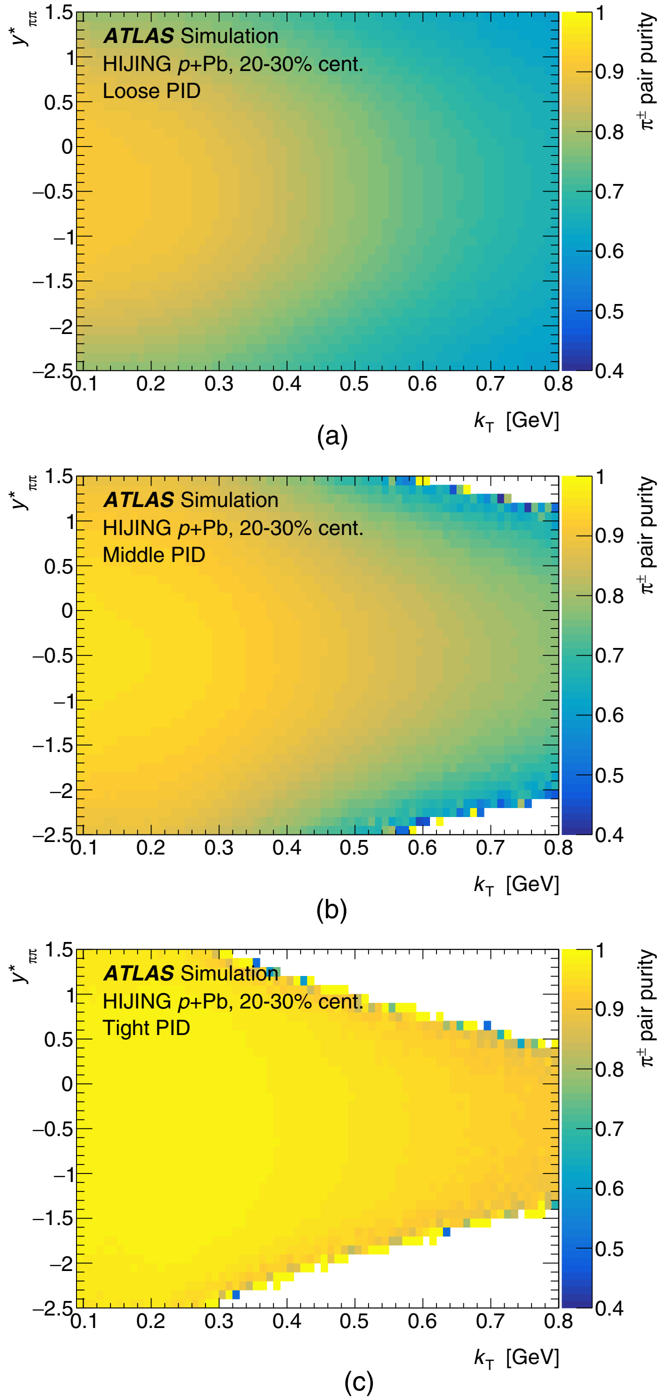

FIG. 2. Purity of identified pion pairs with the loose (a), middle (b), and tight (c) PID selections. The purities are estimated using fully simulated HIJING p+Pb events, as a function of the pair's average transverse momentum k_T and rapidity $y^{\star}_{\pi\pi}$. The rapidity is calculated using the pion mass for both reconstructed charged particles.

values are chosen according to the width of the resonance (for the ρ^0) or the scale of the detector's momentum resolution [K^0_S and $\phi(1020)$]. These requirements are applied when forming both the same- and mixed-event distributions (defined in Sec. IV).

The $q_{\rm inv}$, $q_{\rm long}$, $|q_{\rm side}|$, and $q_{\rm out}$ distributions of the pairs obtained through these procedures are shown in Fig. 3 for the 0–1% and 60–80% centrality intervals. The one-dimensional $q_{\rm inv}$ distribution necessarily decreases to zero at $q_{\rm inv} = 0$ due to the scaling of the phase-space volume element $d^3q \propto q^2 dq$. In contrast the three-dimensional quantities remain finite at zero relative momentum. The distributions are nearly identical for the two centrality intervals, although differences can be seen at small relative momentum in all four distributions.

IV. CORRELATION FUNCTION ANALYSIS

The two-particle correlation function is defined as the ratio of two-particle to single-particle momentum spectra:

$$C(p^a,p^b) \equiv \frac{\left(\frac{dN^{ab}}{d^3p^a d^3p^b}\right)}{\left(\frac{dN^a}{d^3p^a}\right)\left(\frac{dN^b}{d^3p^b}\right)},$$

for pairs of particles with four-momenta p^a and p^b. This definition has the useful feature that most single-particle efficiency, acceptance, and resolution effects cancel in the ratio. The correlation function is expressed as a function of the relative momentum[2] $q \equiv p^a - p^b$ in intervals of average momentum $k \equiv (p^a + p^b)/2$.

The relative momentum distribution $A(q) \equiv dN/dq|_{\rm same}$ (Fig. 3) is formed by selecting like-charge (or unlike-charge) pairs of particles from each event in an event class, which is defined by the collision centrality and z position of the primary vertex ($z_{\rm PV}$). The combinatorial background $B(q) \equiv dN/dq|_{\rm mix}$ is constructed by event mixing; that is, by selecting one particle from each of two events in the same event class as $A(q)$. Each particle in the background fulfills the same selection requirements as those used in the same-event distribution. Event classes are categorized by centrality so that events are only compared to others with similar multiplicities and momentum distributions. Events are sorted by $z_{\rm PV}$ so that the background distribution is constructed with pairs of tracks originating from nearby space points, which is necessary for $B(q)$ to accurately represent the as-installed detector. The $A(q)$ and $B(q)$ distributions are combined over $z_{\rm PV}$ intervals in such a way that each of them samples the same $z_{\rm PV}$ distribution. The ratio of the distributions defines the correlation function:

$$C_{\mathbf{k}}(q) \equiv \frac{A_{\mathbf{k}}(q)}{B_{\mathbf{k}}(q)}. \quad (2)$$

A. Parameterization of the correlation function

Assuming that all particles are identical pions created in a fully chaotic source and that they have no final-state interaction, the enhancement in the correlation function is the Fourier transform of the source density.

[2]While q here refers to the relative four-momentum, it is also used generically to refer to either the Lorentz invariant $q_{\rm inv}$ or three-vector $\mathbf{q}$. The correlation function is studied in terms of both these variables but the description of the analysis is nearly identical for both cases.

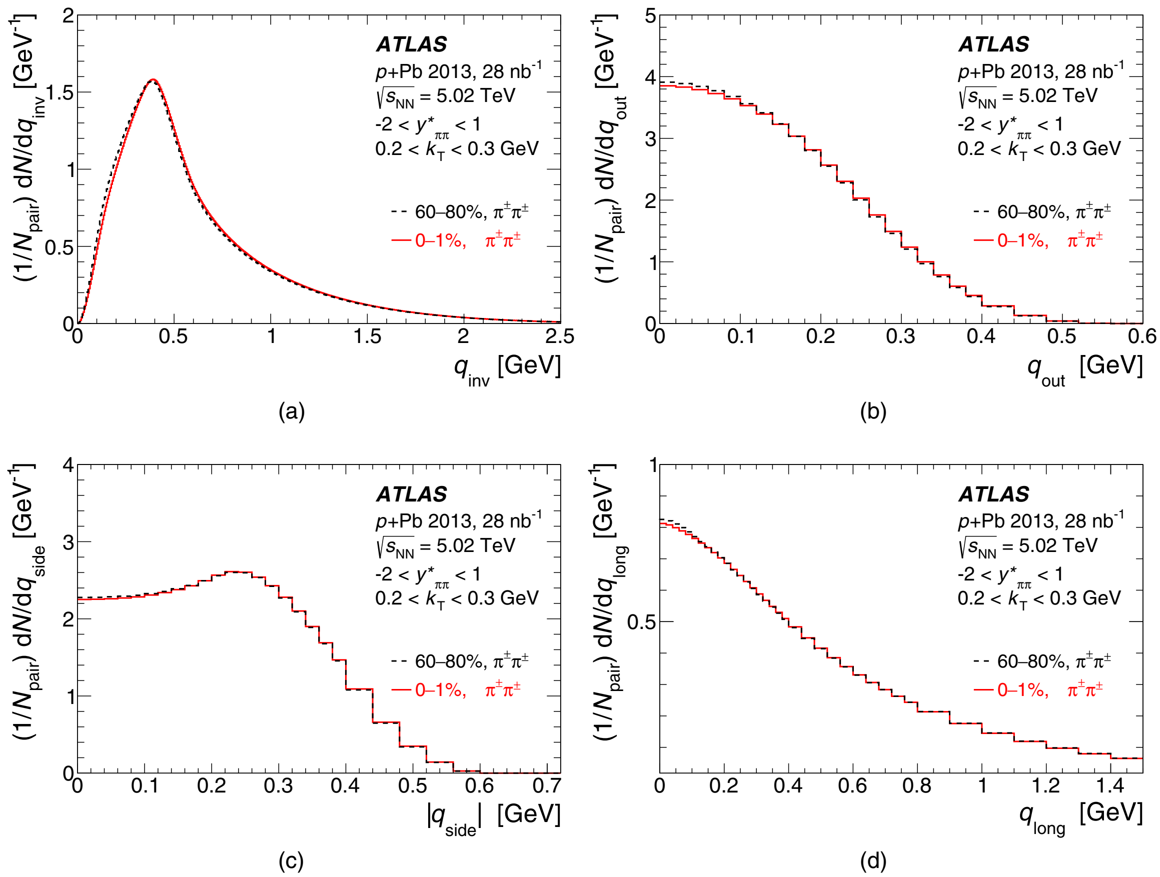

FIG. 3. Pair-normalized distributions of the invariant relative momentum q_{inv} (a) and the three-dimensional relative momentum components q_{long} (b), q_{side} (c), and q_{out} (d) for identified same-charge pion pairs with $0.2 < k_{\mathrm{T}} < 0.3$ GeV obtained from two centrality intervals: 60–80% and 0–1%.

The Bowler-Sinyukov formalism [64,65] is used to account for final-state corrections:

$$C_{\mathbf{k}}(q) = (1-\lambda) + \lambda K(q) C_{\mathrm{BE}}(q),$$

where K is a correction factor for final-state Coulomb interactions, and $C_{\mathrm{BE}}(q) = 1 + \mathcal{F}[S_{\mathbf{k}}](q)$ with $\mathcal{F}[S_{\mathbf{k}}](q)$ denoting the Fourier transform of the two-particle source density function $S_{\mathbf{k}}(r)$. Several factors influence the value of the parameter λ. Including nonidentical particles decreases this parameter, as does coherent particle emission. Products of weak decays or long-lived resonances also lead to a decrease in λ, as they are emitted at a length scale greater than can be resolved by femtoscopic methods given the momentum resolution of the detector. These additional contributions to the source density are not Coulomb-corrected within the Bowler-Sinyukov formalism. When describing pion pairs of opposite charge, there is no Bose-Einstein enhancement and $C_{\mathrm{BE}} \to 1$.

Coulomb interactions suppress the correlation at small relative momentum for identical charged particles. The particular choice of correction factor $K(q)$ is determined using the formalism in Ref. [66]. This uses the approximation that the Coulomb correction is effectively applied not from a point source, but over a Gaussian source density of radius R_{eff}:

$$K(q_{\mathrm{inv}}) = G(q_{\mathrm{inv}})\left[1 + \frac{8R_{\mathrm{eff}}}{\sqrt{\pi}a}\,{}_2F_2\left(\frac{1}{2},1;\frac{3}{2},\frac{3}{2};-R_{\mathrm{eff}}^2 q_{\mathrm{inv}}^2\right)\right], \tag{3}$$

where $a = 388$ fm is the Bohr radius [67] of a two-pion state, ${}_2F_2$ is a generalized hypergeometric function, and $G(q_{\mathrm{inv}})$ is the Gamow factor [68,69]

$$G(q_{\mathrm{inv}}) = \frac{4\pi}{aq_{\mathrm{inv}}}\frac{1}{e^{4\pi/aq_{\mathrm{inv}}} - 1}.$$

For opposite-charge pairs, a is taken to be negative, since its definition includes a product of the two charges.

The Bose-Einstein enhancement in the invariant correlation functions is fit to an exponential form:

$$C_{\mathrm{BE}}(q_{\mathrm{inv}}) = 1 + e^{-R_{\mathrm{inv}} q_{\mathrm{inv}}}, \tag{4}$$

where R_{inv} is the Lorentz-invariant HBT radius. This function corresponds to an underlying Breit-Wigner source density.

The Bose-Einstein component of the three-dimensional correlation functions is fit to a function of the form

$$C_{\mathrm{BE}}(\mathbf{q}) = 1 + e^{-\|R\mathbf{q}\|}, \tag{5}$$

where R is a symmetric matrix of the form

$$R = \begin{pmatrix} R_{\text{out}} & 0 & R_{\text{ol}} \\ 0 & R_{\text{side}} & 0 \\ R_{\text{ol}} & 0 & R_{\text{long}} \end{pmatrix}. \quad (6)$$

The off-diagonal entries other than R_{ol} can be argued to vanish by the average azimuthal symmetry of the source. In hydrodynamic models the out-long term R_{ol} is sensitive to spatio-temporal correlations and, therefore, to the lifetime of the source [70,71]. It couples radial and transverse expansion, and is expected to vanish in the absence of either. If the source is fully boost invariant then this term vanishes, so an observation of a nonzero value demonstrates that the homogeneity region is not boost invariant.

In order to reduce computational demands, a few symmetry arguments are considered. The order of the pairs is chosen such that q_{out} is always positive, which can be done so long as $C(-\mathbf{q}) = C(\mathbf{q})$. The average azimuthal symmetry of the source is invoked in order to allow only the absolute value of q_{side} to be considered. The sign of q_{long} cannot be similarly discarded if a nonzero R_{ol} is allowed.

A Gaussian form for the Bose-Einstein enhancement is often used in the three-dimensional correlation function. However, this form was found to give a poor description of ATLAS data, relative to an exponential form. This was also observed in the ATLAS pp results in Ref. [35]. The chosen form of $\mathcal{F}[S_{\mathbf{k}}](\mathbf{q})$ must be taken into account when interpreting source radii, and there is no simple correspondence between parameters estimated using one form and those from another. An *ad hoc* factor of $\sqrt{\pi}$ is often invoked to relate Gaussian radii to exponential radii by assuming that the first q-moment of the invariant correlation function should be preserved, but this assumption is not rigorously justified and the argument fails in general for three-dimensional correlation functions.

B. Hard-process contribution

Additional nonfemtoscopic enhancements to the correlation functions at $q_{\text{inv}} \lesssim 0.5$–1 GeV are observed in both the opposite-charge ($+-$) and the same-charge ($\pm\pm$) pairs. As discussed later in this section, the enhancement is more prominent in $+-$ pairs than it is in $\pm\pm$ pairs. Monte Carlo (MC) generators do not simulate the final-state two-particle interactions used for femtoscopy, but they do describe the background correlations. The MC generators used in this section to constrain the background description are described in Sec. III B.

The nonfemtoscopic enhancement is more prominent for higher k_{T} and lower multiplicities. This suggests that the correlation is primarily due to jet fragmentation. This hypothesis is verified by studying correlation functions in HIJING, by increasing the minimum hard-scattering p_{T} ($p_{\text{T}}^{\text{HS,min}}$) from 2 to 20 GeV. Increasing $p_{\text{T}}^{\text{HS,min}}$ has the effect of suppressing most hard processes in typical events. Without the resulting jet fragmentation, the nonfemtoscopic enhancement is removed from the correlation function, as demonstrated in Fig. 4 by comparing the panels on the left and right of each row.

The amplitude of the hard-process contribution tends to be larger in the Monte Carlo events than it is in the data. Thus, attempting to account for it by studying the double ratio $C^{\text{data}}(q)/C^{\text{MC}}(q)$ leads to a depletion that is apparent in the region where the Bose-Einstein enhancement disappears [35]. Another commonly used method is to parametrize the minijet contribution using simulation and to allow one or more parameters of the description to vary in the fit [46,47].

To avoid too much reliance on either a full MC description or arbitrary additional free parameters, a data-driven method is derived here to constrain the correlations from jet fragmentation. Opposite-charge correlation functions are used to predict the jet contribution in the same-charge correlation function. This poses two challenges. First, resonance decays appear prominently in the opposite-charge correlations. The most prominent of these are removed by requirements on the invariant mass of the opposite-charge pairs (as described in Sec. III E), and the fits to the opposite-charge correlation functions are restricted to $q_{\text{inv}} > 0.1$ GeV. The lower bound on the domain of the fit reduces sensitivity to effects such as three-body decays that are unrelated to jet fragmentation, which is significant over a broader range of q. Second, jet fragmentation does not affect opposite-charge and same-charge correlations in an identical manner. This is in part because opposite-charge pairs are more likely to have a closer common ancestor in a jet's fragmentation into hadrons.

To account for the remaining differences between $+-$ and $\pm\pm$ pairs, a study of both classes of correlation functions is performed in PYTHIA 8. In order to isolate the effect of jet fragmentation, decays from the relatively longer-lived particles η, η', and ω are excluded. Pairs of particles from two-body resonance decays are also neglected, in order to remove mass peaks in the correlation function. The same-pair mass cut around the ρ resonance that is used in the data is also applied in PYTHIA 8 events, since the removal of the corresponding region of phase space has a significant effect on the shape of the correlation function.

1. Jet fragmentation in q_{inv}

To describe the jet fragmentation in the invariant correlation functions, fits are performed in PYTHIA 8 pp to a stretched exponential function of the form

$$\Omega(q_{\text{inv}}) = \mathcal{N}\left(1 + \lambda_{\text{bkgd}}^{\text{inv}} e^{-|R_{\text{bkgd}}^{\text{inv}} q_{\text{inv}}|^{\alpha_{\text{bkgd}}^{\text{inv}}}}\right), \quad (7)$$

where $\mathcal{N}$ is a normalization factor and the other parameters depend on the charge combination and on k_{T}. The $\Omega(q_{\text{inv}})$ function above is applied as a multiplicative factor to the femtoscopic correlation function. The strategy employed is to estimate these parameters for same-charge correlation functions based on values determined using opposite-charge correlations. First, the shape parameter $\alpha_{\text{bkgd}}^{\text{inv}}$ is determined with fits to same-charge correlation functions, with all parameters allowed to be free. It is only weakly dependent on multiplicity, so a function is fit to parametrize $\alpha_{\text{bkgd}}^{\text{inv}}$ in PYTHIA 8 as a function of k_{T} (with k_{T} in GeV):

$$\alpha_{\text{bkgd}}^{\text{inv}}(k_{\text{T}}) = 2 - 0.050 \ln(1 + e^{50.9(k_{\text{T}} - 0.49)}).$$

The fits are well described by a Gaussian form ($\alpha_{\text{bkgd}}^{\text{inv}} = 2$) at $k_{\text{T}} \lesssim 0.4$ GeV, and $\alpha_{\text{bkgd}}^{\text{inv}}$ decreases to a value around 1.3 in the highest k_{T} interval.

The fits are performed again to the PYTHIA 8 correlation functions, with $\alpha_{\text{bkgd}}^{\text{inv}}$ now fixed to the same value in same- and

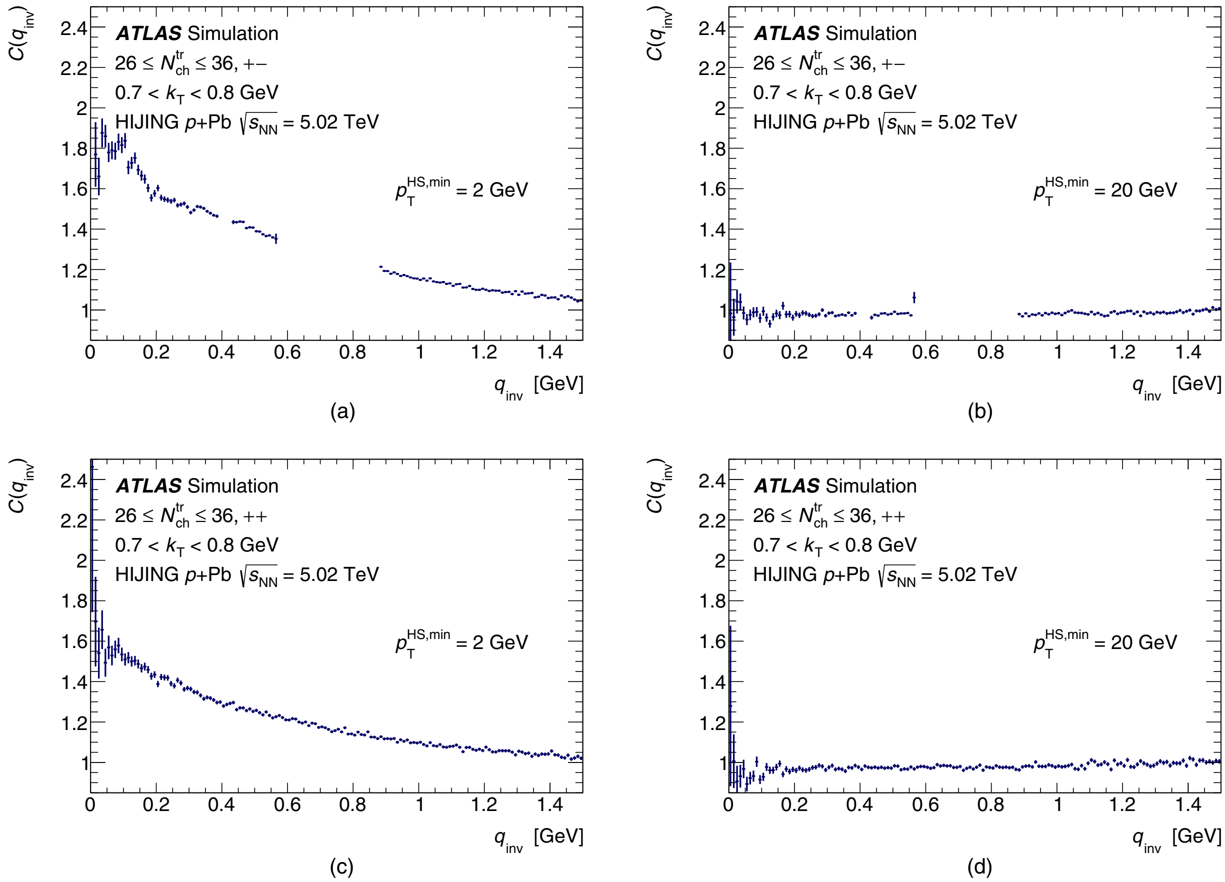

FIG. 4. Correlation functions of charged particles from HIJING for opposite- (a), (b) and same-charge (c), (d) pairs with transverse momentum $0.7 < k_{\mathrm{T}} < 0.8$ GeV, using events with a generated multiplicity $26 \leqslant N_{\mathrm{ch}}^{\mathrm{tr}} \leqslant 36$. The generator is run with the minimum hard-scattering $p_{\mathrm{T}}^{\mathrm{HS,\,min}}$ at the default setting of 2 GeV (a), (c) and increased to 20 GeV (b), (d) to remove the contribution from hard processes. The gaps in the opposite-charge correlation functions are a result of the requirements described in Sec. III E, which remove the largest resonance contributions.

opposite-charged pairs, and a comparison is made between the width parameters $R_{\mathrm{bkgd}}^{\mathrm{inv}\,+-}$ and $R_{\mathrm{bkgd}}^{\mathrm{inv}\,\pm\pm}$. The width of the jet fragmentation correlation for same-charge pairs is found to be correlated to that for opposite-charge pairs, as shown in the right plot of Fig. 5. Four intervals of charged particle multiplicity, N_{ch}, calculated for particles with $p_{\mathrm{T}} >$ 100 MeV and $|\eta| < 2.5$ are shown: $26 \leqslant N_{\mathrm{ch}} \leqslant 36$, $37 \leqslant N_{\mathrm{ch}} \leqslant 48$, $49 \leqslant N_{\mathrm{ch}} \leqslant 64$, and $65 \leqslant N_{\mathrm{ch}}$. The relationship between the invariant background widths is modeled as a direct proportionality,

$$R_{\mathrm{bkgd}}^{\mathrm{inv}\,\pm\pm} = \rho R_{\mathrm{bkgd}}^{\mathrm{inv}\,+-}, \tag{8}$$

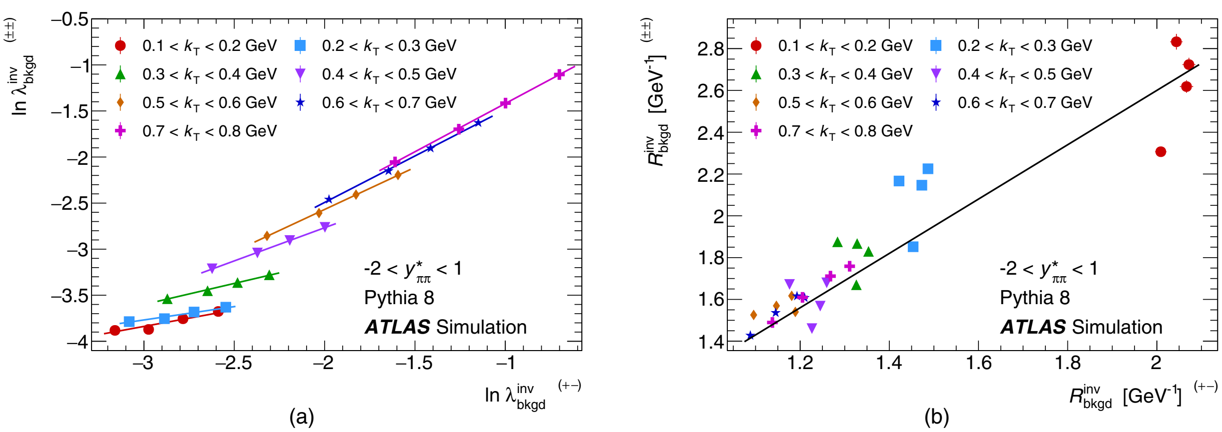

FIG. 5. Comparison of jet fragmentation parameters between opposite- and same-charge correlation functions. The amplitude is shown in (a), and the width is shown in (b). The lines are fits of the data to Eqs. (8) and (9). For each k_{T} interval, four multiplicity intervals are shown ($26 \leqslant N_{\mathrm{ch}} \leqslant 36$, $37 \leqslant N_{\mathrm{ch}} \leqslant 48$, $49 \leqslant N_{\mathrm{ch}} \leqslant 64$, and $65 \leqslant N_{\mathrm{ch}}$).

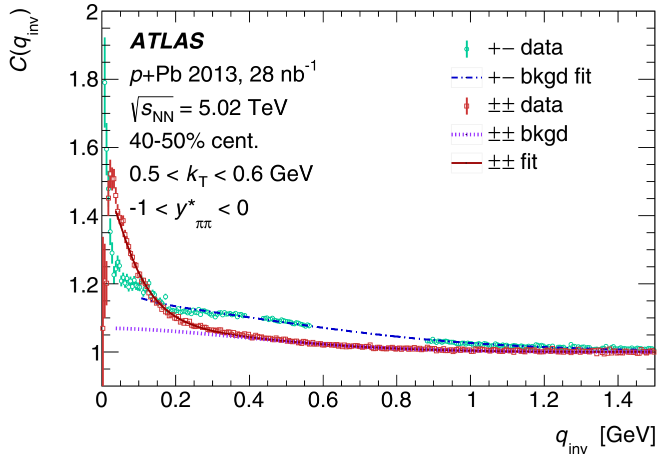

FIG. 6. Correlation functions in p+Pb data for opposite-charge (teal circles) and same-charge (red squares) pairs. The opposite-charge correlation function, with the most prominent resonances removed, is fit to a function of the form in Eq. (7) (blue dashed line). The violet dotted line is the estimated jet contribution in the same-charge correlation function, also of the form of Eq. (7), and the dark red line is the full fit of Eq. (19) to the same-charge data.

with a value of $\rho = 1.3$ extracted from PYTHIA 8. This proportionality begins to break down at low k_T, but the model becomes increasingly accurate at larger k_T, where hard processes give a larger contribution to the correlation function.

Next, $R^{\text{inv}}_{\text{bkgd}}{}^{\pm\pm}$ is fixed from $R^{\text{inv}}_{\text{bkgd}}{}^{+-}$ using the value of ρ, and the fits are performed again to parametrize the relationship between the amplitudes,

$$\lambda^{\text{inv}}_{\text{bkgd}}{}^{\pm\pm} = \mu(k_T)\left(\lambda^{\text{inv}}_{\text{bkgd}}{}^{+-}\right)^{\nu(k_T)}. \tag{9}$$

As shown in the left-hand plot of Fig. 5, μ and ν are fit in each k_T interval to describe four multiplicity intervals. The power-law scaling of Eq. (9) is found to provide a good description of the relation between the same- and opposite-charge amplitudes across all four multiplicity intervals studied. The multiplicity-independence of μ and ν is important in justifying the use of these parameters in p+Pb.

The correspondence between opposite- and same-charge pairs in both pp and p+Pb systems is studied in HIJING, since the study described in this section is performed with PYTHIA 8 in a pp system. While the mapping is mostly consistent between the two systems, it is found that μ is larger in p+Pb than in pp by 8.5% on average. When the mapping is applied to the data, this attenuation factor (along with a corresponding systematic uncertainty described in Sec. V) is also taken into account.

With $\alpha^{\text{inv}}_{\text{bkgd}}(k_T)$, $\mu(k_T)$, $\nu(k_T)$, and ρ determined from Monte Carlo generator samples, the mapping can be applied to the p+Pb data. As illustrated in Fig. 6, the $+-$ correlation function is fit to Eq. (7) for $q_{\text{inv}} > 0.1$ GeV, with α_{bkgd} fixed from PYTHIA 8 and $\lambda^{\text{inv}}_{\text{bkgd}}{}^{+-}$ and $R^{\text{inv}}_{\text{bkgd}}{}^{+-}$ as free parameters. The μ, ν, and ρ parameters are used to infer $\lambda^{\text{inv}}_{\text{bkgd}}{}^{\pm\pm}$ and $R^{\text{inv}}_{\text{bkgd}}{}^{\pm\pm}$, which are fixed before the femtoscopic part of the correlation function is fit to $\pm\pm$ data.

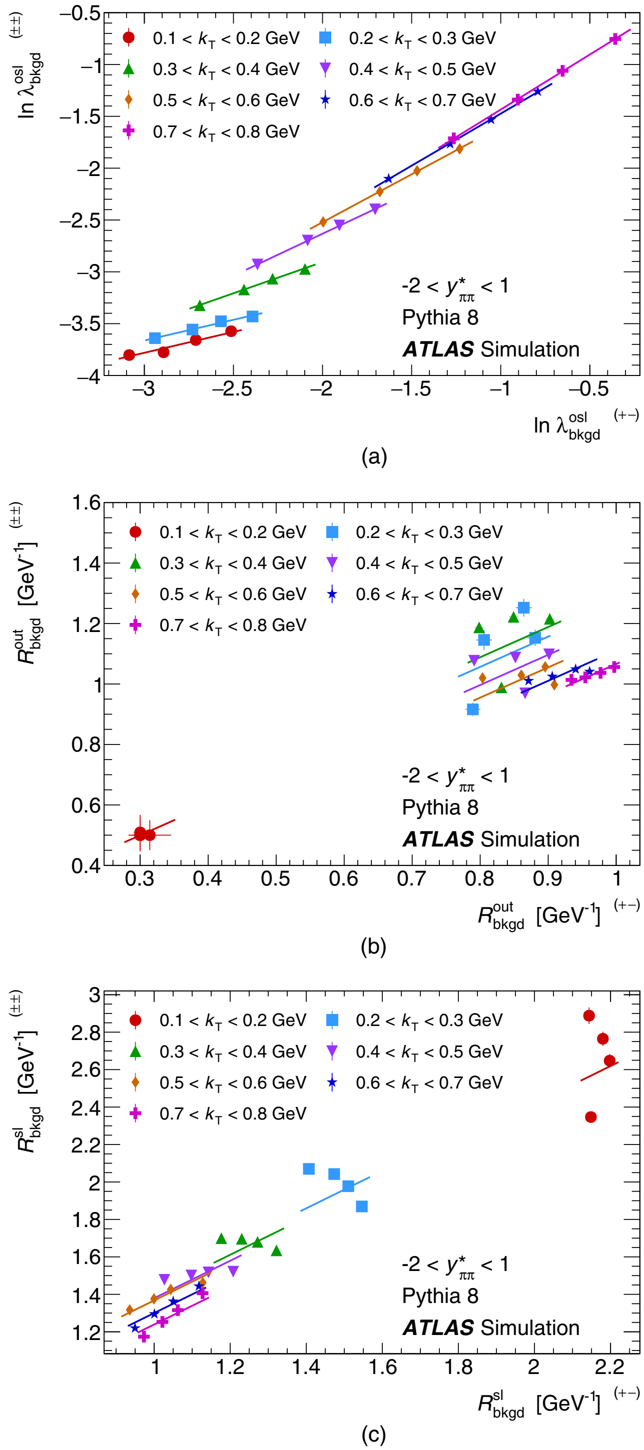

FIG. 7. Comparison of jet fragmentation parameters between opposite- and same-charge correlation functions. The amplitude is shown in (a), and the two widths in (b), (c). The lines are fits of the data to Eqs. (11)–(13). For each k_T interval, four multiplicity intervals are shown ($26 \leqslant N_{\text{ch}} \leqslant 36$, $37 \leqslant N_{\text{ch}} \leqslant 48$, $49 \leqslant N_{\text{ch}} \leqslant 64$, and $65 \leqslant N_{\text{ch}}$).

2. *Jet fragmentation in three dimensions*

In the longitudinally comoving frame of a particle pair produced in a jet, the axis of the jet is aligned on average

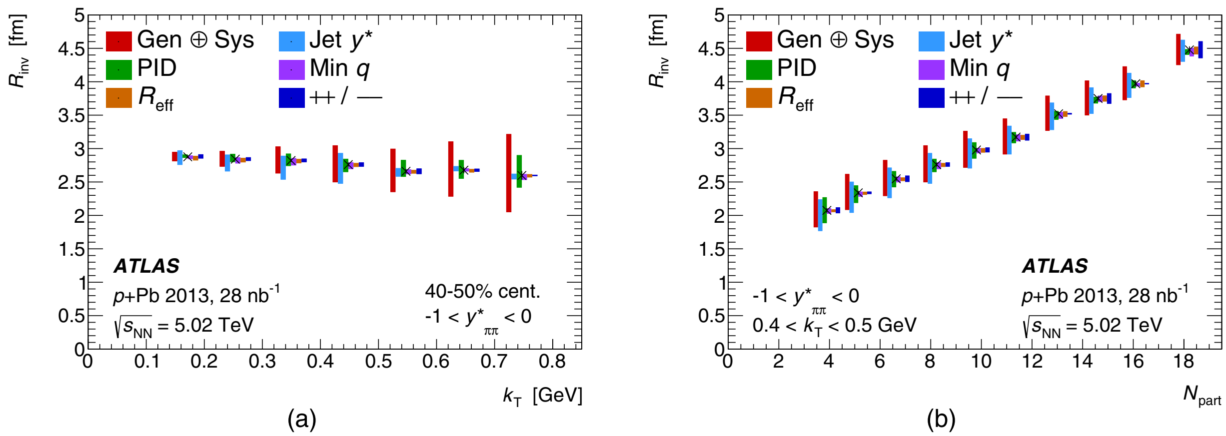

FIG. 8. The contributions of the various sources of systematic uncertainty to the invariant radius $R_{\rm inv}$. The typical trends with the pair's average transverse momentum $k_{\rm T}$ are shown in (a) and the trends with the number of nucleon participants $N_{\rm part}$ are shown in (b). The black crosses indicate the nominal results.

with the "out" direction and the plane transverse to the jet's momentum is spanned by the "side" and "long" directions. In three dimensions the correlation from jet fragmentation is factorized into components which separately describe the "out" direction and both the "side" and "long" directions:

$$\Omega(\mathbf{q}) = 1 + \lambda_{\rm bkgd}^{\rm osl} \exp\left(-\left|R_{\rm bkgd}^{\rm out} q_{\rm out}\right|^{\alpha_{\rm bkgd}^{\rm out}} - \left|R_{\rm bkgd}^{\rm sl} q_{\rm sl}\right|^{\alpha_{\rm bkgd}^{\rm sl}}\right), \tag{10}$$

where $q_{\rm sl} = \sqrt{q_{\rm side}^2 + q_{\rm long}^2}$, $\lambda_{\rm bkgd}^{\rm osl}$ is the background amplitude, and $\alpha_{\rm bkgd}^{\rm out}$ and $\alpha_{\rm bkgd}^{\rm sl}$ parametrize the shape of the fragmentation contribution along and transverse to the jet axis, respectively. The shape parameters $\alpha_{\rm bkgd}^{\rm out}$ and $\alpha_{\rm bkgd}^{\rm sl}$ are taken from PYTHIA 8 and fixed to 1.5 and 1.7 respectively. Fits of these parameters to PYTHIA 8 correlation functions are not fully consistent with these chosen numerical constants at all $k_{\rm T}$ and multiplicities. However, the impact of the somewhat arbitrary choice of fixing these parameters is tested by varying them both by 0.1, and the changes in the results are less than 1%.

Similarly to the procedure used for the $q_{\rm inv}$ correlation functions, the width parameters are compared between opposite- and same-charge correlation functions (bottom panels of Fig. 7); however, in three dimensions the relationships are parameterized as a function of $k_{\rm T}$. Next, as for $q_{\rm inv}$, the amplitudes for three-dimensional jet correlations are compared between opposite- and same-charge pairs (top panel of Fig. 7). While the relationships between opposite- and same-charge correlations are not well described everywhere by the fitted lines, the model becomes increasingly accurate at larger $k_{\rm T}$, where hard processes give a larger contribution to the correlation function. The functional forms of the mappings from opposite- to same-charge three-dimensional parameters are

$$\lambda_{\rm bkgd}^{\rm osl}{}^{\pm\pm} = \mu(k_{\rm T})\left(\lambda_{\rm bkgd}^{\rm osl}{}^{+-}\right)^{\nu(k_{\rm T})}, \tag{11}$$

$$R_{\rm bkgd}^{\rm out}{}^{\pm\pm} = R_{\rm bkgd}^{\rm out}{}^{+-} + \Delta R_{\rm bkgd}^{\rm out}(k_{\rm T}), \tag{12}$$

$$R_{\rm bkgd}^{\rm sl}{}^{\pm\pm} = R_{\rm bkgd}^{\rm sl}{}^{+-} + \Delta R_{\rm bkgd}^{\rm sl}(k_{\rm T}). \tag{13}$$

The widths used in the three-dimensional background description are related by a $k_{\rm T}$-dependent additive factor [Eqs. (12) and (13)] because a simple proportionality [Eq. (8)] is not as successful in describing the behavior.

The invariant and three-dimensional (3D) fragmentation amplitudes are strongly correlated and the mappings from opposite- to same-charge correlation functions are quantitatively similar. Thus, the same 8.5% attenuation factor for μ derived from HIJING for the invariant mapping is used for the three-dimensional fits as well.

The numerical values used for mapping the amplitude $\lambda_{\rm bkgd}^{\rm osl}$, fragmentation width colinear with the jet axis $R_{\rm bkgd}^{\rm out}$, and fragmentation width transverse to the jet axis $R_{\rm bkgd}^{\rm sl}$ are given by the following parametrizations ($k_{\rm T}$ in GeV and $R_{\rm bkgd}$ in GeV^{-1}):

$$\ln \mu(k_{\rm T}) = -3.9 + 9.5 k_{\rm T} - 6.4 k_{\rm T}^2, \tag{14}$$

$$\nu(k_{\rm T}) = 0.03 + 2.6 k_{\rm T} - 1.6 k_{\rm T}^2, \tag{15}$$

$$\Delta R_{\rm bkgd}^{\rm out}(k_{\rm T}) = 0.43 - 0.49 k_{\rm T}, \tag{16}$$

$$\Delta R_{\rm bkgd}^{\rm sl}(k_{\rm T}) = \frac{0.51}{1 + (1.30 k_{\rm T})^2}. \tag{17}$$

The jet fragmentation parameters of the p+Pb data depend on centrality and $k_{\rm T}$. The same-charge amplitude of the background ranges from being negligible at low $k_{\rm T}$ up to a maximum of roughly 0.25 at the largest measured $k_{\rm T}$ of 0.8 GeV for the most peripheral events. The widths of the same-charge fragmentation correlation have length scales which are typically in a range of 0.3–0.5 fm at the largest $k_{\rm T}$ where they are most relevant. The p+Pb femtoscopic measurement is most challenging at high $k_{\rm T}$ in peripheral events, where the fragmentation background amplitude is a significant fraction of the Bose-Einstein amplitude and the HBT radii are smaller and closer in magnitude to the length scale of the jet correlation.

C. Fitting procedure

The bin contents of the histogram representations of $A(q)$ and $B(q)$ are assumed to be Poisson distributed. The correlation function $C(q)$ is assumed to be fit best by the

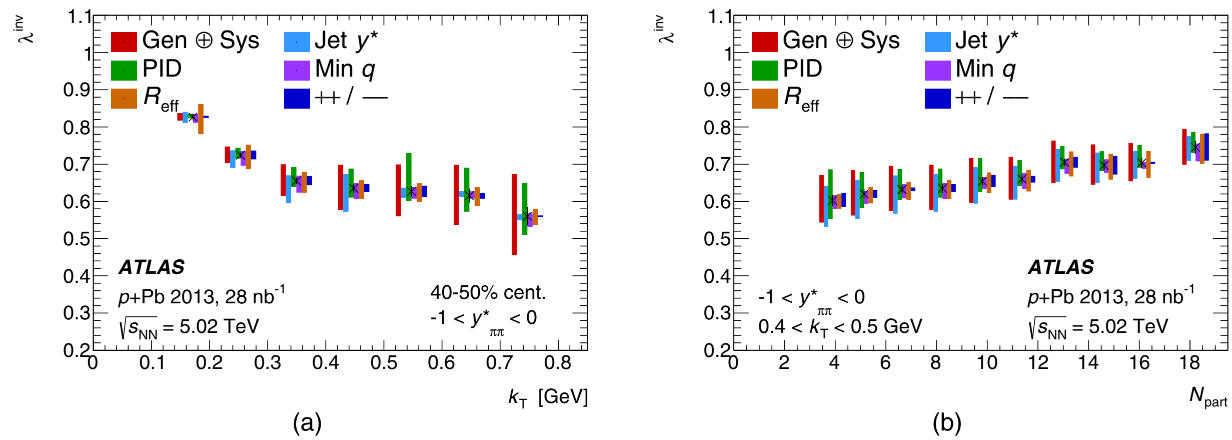

FIG. 9. The contributions of the various sources of systematic uncertainty to the invariant Bose-Einstein amplitude λ_{inv}. The typical trends with the pair's average transverse momentum k_T are shown in (a) and the trends with the number of nucleon participants N_{part} are shown in (b). The black crosses indicate the nominal results.

ratio of their means, and a flat Bayesian prior is assumed for both means. A corresponding χ^2 analog [72], the negative log-likelihood ratio $\mathcal{L}$ [73], is minimized using the MINUIT package [74]:

$$-2\ln\mathcal{L} = 2\sum_i \left\{ A_i \ln\left[\frac{(1+C_i)A_i}{C_i(A_i+B_i+2)}\right] + (B_i+2)\ln\left[\frac{(1+C_i)(B_i+2)}{A_i+B_i+2}\right]\right\}. \quad (18)$$

Here A and B are the signal and background relative momentum distributions in Eq. (2) when represented as histograms, such that A_i and B_i are the contents in bin i, C_i is shorthand for $C(q_i)$ where q_i is the bin center, and $C(q)$ is the fitting function describing the correlation. The multiplicative factor of -2 causes this statistic to approach χ^2 as the sample size increases. The 1σ statistical uncertainties in the fit parameters of $C(q)$ are evaluated using the MINOS routine, and are selected from the points in the parameter space where $-2\ln\mathcal{L} = \min(-2\ln\mathcal{L}) + 1$.

The full form of the invariant-correlation-function fit to like-charge track pair data including the hard-process background description is

$$C(q) = \mathcal{N}[1 - \lambda + \lambda K(q_{\mathrm{inv}})C_{\mathrm{BE}}(q)]\Omega(q), \quad (19)$$

where $C_{\mathrm{BE}}(q)$ is given by Eqs. (4) or (5), $K(q_{\mathrm{inv}})$ is given by Eq. (3), and $\Omega(q)$ is given by Eqs. (7) or (10).

As discussed in Sec. IV B, the opposite-charge correlation functions are fit in the regions where q_{inv} (or $|\mathbf{q}|$ in 3D) is greater than 100 MeV. The opposite-charge parameters are highly insensitive to the choice of cutoff, as the q distributions contribute more statistical weight at larger q. The same-charge correlation functions are fit in the regions $q_{\mathrm{inv}} > 30$ MeV for the invariant fits and $|\mathbf{q}| > 25$ MeV in three dimensions.

V. SYSTEMATIC UNCERTAINTIES

A. Sources of systematic uncertainty

The systematic uncertainties in the extracted parameter values have contributions from several sources: the jet

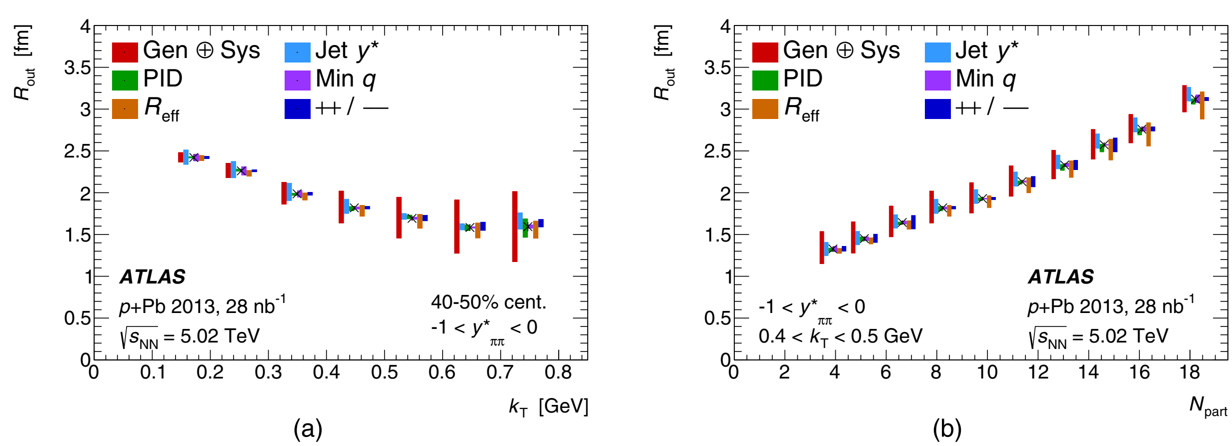

FIG. 10. The contributions of the various sources of systematic uncertainty to the three-dimensional radius R_{out}. The typical trends with the pair's average transverse momentum k_T are shown in (a) and the trends with the number of nucleon participants N_{part} are shown in (b). The black crosses indicate the nominal results.

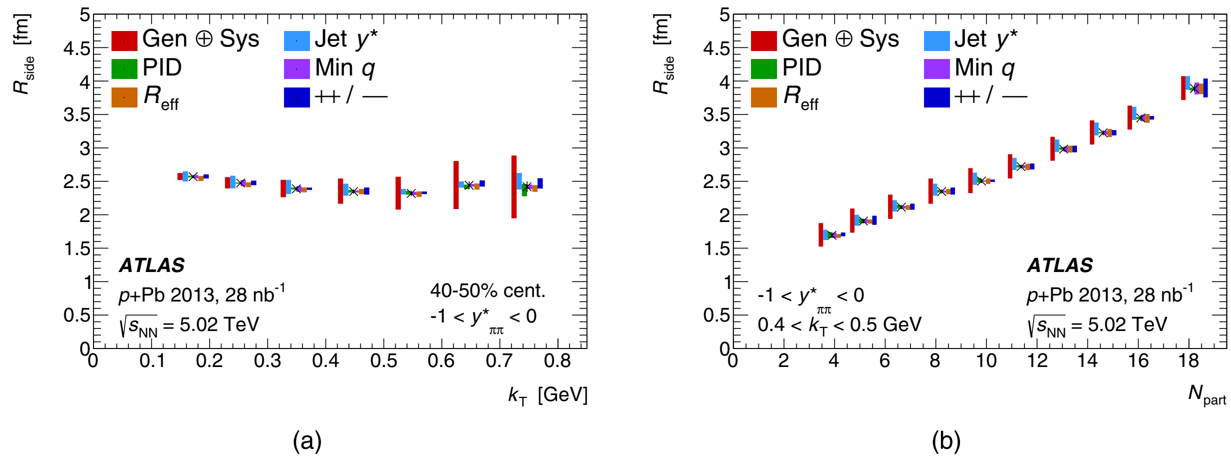

FIG. 11. The contributions of the various sources of systematic uncertainty to the three-dimensional radius R_{side}. The typical trends with the pair's average transverse momentum k_T are shown in (a) and the trends with the number of nucleon participants N_{part} are shown in (b). The black crosses indicate the nominal results.

fragmentation description, PID, the effective Coulomb-correction size R_{eff}, charge asymmetry, and particle reconstruction effects.

One of the largest sources of uncertainty originates from the description of the background correlations $\Omega(q)$ from jet fragmentation. For the uncertainty in the hard-process contribution, three effects are considered. First, the extrapolation from a pp to a p+Pb system is represented with an uncertainty in the background amplitude. Also, to investigate the uncertainty in the Monte Carlo description of jet fragmentation, the amplitude of $C^{+-}(q_{inv})/C^{\pm\pm}(q_{inv})$ is studied in both PYTHIA and Herwig. Herwig does not predict enough difference between $+-$ and $\pm\pm$ correlations to describe the data. Thus, instead of using the ratio of the predicted scalings of the two generators, the standard deviation of the ratio amplitude (across a selection of k_T and multiplicity intervals) is used as a variation reflecting this systematic uncertainty. The hard-process amplitude λ_{bkgd} is scaled up and down by 12.3%, the quadrature sum of the relative variation from the difference between the pp and p+Pb systems (4.1%) and from the generator difference (11.6%). The widths of the background description are highly correlated with the amplitude in the PYTHIA fit results, so varying the widths in addition to the amplitude would overstate the uncertainty. The choice of varying the amplitude instead of the width is found to provide a larger and more consistent variation in the radii, so only the amplitude of the background is varied. The variation from the combination of the generator and the collision system are indicated by a label of "Gen ⊕ Sys" in the figures of Sec. V B. Additionally, the procedure described in Sec. IV B to control the jet fragmentation correlations is repeated in both the central ($|y^\star_{\pi\pi}| < 1$) and forward ($-2 < y^\star_{\pi\pi} < -1$) rapidity intervals. While the relationship between the fragmentation widths (R^{inv}_{bkgd}, R^{sl}_{bkgd}, and R^{out}_{bkgd}) is fairly robust, the mappings of the amplitudes (λ^{inv}_{bkgd} and λ^{osl}_{bkgd}) from opposite- to same-charge correlations vary between the two rapidity intervals. This

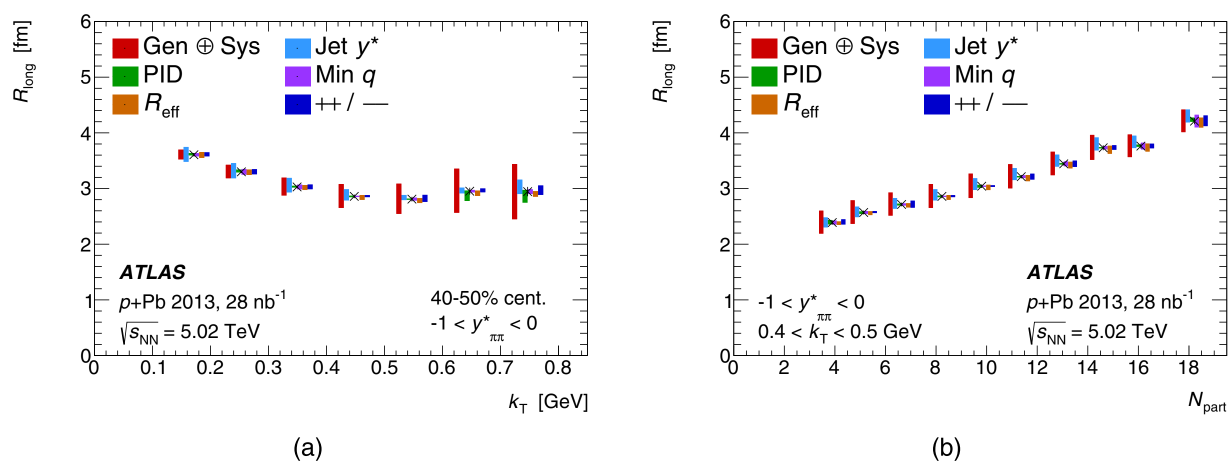

FIG. 12. The contributions of the various sources of systematic uncertainty to the three-dimensional radius R_{long}. The typical trends with the pair's average transverse momentum k_T are shown in (a) and the trends with the number of nucleon participants N_{part} are shown in (b). The black crosses indicate the nominal results.

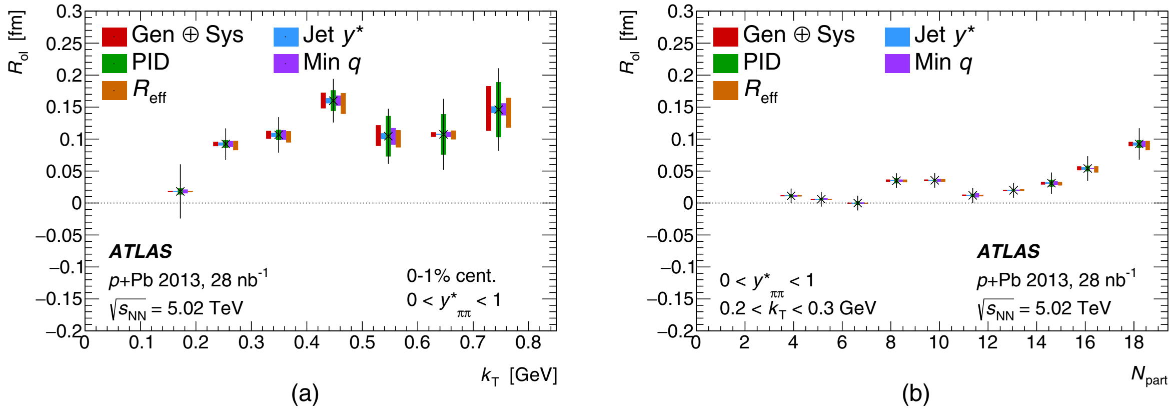

FIG. 13. The contributions of the various sources of systematic uncertainty to the three-dimensional radius R_{ol}. The typical trends with the pair's average transverse momentum k_T are shown in (a) and the trends with the number of nucleon participants N_{part} are shown in (b). The large uncertainties from PID at high k_T are mostly the result of statistical fluctuations, and including them in the reported uncertainty is a conservative choice. The uncertainties for Jet $y^\star$ and PID are explicitly symmetrized. The black crosses indicate the nominal results, and the dotted line at $R_{ol} = 0$ is drawn for visibility.

variation represents the breakdown of the assumptions used to describe the jet fragmentation. The mapping procedure is repeated with the results from each rapidity interval, and the variation is used as an additional systematic uncertainty in the amplitude. The HBT radii and amplitudes are both highly correlated with the amplitude of the jet background, so varying λ_{bkgd} is a robust method of evaluating the uncertainties from the background description procedure. This systematic variation is represented by the "Jet $y^\star_{\pi\pi}$" label in the figures of Sec. V B.

The analysis is repeated at both a looser and a tighter PID selection than the nominal definition, and the variations are included as a systematic uncertainty. The effect on the radii is at the 1–2% level for the lower k_T intervals, but becomes more significant at higher momentum, where there are relatively more kaons and protons and the dE/dx separation is not as large. In the highest k_T intervals studied, variations are typically in the range of 5–30%. The PID systematic variation is labeled by "PID" in the figures of Sec. V B.

The nonzero effective size of the Coulomb correction R_{eff} should only cause a bin-by-bin change of a few percent in the correlation function, even with a value up to several femtometers, since the Bohr radius of pion pairs is nearly 400 fm. However, since this parameter changes the width in q_{inv} over which the Coulomb correction is applied, varying this parameter can affect the source radii measurably. The effective size is assumed to scale with the size of the source itself, so a scaling constant ξ is chosen such that $R_{eff} = \xi R_{inv}$. The nominal value of ξ is taken to be equal to 1 and the associated systematic uncertainty is evaluated by varying this between 1/2 and 2. The Coulomb size systematic variation is indicated by a label of "R_{eff}" in the figures of Sec. V B.

A small difference between positive and negative charge pairs is observed, attributable to detector effects such as

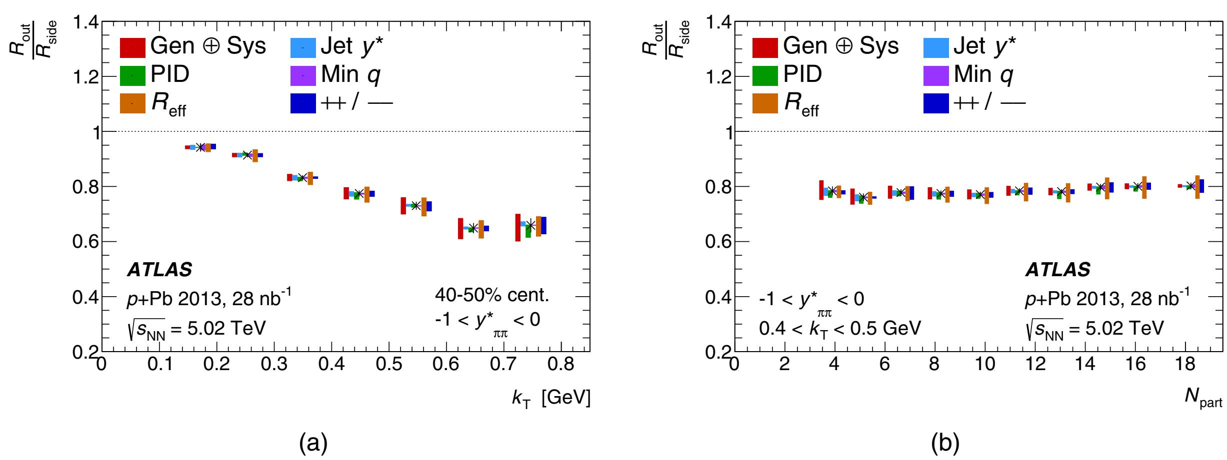

FIG. 14. The contributions of the various sources of systematic uncertainty to the ratio R_{out}/R_{side}. The typical trends with the pair's average transverse momentum k_T are shown in (a) and the trends with the number of nucleon participants N_{part} are shown in (b). The black crosses indicate the nominal results, and the dotted line at $R_{out}/R_{side} = 1$ is drawn for visibility.

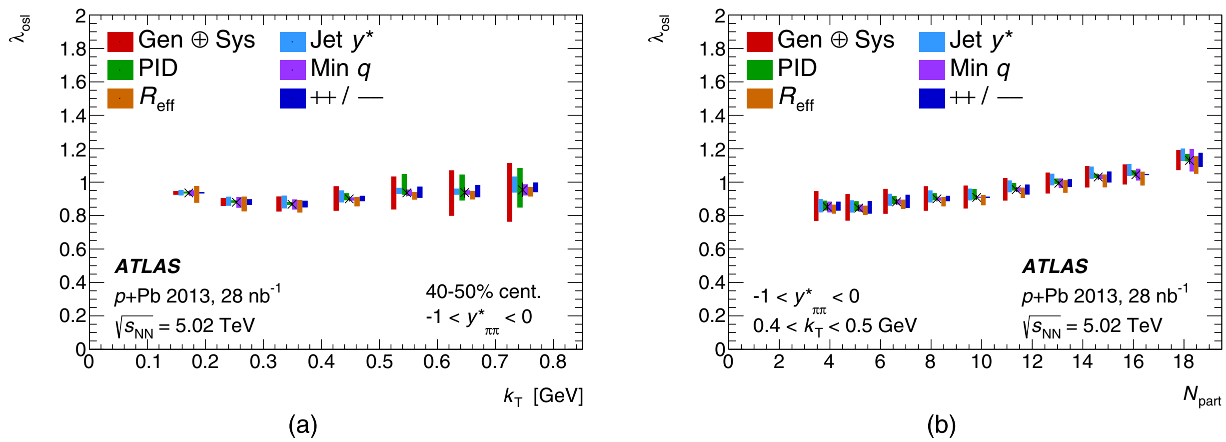

FIG. 15. The contributions of the various sources of systematic uncertainty to the three-dimensional Bose-Einstein amplitude λ_{osl}. The typical trends with the pair's average transverse momentum k_T are shown in (a) and the trends with the number of nucleon participants N_{part} are shown in (b). The black crosses indicate the nominal results.

the orientation of the azimuthal overlap of the inner detector's component staves. The nominal results use all of the same-charge pairs, and a systematic variation accounting for this charge asymmetry is assigned which covers the results for both of the separate charge states. The variation from this effect is labeled by "++/−−" in the figures of Sec. V B.

Single-particle correction factors for track reconstruction efficiency cancel in the ratio $A(q)/B(q)$. However, two-particle effects in the track reconstruction can affect the correlation function at small relative momentum. Single- and multitrack reconstruction effects are both studied with the fully simulated HIJING sample. The generator-level and reconstructed correlation functions are compared, and a deficit in the latter, due to the impact of the two-particle reconstruction efficiency, is observed at q_{inv} below approximately 50 MeV. At larger q_{inv} the two-particle reconstruction efficiency is found to not depend on q_{inv} within statistical uncertainties. A minimum q cutoff is applied in the fits to minimize the impact of these detector effects. The sensitivity of the results to this cutoff is checked by taking $q_{inv}^{min} = 30 \pm 10$ MeV in the one-dimensional fits, and symmetrizing the effect of the variation from $|\mathbf{q}|^{min} = 25$ to 50 MeV in the 3D fits. Because this variation has only a small effect on the radii, this procedure is taken to be sufficient to account for two-particle reconstruction effects. The effects of this variation have the label "Min q" in the figures of Sec. V B.

B. Magnitude of systematic effects

In this section the contributions of each source of systematic uncertainty are illustrated. Examples of the systematic uncertainties in the invariant parameters R_{inv} and λ_{inv} are shown as a function of k_T and centrality in Figs. 8 and 9.

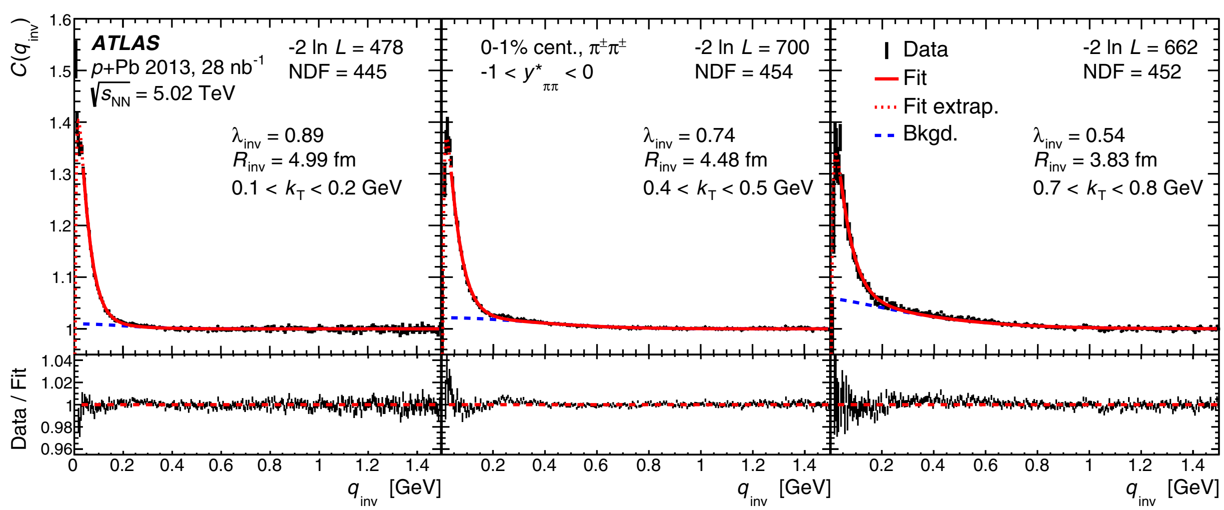

FIG. 16. Results of the fit to the one-dimensional correlation function in very central (0–1%) events in three k_T intervals. The dashed blue line indicates the description of the contribution from jet fragmentation and the red line shows the full correlation function fit. The dotted red line indicates the extrapolation of the fit function beyond the interval over which the fit is performed.

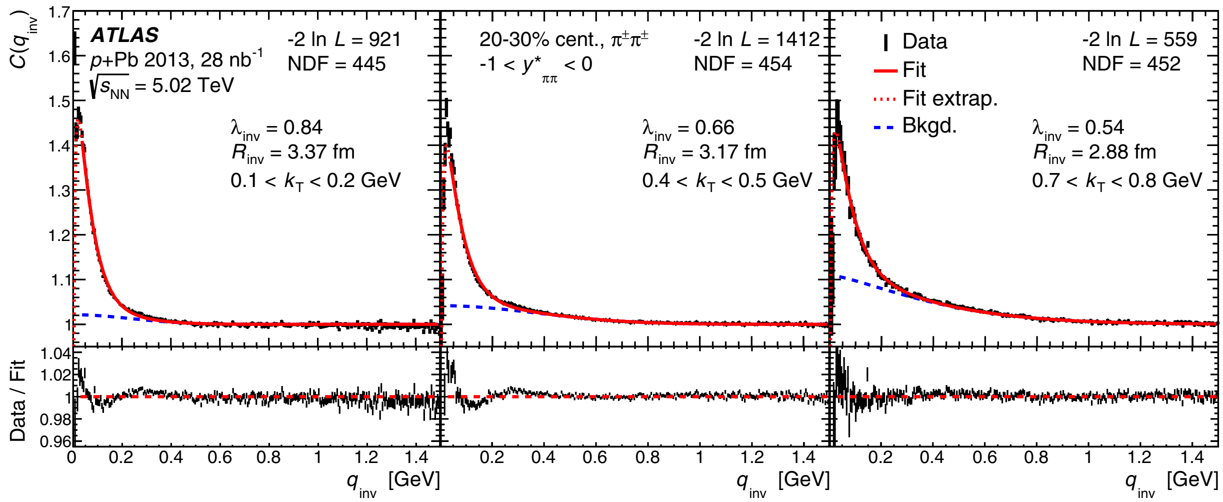

FIG. 17. Results of the fit to the one-dimensional correlation function in semicentral (20–30%) events in three k_T intervals. The dashed blue line indicates the description of the contribution from jet fragmentation and the red line shows the full correlation function fit. The dotted red line indicates the extrapolation of the fit function beyond the interval over which the fit is performed.

Systematic uncertainties are also shown for the 3D radii R_{out} (Fig. 10), R_{side} (Fig. 11), R_{long} (Fig. 12), and R_{ol} (Fig. 13), as well as the ratio $R_{\text{out}}/R_{\text{side}}$ (Fig. 14) and the amplitude (Fig. 15). These are all shown for typical choices of centrality, k_T, and $y^{\star}_{\pi\pi}$ so that they represent standard, rather than exceptional, values of the uncertainties.

The uncertainties in the HBT radii (Figs. 8, 10, 11, and 12) are dominated by the jet background description. At larger k_T the generator (PYTHIA vs Herwig) and system (pp vs p+Pb) contributions constitute the larger portion of this, and at lower k_T the variation of the mapping over $y^{\star}_{\pi\pi}$ is more significant.

The Bose-Einstein amplitudes λ_{inv} (Fig. 9) and λ_{osl} (Fig. 15) are also affected strongly by the jet fragmentation description, but at sufficiently large k_T ($\gtrsim$0.4 GeV) pion identification contributes a comparable systematic uncertainty. This is expected because other particles misidentified as pions do not exhibit Bose-Einstein interference with real pions, and the most significant effect of their inclusion in the correlation function is to decrease the amplitude of the Bose-Einstein enhancement.

The systematic uncertainties in the ratio $R_{\text{out}}/R_{\text{side}}$ (Fig. 14) are estimated by evaluating the ratio after each variation reflecting a systematic uncertainty and taking the difference from the nominal value. Thus, the uncertainties that are correlated between R_{out} and R_{side} cancel properly in the ratio. The uncertainties in the ratio are not universally dominated by any single effect. At sufficiently large k_T in central events, the effective Coulomb size becomes the largest contributor. This

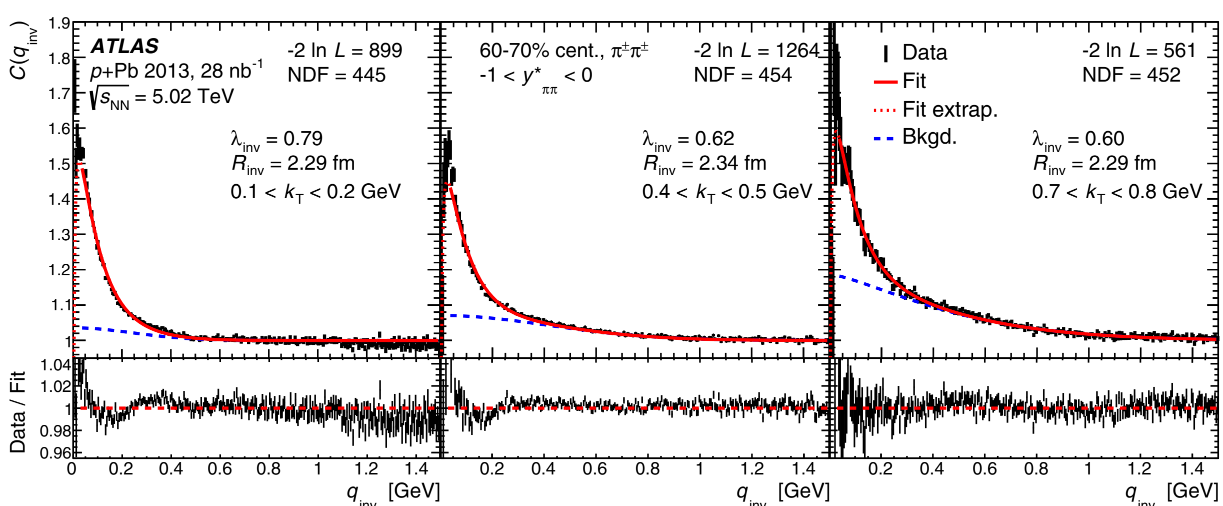

FIG. 18. Results of the fit to the one-dimensional correlation function in relatively peripheral (60–70%) events in three k_T intervals. The dashed blue line indicates the description of the contribution from jet fragmentation and the red line shows the full correlation function fit. The dotted red line indicates the extrapolation of the fit function beyond the interval over which the fit is performed.

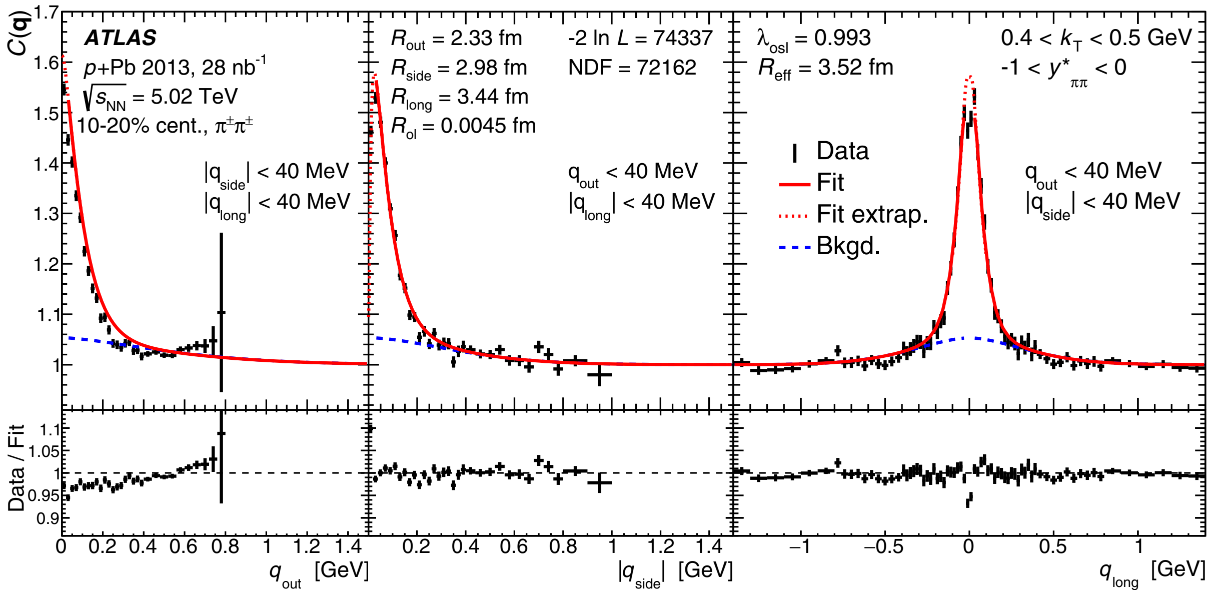

FIG. 19. Results of the 3D fit to the correlation function in the $0.4 < k_T < 0.5$ GeV, $-1 < y^{\star}_{\pi\pi} < 0$ kinematic intervals and for the 10–20% centrality interval. The left, middle, and right panels show the distributions versus q_{out}, q_{side}, and q_{long}, respectively, with limits on the other two components of $\mathbf{q}$ such that $|q_i| < 40$ MeV. The dashed blue line indicates the description of the contribution from hard processes and the red line shows the full correlation function fit. The dotted red line indicates the extrapolation of the fit function beyond the interval over which the fit is performed.

is understandable because the Coulomb correction is applied as a function of q_{inv}, and as a result it is applied over a wider range in q_{out} than in q_{side} at larger k_T.

Similarly, systematic effects in the cross term R_{ol} (Fig. 13) are not dominated by any one source, and in fact the uncertainties in this quantity are predominantly statistical. At large k_T the systematic uncertainties from PID appear large. However, these are mostly a result of statistical fluctuations that arise because the fit in the tight PID selection is performed on a sample even smaller than the nominal dataset. Therefore, the reported systematic uncertainties are overly conservative for this quantity. For a similar reason, the systematic uncertainty for charge-asymmetric detector effects is not included in the error bars for R_{ol}. No systematic dependence of R_{ol} is observed when measuring $++$ and $--$ correlations independently, so they are excluded from the total systematic uncertainties in order not to include additional statistical fluctuations as systematic effects.

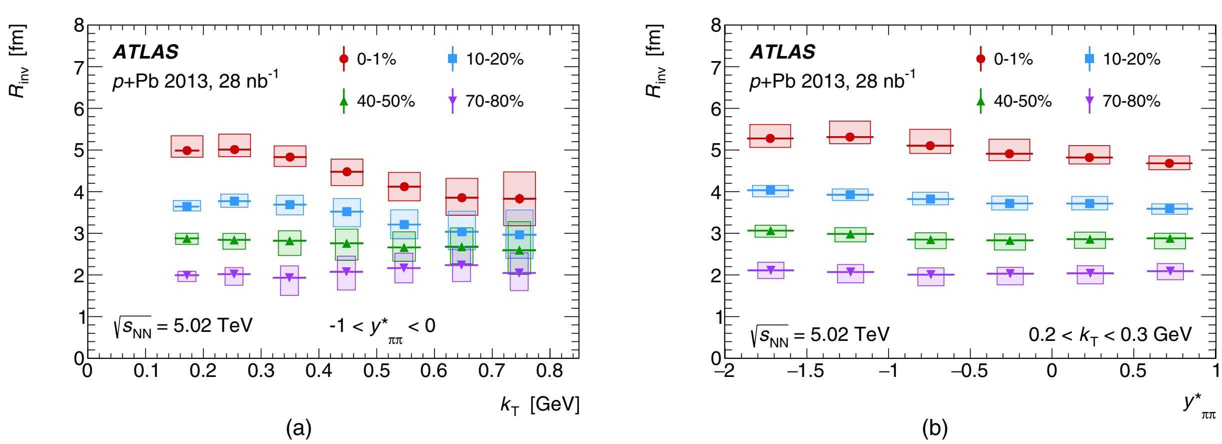

FIG. 20. The exponential invariant radii, R_{inv}, obtained from one-dimensional fits to the q_{inv} correlation functions shown as a function of pair transverse momentum k_T (a) and rapidity $y^{\star}_{\pi\pi}$ (b). Four nonadjacent centrality intervals are shown. The vertical size of each box represents the quadrature sum of the systematic uncertainties described in Sec. V, and statistical uncertainties are shown with vertical lines. The horizontal positions of the points are the average k_T or $y^{\star}_{\pi\pi}$ in each interval, and the horizontal lines indicate the standard deviation of k_T or $y^{\star}_{\pi\pi}$. The widths of the boxes differ among centrality intervals only for visual clarity.

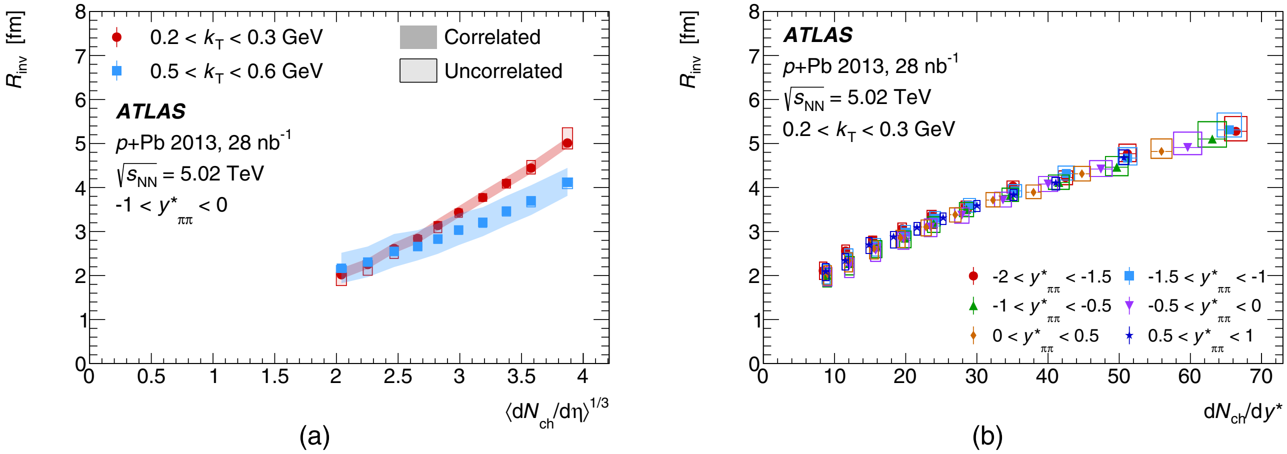

FIG. 21. Exponential fit results for R_{inv} as a function of the cube root of average charged-particle multiplicity $\langle dN_{\mathrm{ch}}/d\eta\rangle^{1/3}$ (a), where the average is taken over $|\eta| < 1.5$, and as a function of the local density, $dN_{\mathrm{ch}}/dy^{\star}$, over several centrality and rapidity intervals (b). In the left plot the systematic uncertainties from pion identification and from the generator and collision system components of the background amplitude are treated as correlated and shown as error bands, and the systematic uncertainties from charge asymmetry, R_{eff}, the rapidity variation of the jet fragmentation description, and two-particle reconstruction are treated as uncorrelated and indicated by the height of the boxes. The horizontal error bars indicate the systematic uncertainty from $\langle dN_{\mathrm{ch}}/d\eta\rangle$ or $dN_{\mathrm{ch}}/dy^{\star}$.

VI. RESULTS

This section shows examples of one- and three-dimensional fits to correlation functions, then presents results for extracted invariant and 3D source radii. The results are shown as a function of k_{T}, which can illustrate the time dependence of the source size. They are also shown as a function of $y^{\star}_{\pi\pi}$, showing any variations in source size along the collision axis, and against several quantities related to multiplicity and centrality. These results show the freeze-out density and the evolution of the source with the size of the initial geometry.

A. Performance of fit procedure

An example of a one-dimensional fit to $C(q_{\mathrm{inv}})$ using the functional form of Eq. (19) is included in Fig. 6. Additional examples of one-dimensional fits for different k_{T} intervals are shown in Figs. 16–18 for very central (0–1%), semicentral (20–30%), and peripheral (60–70%) centrality intervals, respectively. The test statistic $-2\ln\mathcal{L}$, defined in Eq. (18), is displayed on these figures. The values of this χ^2 analog indicate that the fits to the same-charge correlation functions generally describe the data well when compared to

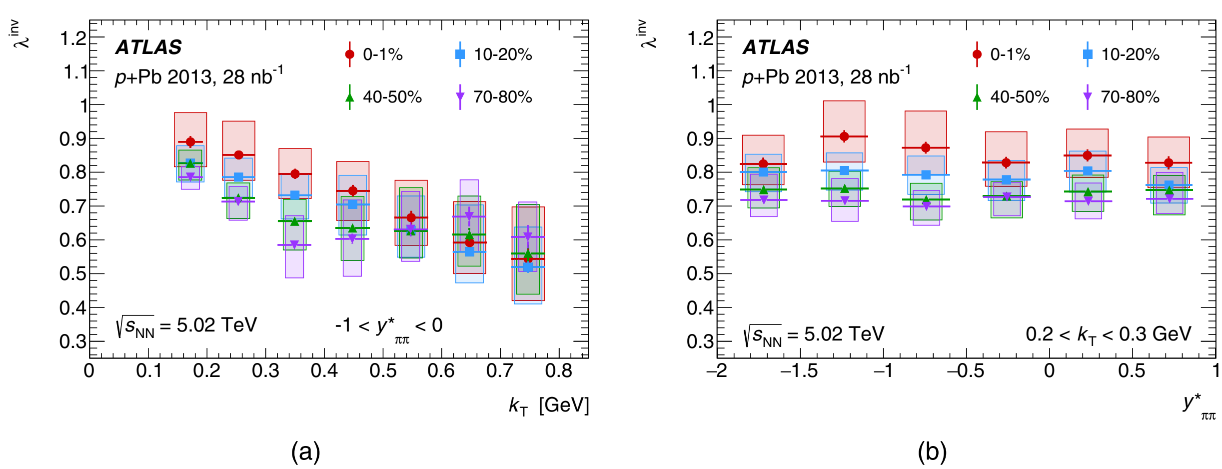

FIG. 22. The Bose-Einstein amplitude, λ_{inv}, obtained from one-dimensional fits to the q_{inv} correlation functions shown as a function of pair transverse momentum k_{T} (a) and rapidity $y^{\star}_{\pi\pi}$ (b). Four nonadjacent centrality intervals are shown. The vertical size of each box represents the quadrature sum of the systematic uncertainties described in Sec. V, and statistical uncertainties are shown with vertical lines. The horizontal positions of the points are the average k_{T} or $y^{\star}_{\pi\pi}$ in each interval, and the horizontal lines indicate the standard deviation of k_{T} or $y^{\star}_{\pi\pi}$. The widths of the boxes differ among centrality intervals only for visual clarity.

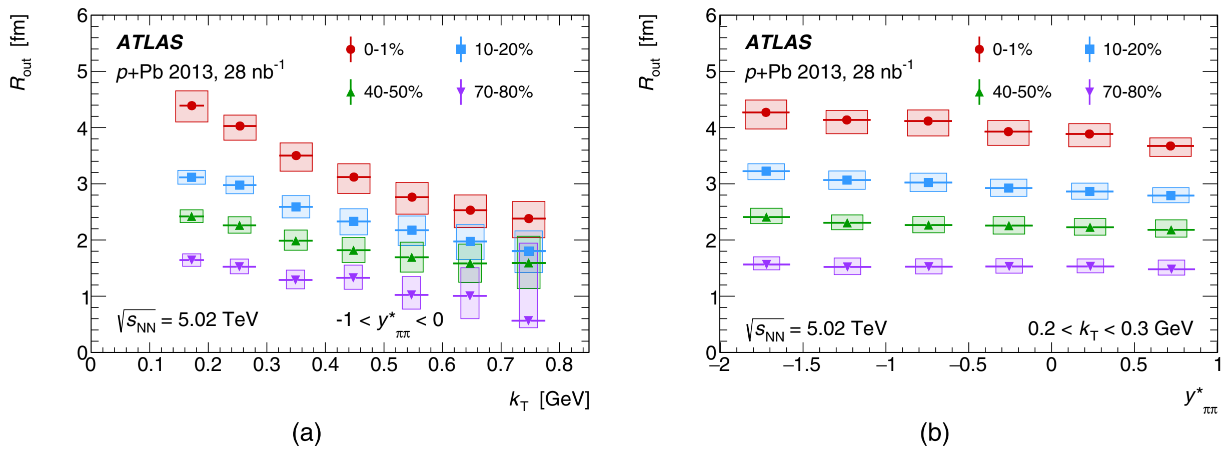

FIG. 23. Exponential fit results for the 3D source radius, $R_{\rm out}$, as a function of pair transverse momentum $k_{\rm T}$ (a) and rapidity $y^{\star}_{\pi\pi}$ (b). Four nonadjacent centrality intervals are shown. The vertical size of each box represents the quadrature sum of the systematic uncertainties described in Sec. V, and statistical uncertainties are shown with vertical lines. The horizontal positions of the points are the average $k_{\rm T}$ or $y^{\star}_{\pi\pi}$ in each interval, and the horizontal lines indicate the standard deviation of $k_{\rm T}$ or $y^{\star}_{\pi\pi}$. The widths of the boxes differ among centrality intervals only for visual clarity.

the number of degrees of freedom (NDF), with only small departures from an exponential description.

Slices of a three-dimensional fit of $C(\mathbf{q})$ to the three-dimensional variant of Eq. (19) are shown in Fig. 19. The apparently imperfect fit along the $q_{\rm out}$ axis is characteristic of $q_{\rm side} \approx q_{\rm long} \approx 0$, and away from this slice the fit agrees better with the data (the test statistic per degree of freedom is 1.03 for the fit shown).

B. One-dimensional results

The results from fits of $C(q_{\rm inv})$ to Eq. (19) for the invariant radius, $R_{\rm inv}$, are shown in Fig. 20 in four selected centrality intervals. Only an intermediate rapidity interval $-1 < y^{\star}_{\pi\pi} < 0$ is shown for these and similar results as a function of $k_{\rm T}$, as the qualitative behavior is consistent in forward and backward rapidities. The clear decrease in size with increasing $k_{\rm T}$ that is observed in central events is not observed in peripheral events. This is consistent with the interpretation that central events undergo transverse expansion, since in hydrodynamic models higher-$p_{\rm T}$ particles are more likely to freeze out earlier in the event. Another way of understanding this trend as evidence for transverse expansion is that there is a smaller homogeneity region for particles with higher $p_{\rm T}$ [39]. At low $k_{\rm T}$, ultracentral (0–1%) events have an invariant radius significantly greater than peripheral (70–80%) events by a factor of about 2.6. This difference becomes less prominent at high $k_{\rm T}$. In central events $R_{\rm inv}$ is larger on the lead-going side than on the proton-going

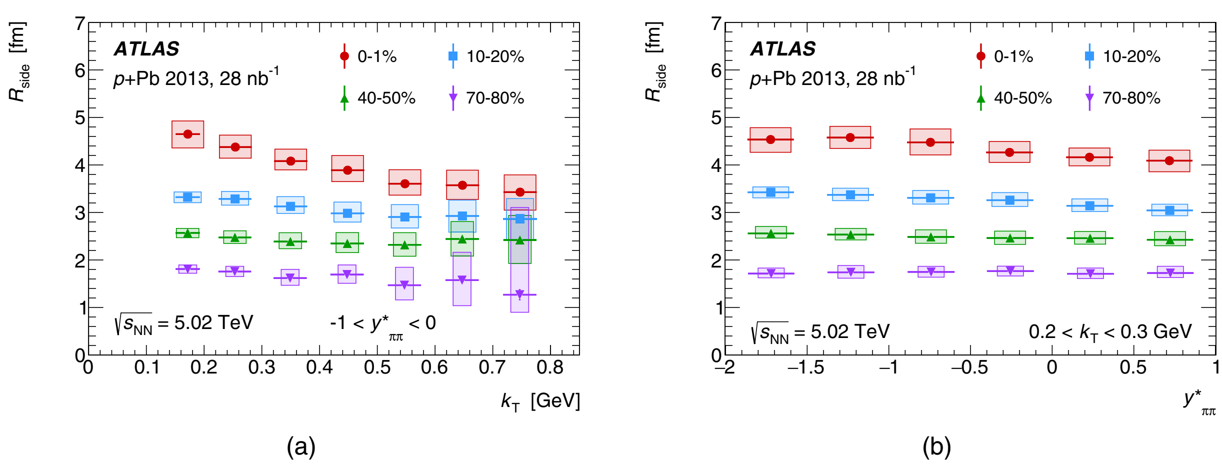

FIG. 24. Exponential fit results for the 3D source radius, $R_{\rm side}$, as a function of pair transverse momentum $k_{\rm T}$ (a) and rapidity $y^{\star}_{\pi\pi}$ (b). Four nonadjacent centrality intervals are shown. The vertical size of each box represents the quadrature sum of the systematic uncertainties described in Sec. V, and statistical uncertainties are shown with vertical lines. The horizontal positions of the points are the average $k_{\rm T}$ or $y^{\star}_{\pi\pi}$ in each interval, and the horizontal lines indicate the standard deviation of $k_{\rm T}$ or $y^{\star}_{\pi\pi}$. The widths of the boxes differ among centrality intervals only for visual clarity.

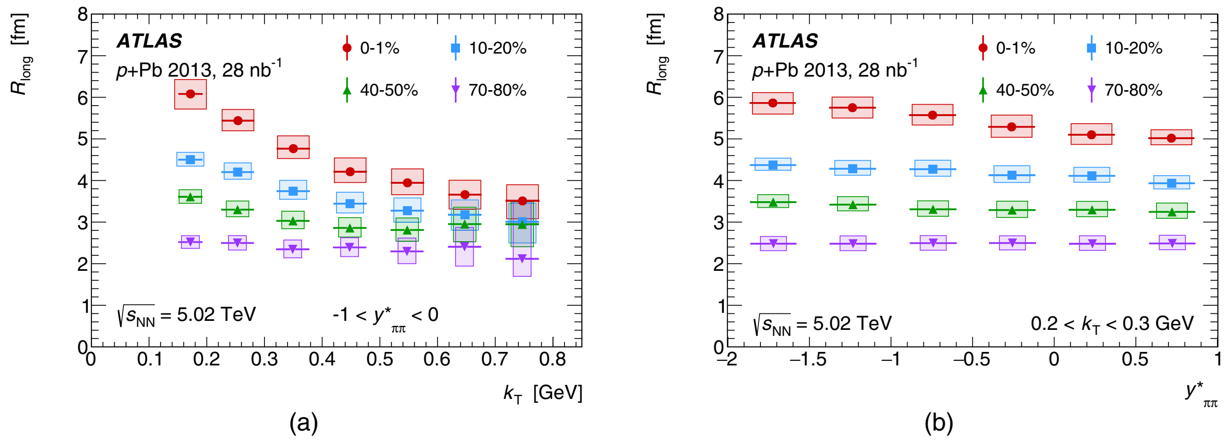

FIG. 25. Exponential fit results for 3D source radius, R_{long}, as a function of pair transverse momentum k_{T} (a) and rapidity $y^{\star}_{\pi\pi}$ (b). Four nonadjacent centrality intervals are shown. The vertical size of each box represents the quadrature sum of the systematic uncertainties described in Sec. V, and statistical uncertainties are shown with vertical lines. The horizontal positions of the points are the average k_{T} or $y^{\star}_{\pi\pi}$ in each interval, and the horizontal lines indicate the standard deviation of k_{T} or $y^{\star}_{\pi\pi}$. The widths of the boxes differ among centrality intervals only for visual clarity.

side, while in peripheral events the rapidity dependence of the radius becomes constant.

Invariant radii are shown for several centralities in Fig. 21 (left) as a function of the cube root of average $dN_{\mathrm{ch}}/d\eta$. For both k_{T} intervals shown, the scaling of R_{inv} with $\langle dN_{\mathrm{ch}}/d\eta\rangle^{1/3}$ is close to linear but with a slightly increasing slope at higher multiplicities. The invariant radius, R_{inv}, has a steeper trend versus multiplicity at lower k_{T}. Figure 21 (right) shows R_{inv} in several centrality and rapidity intervals as a function of the local particle density, $dN_{\mathrm{ch}}/dy^{\star}$, which is evaluated by taking the average over the same interval used for the pair's rapidity. The extracted radius and the local particle density are seen to be tightly correlated, such that the radius can be predicted, within uncertainties, by the local density alone.

The Bose-Einstein amplitude of the invariant fits, λ_{inv}, is shown in Fig. 22 as a function of k_{T} and $y^{\star}_{\pi\pi}$. At low k_{T}, λ_{inv} has values near unity, and it decreases with rising k_{T}. In the lower k_{T} intervals a systematic difference is observed between centrality intervals, with λ_{inv} having larger values in central events. In contrast, at larger k_{T} the amplitudes are indistinguishable between different centralities. The amplitude exhibits no significant variation over rapidity.

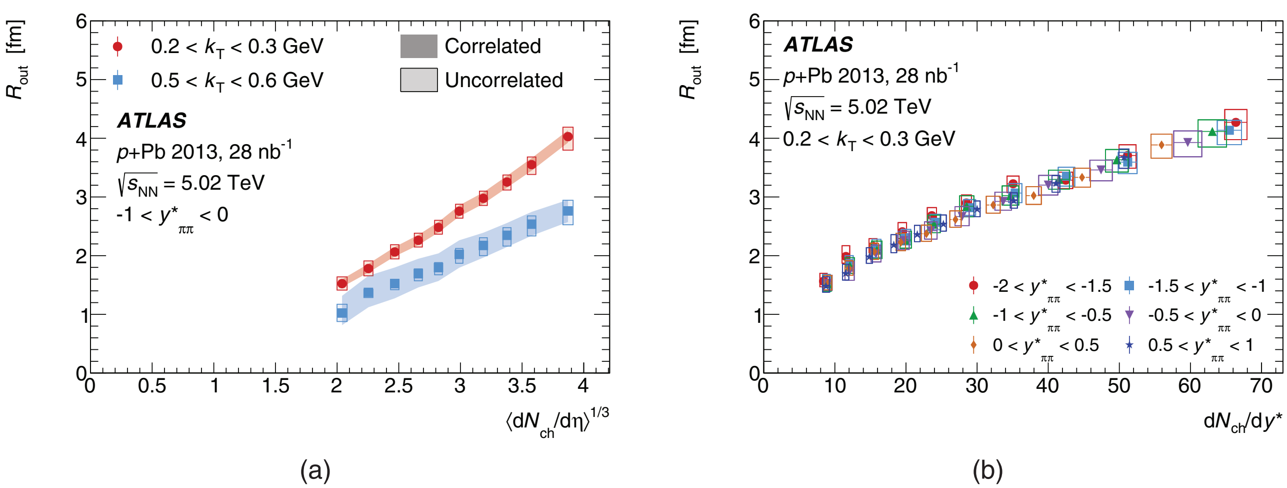

FIG. 26. Exponential fit results for R_{out} as a function of (a) the cube root of average charged-particle multiplicity, $\langle dN_{\mathrm{ch}}/d\eta\rangle^{1/3}$, where the average is taken over $|\eta| < 1.5$, and (b) the local density, $dN_{\mathrm{ch}}/dy^{\star}$, in intervals of $y^{\star}_{\pi\pi}$. In the left plot the systematic uncertainties from pion identification and from the generator and collision system components of the background amplitude are treated as correlated and shown as error bands, while the systematic uncertainties from charge asymmetry, R_{eff}, the rapidity variation of the jet fragmentation description, and two-particle reconstruction are treated as uncorrelated and indicated by the height of the boxes. The horizontal error bars indicate the systematic uncertainty from $\langle dN_{\mathrm{ch}}/d\eta\rangle$ or $dN_{\mathrm{ch}}/dy^{\star}$.

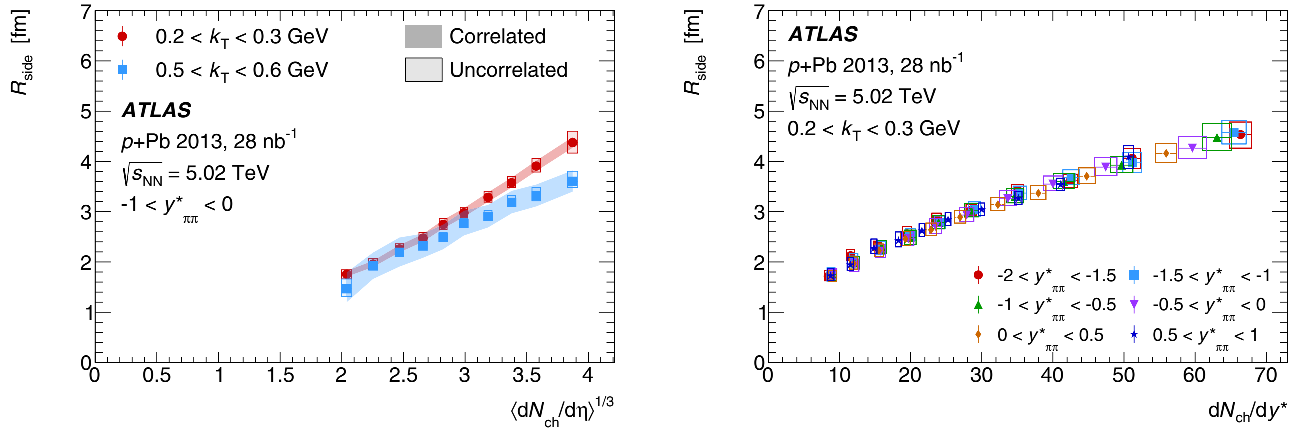

(a) (b)

FIG. 27. Exponential fit results for R_{side} as a function of (a) the cube root of average charged-particle multiplicity, $\langle dN_{\mathrm{ch}}/d\eta\rangle^{1/3}$, where the average is taken over $|\eta| < 1.5$, and (b) the local density, $dN_{\mathrm{ch}}/dy^{\star}$, in intervals of $y^{\star}_{\pi\pi}$. In the left plot the systematic uncertainties from pion identification and from the generator and collision system components of the background amplitude are treated as correlated and shown as error bands, while the systematic uncertainties from charge asymmetry, R_{eff}, the rapidity variation of the jet fragmentation description, and two-particle reconstruction are treated as uncorrelated and indicated by the height of the boxes. The horizontal error bars indicate the systematic uncertainty from $\langle dN_{\mathrm{ch}}/d\eta\rangle$ or $dN_{\mathrm{ch}}/dy^{\star}$.

C. Three-dimensional results

The three-dimensional radii R_{out}, R_{side}, and R_{long} are shown as a function of k_{T} and $y^{\star}_{\pi\pi}$ in four selected centrality intervals in Figs. 23–25. In central collisions, the 3D radii exhibit an even steeper decrease with increasing k_{T} relative to that observed for the invariant radii in Fig. 20. A similar, but weaker trend is present in peripheral events. Central collisions exhibit larger radii on the backward (Pb-going) side of the event, while peripheral events show no distinguishable variation of the radii with rapidity.

The 3D radii are also shown as a function of the cube root of both average event multiplicity and local density in Figs. 26–28. These plots demonstrate the relationship between the size and the density of the source at freeze-out. All of the radii are seen to be very strongly correlated with the local density. The scaling of the radii is not far from being linear with the cube root of multiplicity. This behavior is qualitatively similar to the scaling of R_{inv} with $\langle dN_{\mathrm{ch}}/d\eta\rangle$ in Fig. 21.

The Bose-Einstein amplitude in the 3D fits, λ_{osl}, is shown in Fig. 29 as a function of k_{T} and $y^{\star}_{\pi\pi}$. Like the invariant

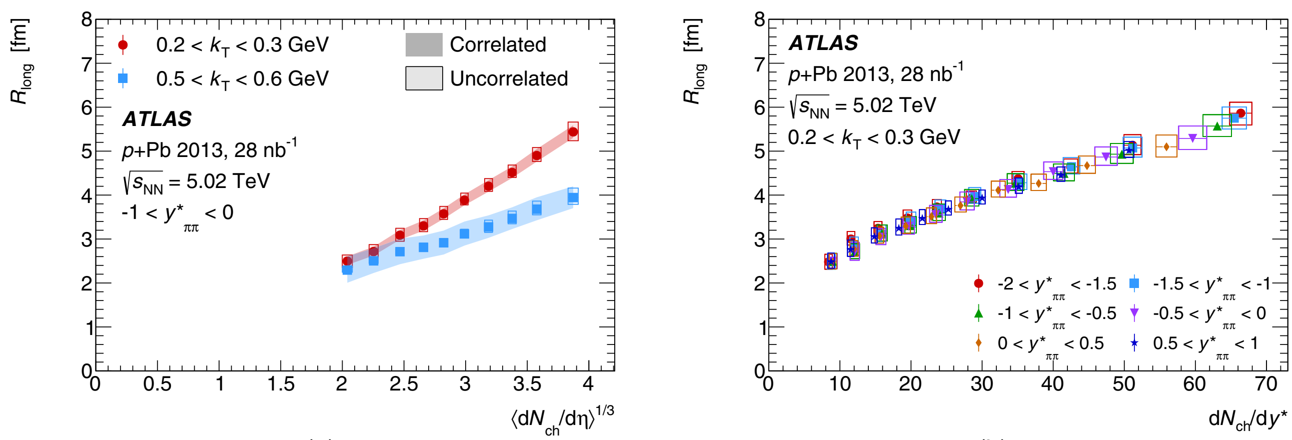

(a) (b)

FIG. 28. Exponential fit results for R_{long} as a function of (a) the cube root of average charged-particle multiplicity, $\langle dN_{\mathrm{ch}}/d\eta\rangle^{1/3}$, where the average is taken over $|\eta| < 1.5$, and (b) the local density, $dN_{\mathrm{ch}}/dy^{\star}$, in intervals of $y^{\star}_{\pi\pi}$. In the left plot the systematic uncertainties from pion identification and from the generator and collision system components of the background amplitude are treated as correlated and shown as error bands, while the systematic uncertainties from charge asymmetry, R_{eff}, the rapidity variation of the jet fragmentation description, and two-particle reconstruction are treated as uncorrelated and indicated by the height of the boxes. The horizontal error bars indicate the systematic uncertainty from $\langle dN_{\mathrm{ch}}/d\eta\rangle$ or $dN_{\mathrm{ch}}/dy^{\star}$.

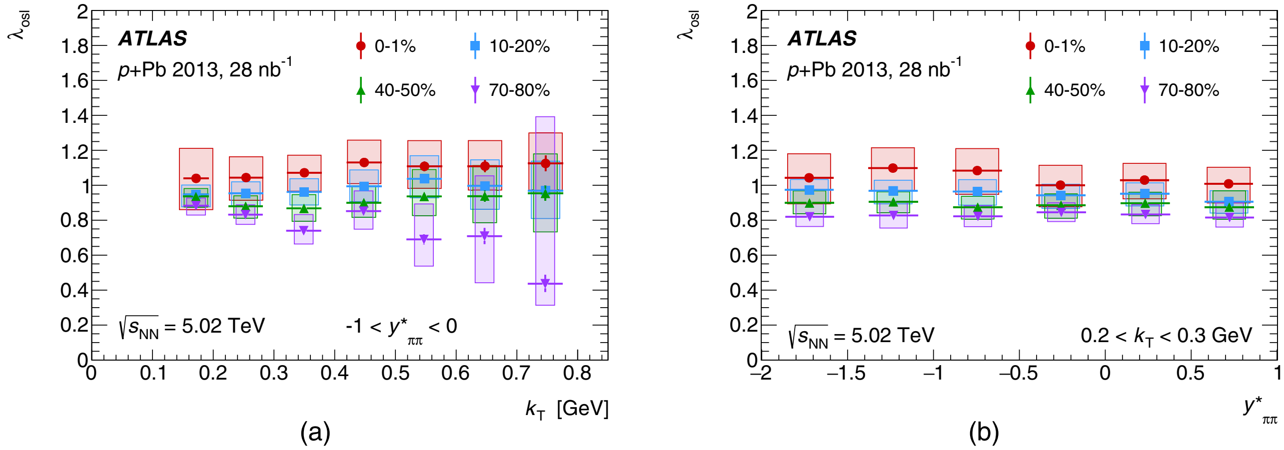

FIG. 29. The Bose-Einstein amplitude, λ_{osl}, as a function of pair transverse momentum k_{T} (a) and rapidity $y^{\star}_{\pi\pi}$ (b). Four nonadjacent centrality intervals are shown. The vertical size of each box represents the quadrature sum of the systematic uncertainties described in Sec. V, and statistical uncertainties are shown with vertical lines. The horizontal positions of the points are the average k_{T} or $y^{\star}_{\pi\pi}$ in each interval, and the horizontal lines indicate the standard deviation of k_{T} or $y^{\star}_{\pi\pi}$. The widths of the boxes differ among centrality intervals only for visual clarity.

amplitude, at low k_{T} it is larger for central events than for peripheral ones. The three-dimensional amplitude does not decrease significantly with rising k_{T} as the invariant amplitude does, except in the most peripheral events. The 3D amplitude also exhibits no significant variation over rapidity.

The ratio $R_{\mathrm{out}}/R_{\mathrm{side}}$ (Fig. 30) is often studied because in models with radial flow, R_{out} includes components of the source's lifetime but R_{side} does not (see, for instance, the discussion in Ref. [31]). A value of $R_{\mathrm{out}}/R_{\mathrm{side}}$ less than one is observed and it decreases with increasing k_{T}. The ratio is observed to be the same in different centrality intervals within uncertainties. As explained in Ref. [75], several improvements to naive hydrodynamic models—primarily prethermal acceleration, a stiffer equation of state, and shear viscosity—all result in more sudden emission. This implies that a value of $R_{\mathrm{out}}/R_{\mathrm{side}} \lesssim 1$ does not necessarily rule out collective behavior.

The transverse area scale $R_{\mathrm{out}}R_{\mathrm{side}}$ is shown in Fig. 31 as a function of both event and local density. At lower k_{T}, the transverse area scales linearly with multiplicity over all centralities and rapidities. This result is consistent with a picture in which the longitudinal dynamics can be separated from the transverse particle production, and low-k_{T} particles freeze out at a constant transverse area density.

The determinant of the 3D radius matrix, $\det(R)$ [Eq. (6)], is shown in Fig. 32 as a function of both the average and local density. While the transverse area scales linearly with multiplicity at low k_{T}, the volume scale grows linearly at

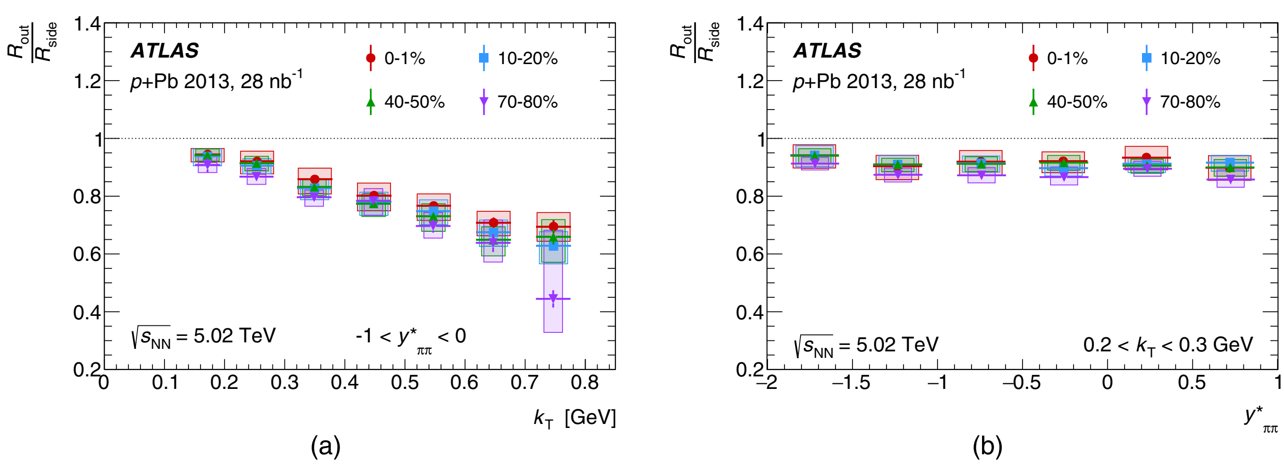

FIG. 30. The ratio of exponential radii $R_{\mathrm{out}}/R_{\mathrm{side}}$ as a function of pair transverse momentum k_{T} (a) and rapidity $y^{\star}_{\pi\pi}$ (b). Four nonadjacent centrality intervals are shown. The vertical size of each box represents the quadrature sum of the systematic uncertainties described in Sec. V, and statistical uncertainties are shown with vertical lines. The horizontal positions of the points are the average k_{T} or $y^{\star}_{\pi\pi}$ in each interval, and the horizontal lines indicate the standard deviation of k_{T} or $y^{\star}_{\pi\pi}$. The widths of the boxes differ among centrality intervals only for visual clarity.

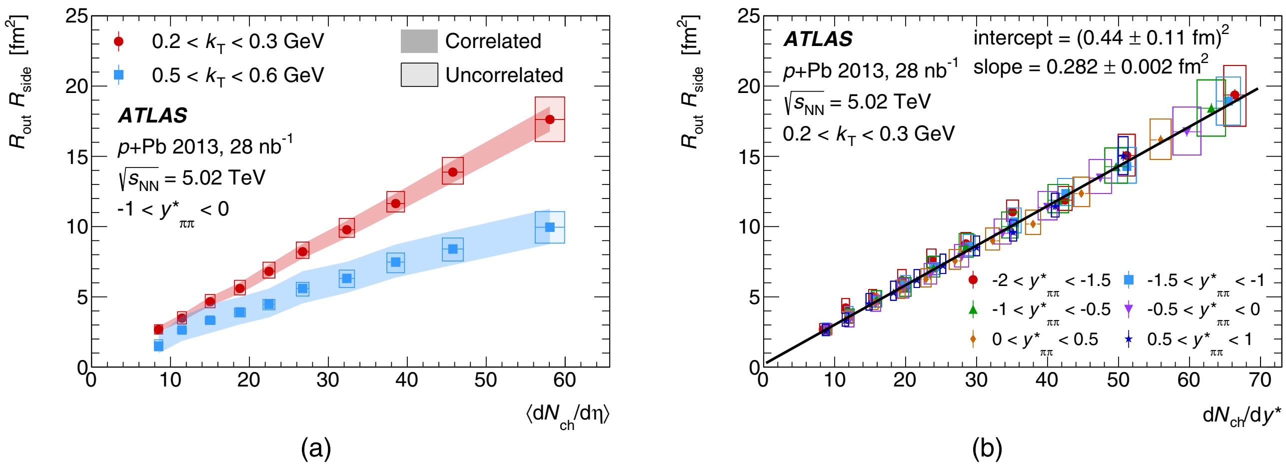

FIG. 31. The transverse area scale, $R_{\mathrm{out}}R_{\mathrm{side}}$, plotted against the average multiplicity $\langle dN_{\mathrm{ch}}/d\eta\rangle$ (a) and the local density $dN_{\mathrm{ch}}/dy^{\star}$ as a function of rapidity (b). The systematic uncertainties from pion identification and the generator and collision system components of the jet background description are treated as correlated and shown as error bands. The systematic uncertainties from charge asymmetry, R_{eff}, rapidity variation of the jet fragmentation, and two-particle track reconstruction effects are treated as uncorrelated and indicated by the height of the boxes. The horizontal error bars indicate the systematic uncertainty from $\langle dN_{\mathrm{ch}}/d\eta\rangle$ or $dN_{\mathrm{ch}}/dy^{\star}$. The slope and intercept of the best fit to the right-hand plot are shown with combined statistical and systematic uncertainties.

higher k_{T}, implying a constant freeze-out volume density for particles with higher momentum. Figure 33 compares the volume scaling with $\langle N_{\mathrm{part}}\rangle$ for the standard Glauber model as well as for two choices of the Glauber-Gribov color fluctuation (GGCF) model [61]. The parameter ω_{σ} controls the size of the fluctuations in the nucleon-nucleon cross section within the Glauber-Gribov model. With the Glauber model, the scaling of the volume element with $\langle N_{\mathrm{part}}\rangle$ has a significant upwards curvature. Including Glauber-Gribov fluctuations in the $\langle N_{\mathrm{part}}\rangle$ calculation results in a more modest curvature in the scaling of $\det(R)$. This result suggests that the fluctuations in the nucleon-nucleon cross section are a crucial component of the initial geometry description in p+Pb systems. The values and systematic uncertainties of $\langle N_{\mathrm{part}}\rangle$ in each model are listed in Table I.

The cross term, R_{ol} [Eq. (6)], which couples to the lifetime of the source [70], is shown in Figs. 34 and 35. A significant departure from zero is observed in this parameter in central events, but only for rapidities $y^{\star}_{\pi\pi} \gtrsim -1$. For the 0–1% centrality interval, in $0.2 < k_{\mathrm{T}} < 0.4$ and $-1 < y^{\star}_{\pi\pi} < 1$, R_{ol} is measured to be nonzero with a significance of 7.1/7.3/5.1 σ (statistical/systematic/combined). The next most central interval, 1–5%, has a nonzero R_{ol} with a significance of 5.2/5.8/3.9 σ (statistical/systematic/combined). This suggests that the particle production at middle and forward rapidities is sensitive to the local z asymmetry of the system.

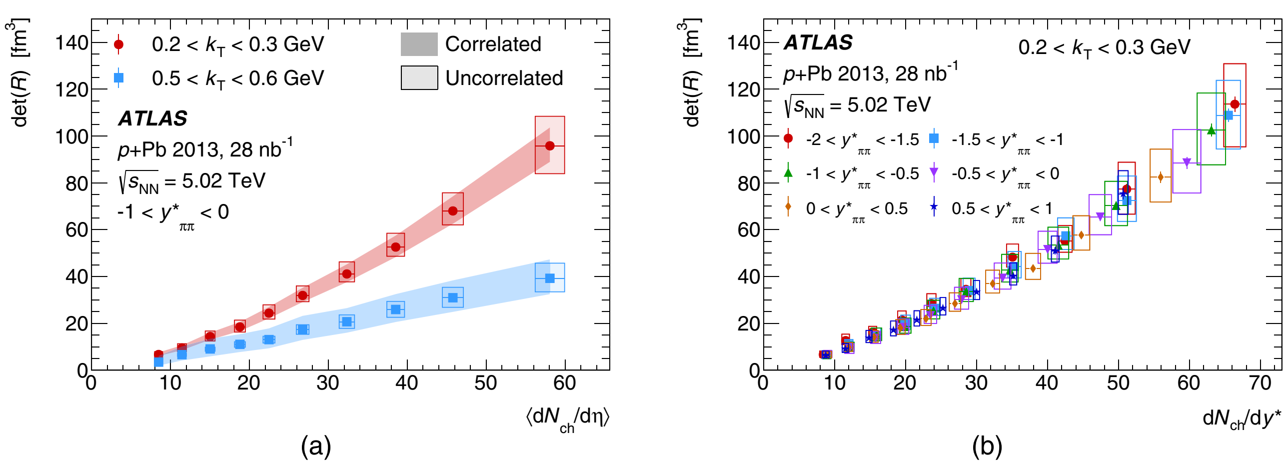

FIG. 32. The volume scale, $\det(R)$, plotted against the average multiplicity $\langle dN_{\mathrm{ch}}/d\eta\rangle$ (a) and the local density, $dN_{\mathrm{ch}}/dy^{\star}$, as a function of rapidity (b). In the left plot, the systematic uncertainties from pion identification and the generator and collision system components of the jet background description are treated as correlated and shown as error bands, while those from charge asymmetry, R_{eff}, rapidity variation of the jet fragmentation, and two-particle track reconstruction effects are treated as uncorrelated and indicated by the height of the boxes. The widths of the boxes indicate the systematic uncertainty in $\langle dN_{\mathrm{ch}}/d\eta\rangle$ or $dN_{\mathrm{ch}}/dy^{\star}$.

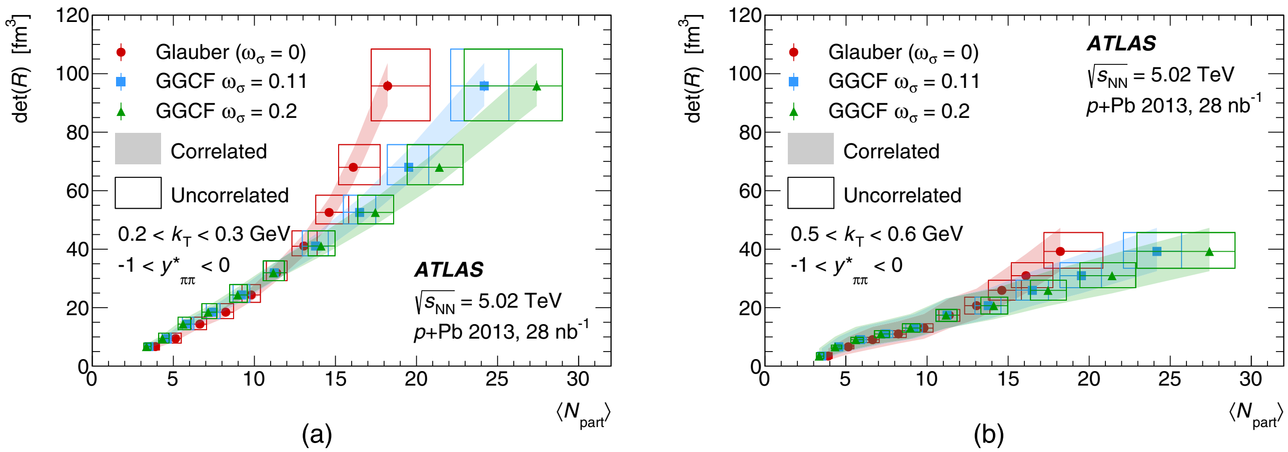

FIG. 33. The scaling of the volume element, det(R), with $\langle N_{\text{part}}\rangle$ calculated with three initial geometry models: standard Glauber as well as Glauber-Gribov (GGCF) for two choices of the color fluctuation parameter, ω_σ. Each of the panels shows a different k_T interval. The systematic uncertainties from the pion identification and the generator and collision system components of the background description are treated as correlated and shown as error bands. The systematic uncertainties from charge asymmetry, R_{eff}, rapidity variation of the jet background, and two-particle reconstruction are treated as uncorrelated and indicated by the height of the boxes. The horizontal error bars indicate the systematic uncertainties in $\langle N_{\text{part}}\rangle$.

The argument from Sec. IV A for why the order of the particles in a pair can be chosen so that q_{out} is greater than zero relies on the assumption that both particles in the pair are the same species, or at least that they are characterised by the same momentum distributions. In principle, final-state interactions between different particle species could break this symmetry of the correlation function and lead to a nonzero R_{ol} term. However, the systematic uncertainties shown in Fig. 13 demonstrate that R_{ol} is not sensitive to particle identification, particularly at low k_T. At larger k_T the systematic effect from PID looks larger, but the variations are likely driven by statistical fluctuations.

VII. SUMMARY AND CONCLUSIONS

This paper presents ATLAS measurements of two-identified-pion HBT correlations in p+Pb collisions at the LHC at $\sqrt{s_{NN}} = 5.02$ TeV using a total integrated luminosity of 28 nb^{-1}. Two-particle correlation functions were measured in one dimension as a function of q_{inv} and in three dimensions using the out-side-long decomposition as a function of the pair's average transverse momentum and the pair's rapidity. The measurements were performed for several intervals of p+Pb centrality characterized by ΣE_T^{Pb}, the total transverse energy measured in the Pb-going forward calorimeter. A

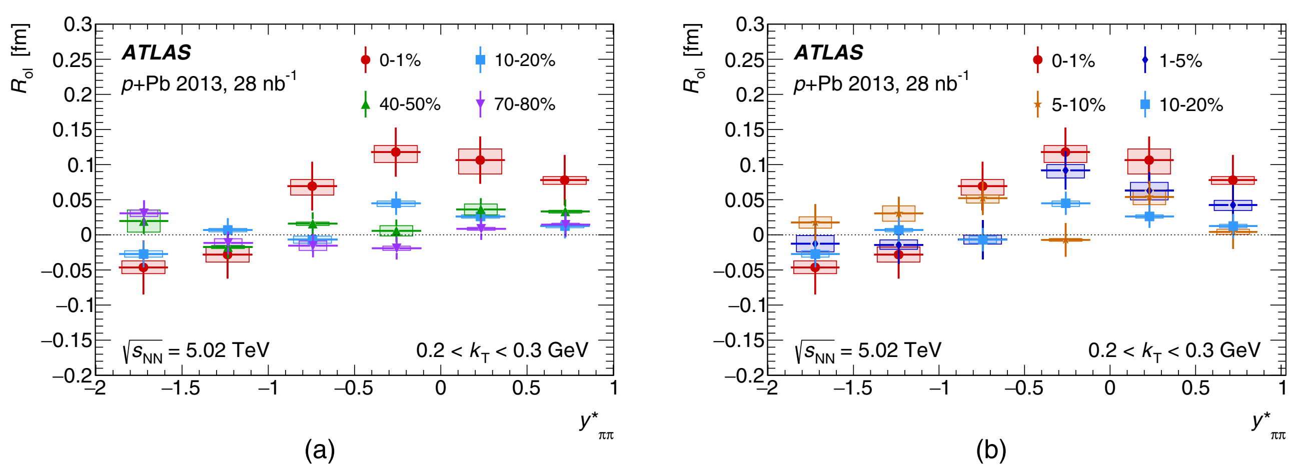

FIG. 34. The cross term, R_{ol}, as a function of the pair's rapidity, $y^\star_{\pi\pi}$, in a wide range of centrality intervals (a) and in the four most central event classes (b). The vertical size of each box represents the quadrature sum of the systematic uncertainties described in Sec. V, and statistical uncertainties are shown with vertical lines. The horizontal positions of the points are the average $y^\star_{\pi\pi}$ in each interval, and the horizontal lines indicate the standard deviation of $y^\star_{\pi\pi}$ in the corresponding interval. The widths of the boxes differ only for visual clarity.

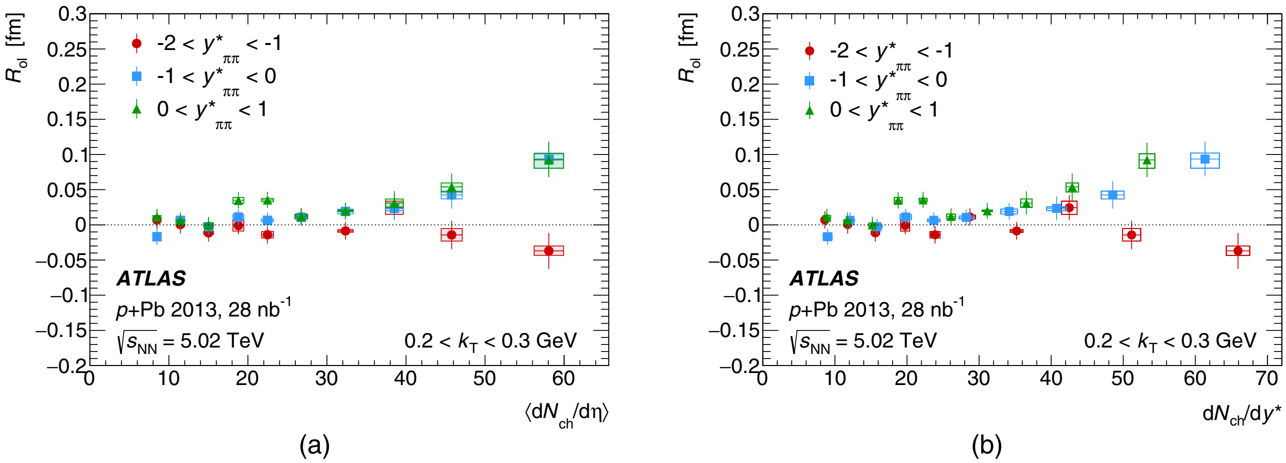

FIG. 35. The cross term, R_{ol}, as a function of average event multiplicity $\langle dN_{ch}/d\eta \rangle$ (a) and the local density $dN_{ch}/dy^{\star}$ (b). The vertical size of each box represents the quadrature sum of the systematic uncertainties described in Sec. V, and statistical uncertainties are shown with vertical lines. The widths of the boxes indicate the systematic uncertainties in the corresponding quantities.

data-driven technique was developed for constraining the contribution of jet fragmentation to the correlation function. The correlation functions were fit to a Bowler-Sinyukov parametrization of the Bose-Einstein and Coulomb form with a contribution that describes the jet background. The HBT correlation is described by an exponential form that provides a good description of the data. For the out-side-long fits, the parametrization includes a non-diagonal coupling between q_{out} and q_{long} in the correlation function.

The radii extracted from the one-dimensional and three-dimensional fits show a significant variation with transverse momentum k_T that is strongest for the most central events and weakest or not present in the most peripheral centrality interval. For the three-dimensional fits, the k_T dependence is found to be the largest for the out and long directions. A small but significant dependence of the three-dimensional source radii on the pair's rapidity is observed in the more central collisions while in the most peripheral collisions the radii do not depend on rapidity.

The one-dimensional and three-dimensional source radii increase monotonically between peripheral and central collisions with a slope that decreases with rising k_T. The dependence of the radii on centrality was studied as a function of both the cube root of the rapidity-averaged charged-particle multiplicity, $\langle dN_{ch}/d\eta \rangle^{1/3}$, and the local charged-particle density, $dN_{ch}/dy^{\star}$. When evaluated in intervals of both centrality and rapidity, the radii as a function of $dN_{ch}/dy^{\star}$ fall on a single curve. At low k_T the rapidity-averaged radii are observed to increase approximately linearly with $\langle dN_{ch}/d\eta \rangle^{1/3}$. A nonzero out-long cross term R_{ol} is observed in central (0–5%) collisions for rapidities greater than -1, with a combined significance of 5.1σ in the most central (0–1%) events.

The transverse area, $R_{side}\,R_{long}$, is observed to vary linearly with $dN_{ch}/dy^{\star}$ at low k_T. The volume scale represented by $\det(R)$ increases faster than linearly with $\langle dN_{ch}/d\eta \rangle^{1/3}$ or $dN_{ch}/dy^{\star}$ at low k_T, but increases approximately linearly with $\langle dN_{ch}/d\eta \rangle^{1/3}$ at higher momentum ($k_T > 0.5$ GeV). When plotted versus the mean number of nucleon participants N_{part} obtained from three different geometric models, the volume shows a steady increase with $\langle N_{part} \rangle$ for the GGCF-derived $\langle N_{part} \rangle$ values, but a sudden increase with $\langle N_{part} \rangle$ for $\langle N_{part} \rangle \gtrsim 12$ when $\langle N_{part} \rangle$ is obtained from the Glauber model. While the freeze-out volume scale $\det(R)$ should only be strictly linear with the initial size, represented by N_{part}, if the expansion is independent of centrality, an extreme deviation from a naive linear scaling is not expected. This observation supports the conclusion drawn from previous studies that the Glauber-Gribov color fluctuation model provides a better description of p+Pb collision geometry.

The R_{out} to R_{side} ratio is found to be less than unity for all centrality and kinematic selections studied in this analysis, and it is observed to decrease approximately linearly with increasing k_T. This result, combined with the k_T dependence of the radii, suggests a collective, explosive expansion of the source. The nonzero out-long cross term indicates that the freeze-out behavior of the source is sensitive to the local z asymmetry of the particle production away from the Pb-going region.

The results presented in this paper provide detailed measurements of the space-time extent of the particle source in p+Pb systems. In particular, the rapidity sensitivity of the results demonstrate the asymmetry of the p+Pb system and show that k_T and local charged-particle density are sufficient to predict the radii. These conclusions present a significant opportunity for theoretical models.

ACKNOWLEDGMENTS

We thank CERN for the very successful operation of the LHC, as well as the support staff from our institutions without whom ATLAS could not be operated efficiently. We acknowledge the support of ANPCyT, Argentina; YerPhI, Armenia; ARC, Australia; BMWFW and FWF, Austria; ANAS, Azerbaijan; SSTC, Belarus; CNPq and FAPESP, Brazil; NSERC, NRC and CFI, Canada; CERN; CONICYT, Chile; CAS, MOST, and NSFC, China; COLCIENCIAS, Colombia; MSMT CR, MPO CR, and VSC CR, Czech Republic; DNRF and DNSRC, Denmark; IN2P3-CNRS, CEA-DSM/IRFU, France; SRNSF, Georgia; BMBF, HGF, and MPG, Germany; GSRT, Greece; RGC, Hong Kong SAR, China; ISF, I-CORE, and Benoziyo Center, Israel; INFN, Italy; MEXT and JSPS, Japan; CNRST, Morocco; NWO, Netherlands; RCN, Norway; MNiSW and NCN, Poland; FCT, Portugal; MNE/IFA, Romania; MES of Russia and NRC KI, Russian Federation; JINR; MESTD, Serbia; MSSR, Slovakia; ARRS and MIZŠ, Slovenia; DST/NRF, South Africa; MINECO, Spain; SRC and Wallenberg Foundation, Sweden; SERI, SNSF, and Cantons of Bern and Geneva, Switzerland; MOST, Taiwan; TAEK, Turkey; STFC, United Kingdom; DOE and NSF, United States of America. In addition, individual groups and members have received support from BCKDF, the Canada Council, CANARIE, CRC, Compute Canada, FQRNT, and the Ontario Innovation Trust, Canada; EPLANET, ERC, ERDF, FP7, Horizon 2020, and Marie Skłodowska-Curie Actions, European Union; Investissements d'Avenir Labex and Idex, ANR, Région Auvergne, and Fondation Partager le Savoir, France; DFG and AvH Foundation, Germany; Herakleitos, Thales, and Aristeia programs cofinanced by EU-ESF and the Greek NSRF; BSF, GIF, and Minerva, Israel; BRF, Norway; CERCA Programme Generalitat de Catalunya, Generalitat Valenciana, Spain; the Royal Society and Leverhulme Trust, United Kingdom. The crucial computing support from all WLCG partners is acknowledged gratefully, in particular from CERN, the ATLAS Tier-1 facilities at TRIUMF (Canada), NDGF (Denmark, Norway, Sweden), CC-IN2P3 (France), KIT/GridKA (Germany), INFN-CNAF (Italy), NL-T1 (Netherlands), PIC (Spain), ASGC (Taiwan), RAL (UK), and BNL (USA), the Tier-2 facilities worldwide, and large non-WLCG resource providers. Major contributors of computing resources are listed in Ref. [76].

[1] B. Abelev *et al.* (ALICE Collaboration), Long-range angular correlations on the near and away side in *p*-Pb collisions at $\sqrt{s_{NN}} = 5.02$ TeV, Phys. Lett. B **719**, 29 (2013).

[2] G. Aad *et al.* (ATLAS Collaboration), Observation of Associated Near-Side and Away-Side Long-Range Correlations in $\sqrt{s_{NN}} = 5.02$ TeV Proton-Lead Collisions with the ATLAS Detector, Phys. Rev. Lett. **110**, 182302 (2013).

[3] CMS Collaboration, Multiplicity and transverse momentum dependence of two- and four-particle correlations in pPb and PbPb collisions, Phys. Lett. B **724**, 213 (2013).

[4] G. Aad *et al.* (ATLAS Collaboration), Measurement of long-range pseudorapidity correlations and azimuthal harmonics in $\sqrt{s_{NN}} = 5.02$ TeV proton-lead collisions with the ATLAS detector, Phys. Rev. C **90**, 044906 (2014).

[5] V. Khachatryan *et al.* (CMS Collaboration), Evidence for Collective Multiparticle Correlations in *p*-Pb Collisions, Phys. Rev. Lett. **115**, 012301 (2015).

[6] G. Aad *et al.* (ATLAS Collaboration), Observation of Long-Range Elliptic Azimuthal Anisotropies in $\sqrt{s} = 13$ and 2.76 TeV *pp* Collisions with the ATLAS Detector, Phys. Rev. Lett. **116**, 172301 (2016).

[7] A. Adare *et al.* (PHENIX Collaboration), Quadrupole Anisotropy in Dihadron Azimuthal Correlations in Central d+Au Collisions at $\sqrt{s_{NN}} = 200$ GeV, Phys. Rev. Lett. **111**, 212301 (2013).

[8] A. Adare *et al.* (PHENIX Collaboration), Measurement of Long-Range Angular Correlation and Quadrupole Anisotropy of Pions and (Anti)Protons in Central d+Au Collisions at $\sqrt{s_{NN}} = 200$ GeV, Phys. Rev. Lett. **114**, 192301 (2015).

[9] L. Adamczyk *et al.* (STAR Collaboration), Long-range pseudorapidity dihadron correlations in d+Au collisions at $\sqrt{s_{NN}} = 200$ GeV, Phys. Lett. B **747**, 265 (2015).

[10] A. Adare *et al.* (PHENIX Collaboration), Measurements of Elliptic and Triangular Flow in High-Multiplicity ^{3}He + Au Collisions at $\sqrt{s_{NN}} = 200$ GeV, Phys. Rev. Lett. **115**, 142301 (2015).

[11] K. H. Ackermann *et al.* (STAR Collaboration), Elliptic Flow in Au+Au Collisions at $\sqrt{s_{NN}} = 130$ GeV, Phys. Rev. Lett. **86**, 402 (2001).

[12] A. Adare *et al.* (PHENIX Collaboration), Dihadron azimuthal correlations in Au+Au collisions at $\sqrt{s_{NN}} = 200$ GeV, Phys. Rev. C **78**, 014901 (2008).

[13] B. Alver *et al.* (PHOBOS Collaboration), High Transverse Momentum Triggered Correlations Over a Large Pseudorapidity Acceptance in Au+Au Collisions at $\sqrt{s_{NN}} = 200$ GeV, Phys. Rev. Lett. **104**, 062301 (2010).

[14] K. Aamodt *et al.* (ALICE Collaboration), Higher Harmonic Anisotropic Flow Measurements of Charged Particles in Pb-Pb Collisions at $\sqrt{s_{NN}} = 2.76$ TeV, Phys. Rev. Lett. **107**, 032301 (2011).

[15] CMS Collaboration, Long-range and short-range dihadron angular correlations in central PbPb collisions at $\sqrt{s_{NN}} = 2.76$ TeV, J. High Energy Phys. 07 (2011) 076.

[16] G. Aad *et al.* (ATLAS Collaboration), Measurement of the azimuthal anisotropy for charged particle production in $\sqrt{s_{NN}} = 2.76$ TeV lead-lead collisions with the ATLAS detector, Phys. Rev. C **86**, 014907 (2012).

[17] CMS Collaboration, Observation of long-range near-side angular correlations in p+Pb collisions at the LHC, Phys. Lett. B **718**, 795 (2013).

[18] CMS Collaboration, Observation of long-range near-side angular correlations in proton-proton collisions at the LHC, J. High Energy Phys. 09 (2010) 091.

[19] P. Huovinen, P. F. Kolb, Ulrich W. Heinz, P. V. Ruuskanen, and S. A. Voloshin, Radial and elliptic flow at RHIC: Further predictions, Phys. Lett. B **503**, 58 (2001).

[20] P. Romatschke and M. Strickland, Collective modes of an anisotropic quark gluon plasma, Phys. Rev. D **68**, 036004 (2003).

[21] U. Heinz and R. Snellings, Collective flow and viscosity in relativistic heavy-ion collisions, Annu. Rev. Nucl. Part. Sci. **63**, 123 (2013).

[22] P. Bożek, Collective flow in *p*-Pb and *d*-Pb collisions at TeV energies, Phys. Rev. C **85**, 014911 (2012).

[23] E. Shuryak and I. Zahed, High-multiplicity *pp* and *pA* collisions: Hydrodynamics at its edge, Phys. Rev. C **88**, 044915 (2013).

[24] P. Bożek and W. Broniowski, Collective dynamics in high-energy proton-nucleus collisions, Phys. Rev. C **88**, 014903 (2013).

[25] G.-Y. Qin and B. Müller, Elliptic and triangular flow anisotropy in deuteron-gold collisions at $\sqrt{s_{NN}} = 200$ GeV at RHIC and in proton-lead collisions at $\sqrt{s_{NN}} = 5.02$ TeV at the LHC, Phys. Rev. C **89**, 044902 (2014).

[26] K. Dusling and R. Venugopalan, Evidence for BFKL and saturation dynamics from dihadron spectra at the LHC, Phys. Rev. D **87**, 051502 (2013).

[27] K. Dusling and R. Venugopalan, Explanation of systematics of CMS p+Pb high multiplicity dihadron data at $\sqrt{s_{NN}} = 5.02$ TeV, Phys. Rev. D **87**, 054014 (2013).

[28] Y. V. Kovchegov and D. E. Wertepny, Long-range rapidity correlations in heavy-light ion collisions, Int. J. Mod. Phys.: Conf. Ser. **25**, 1460023 (2014).

[29] L. McLerran, M. Praszalowicz, and B. Schenke, Transverse momentum of protons, pions and kaons in high multiplicity pp and pA collisions: Evidence for the color glass condensate? Nucl. Phys. A **916**, 210 (2013).

[30] K. Dusling and R. Venugopalan, Comparison of the color glass condensate to dihadron correlations in proton-proton and proton-nucleus collisions, Phys. Rev. D **87**, 094034 (2013).

[31] M. A. Lisa, S. Pratt, R. Soltz, and U. Wiedemann, Femtoscopy in relativistic heavy ion collisions: Two decades of progress, Annu. Rev. Nucl. Part. Sci. **55**, 357 (2005).

[32] R. H. Brown and R. Q. Twiss, A test of a new type of stellar interferometer on Sirius, Nature (London) **178**, 1046 (1956).

[33] R. H. Brown and R. Q. Twiss, LXXIV. A new type of interferometer for use in radio astronomy, Philos. Mag. **45**, 663 (1954).

[34] G. Goldhaber, S. Goldhaber, W. Lee, and A. Pais, Influence of Bose-Einstein Statistics on the Antiproton-Proton Annihilation Process, Phys. Rev. **120**, 300 (1960).

[35] G. Aad *et al.* (ATLAS Collaboration), Two-particle Bose-Einstein correlations in pp collisions at $\sqrt{s} = 0.9$ and 7 TeV measured with the ATLAS detector, Eur. Phys. J. C **75**, 466 (2015).

[36] CMS Collaboration, Measurement of Bose-Einstein correlations in pp collisions at $\sqrt{s} = 0.9$ and 7 TeV, J. High Energy Phys. 05 (2011) 029.

[37] K. Aamodt *et al.* (ALICE Collaboration), Femtoscopy of pp collisions at $\sqrt{s} = 0.9$ and 7 TeV at the LHC with two-pion Bose-Einstein correlations, Phys. Rev. D **84**, 112004 (2011).

[38] R. Lednicky, Progress in correlation femtoscopy, in *Multi-particle Dynamics*, Proceedings of the XXXII International Symposium, Alushta, Crimea, Ukraine, September 2002 (World Scientific, Singapore, 2003), p. 21.

[39] P. F. Kolb and U. W. Heinz, Hydrodynamic description of ultrarelativistic heavy ion collisions, *Quark Gluon Plasma 3*, edited by R. C. Hwa and X.-N. Wang (World Scientific, Singapore), pp. 634–714, arXiv:nucl-th/0305084.

[40] S. Pratt, Pion interferometry of quark-gluon plasma, Phys. Rev. D **33**, 1314 (1986).

[41] G. Bertsch, M. Gong, and M. Tohyama, Pion interferometry in ultrarelativistic heavy-ion collisions, Phys. Rev. C **37**, 1896 (1988).

[42] G. F. Bertsch, Pion interferometry as a probe of the plasma, Nucl. Phys. A **498**, 173 (1989).

[43] T. Csörgo, J. Zimanyi, J. Bondorf, H. Heiselberg, and S. Pratt, Two-pion correlations from spacer, Phys. Lett. B **241**, 301 (1990).

[44] J. Adam *et al.* (ALICE Collaboration), Centrality dependence of particle production in p-Pb collisions at $\sqrt{s_{NN}} = 5.02$ TeV, Phys. Rev. C **91**, 064905 (2015).

[45] G. Aad *et al.* (ATLAS Collaboration), Measurement of the centrality dependence of the charged-particle pseudorapidity distribution in proton-lead collisions at $\sqrt{s_{NN}} = 5.02$ TeV with the ATLAS detector, Eur. Phys. J. C **76**, 199 (2016).

[46] J. Adam *et al.* (ALICE Collaboration), Two-pion femtoscopy in p-Pb collisions at $\sqrt{s_{NN}} = 5.02$ TeV, Phys. Rev. C **91**, 034906 (2015).

[47] B. Abelev *et al.* (ALICE Collaboration), Freeze-out radii extracted from three-pion cumulants in pp, p-Pb and Pb-Pb collisions at the LHC, Phys. Lett. B **739**, 139 (2014).

[48] M. L. Miller, K. Reygers, S. J. Sanders, and P. Steinberg, Glauber modeling in high energy nuclear collisions, Annu. Rev. Nucl. Part. Sci. **57**, 205 (2007).

[49] ATLAS Collaboration, The ATLAS Experiment at the CERN Large Hadron Collider, J. Instrum. **3**, S08003 (2008).

[50] G. Aad *et al.* (ATLAS Collaboration), The ATLAS Inner Detector commissioning and calibration, Eur. Phys. J. C **70**, 787 (2010).

[51] M. Gyulassy and X.-N. Wang, HIJING1.0: A Monte Carlo program for parton and particle production in high-energy hadronic and nuclear collisions, Comput. Phys. Commun. **83**, 307 (1994).

[52] S. Agostinelli *et al.*, GEANT4: A simulation toolkit, Nucl. Instrum. Methods A **506**, 250 (2003).

[53] G. Aad *et al.* (ATLAS Collaboration), The ATLAS simulation infrastructure, Eur. Phys. J. C **70**, 823 (2010).

[54] T. Sjöstrand, S. Mrenna, and P. Z. Skands, A brief introduction to PYTHIA 8.1, Comput. Phys. Commun. **178**, 852 (2008).

[55] ATLAS Collaboration, Summary of ATLAS PYTHIA 8 tunes, 2012, https://cds.cern.ch/record/1474107

[56] J. Pumplin *et al.*, New generation of parton distributions with uncertainties from global QCD analysis, J. High Energy Phys. 07 (2002) 012.

[57] A. Buckley *et al.*, LHAPDF6: Parton density access in the LHC precision era, Eur. Phys. J. C **75**, 132 (2015).

[58] Bähr *et al.*, Herwig++ physics and manual, Eur. Phys. J. C **58**, 639 (2008).

[59] A. D. Martin, R. G. Roberts, W. J. Stirling, and R. S. Thorne, NNLO global parton analysis, Phys. Lett. B **531**, 216 (2002).

[60] G. Aad *et al.* (ATLAS Collaboration), Charged-particle multiplicities in pp interactions measured with the ATLAS detector at the LHC, New J. Phys. **13**, 053033 (2011).

[61] M. Alvioli and M. Strikman, Color fluctuation effects in proton-nucleus collisions, Phys. Lett. B **722**, 347 (2013).

[62] G. Aad *et al.* (ATLAS Collaboration), The differential production cross section of the ϕ (1020) meson in $\sqrt{s} = 7$ TeV pp collisions measured with the ATLAS detector, Eur. Phys. J. C **74**, 2895 (2014).

[63] ATLAS Collaboration, dE/dx measurement in the ATLAS Pixel Detector and its use for particle identification2011, https://cds.cern.ch/record/1336519

[64] M. G. Bowler, Coulomb corrections to Bose-Einstein correlations have been greatly exaggerated, Phys. Lett. B **270**, 69 (1991).

[65] Y. M. Sinyukov, R. Lednicky, S. Akkelin, J. Pluta, and B. Erazmus, Coulomb corrections for interferometry analysis of expanding hadron systems, Phys. Lett. B **432**, 248 (1998).

[66] R. Maj and S. Mrówczyński, Coulomb effects in Femtoscopy, Phys. Rev. C **80**, 034907 (2009).

[67] N. Bohr, I. On the constitution of atoms and molecules, Philos. Mag. Ser. 6 **26**, 1 (1913).

[68] M. Gyulassy, S. K. Kauffmann, and L. W. Wilson, Pion interferometry of nuclear collisions, I. Theory, Phys. Rev. C **20**, 2267 (1979).

[69] M. Gyulassy and S. K. Kauffmann, Coulomb effects in relativistic nuclear collisions, Nucl. Phys. A **362**, 503 (1981).

[70] S. Chapman, P. Scotto, and U. W. Heinz, New Cross Term in the Two-Particle Hanbury Brown–Twiss Correlation Function in Ultrarelativistic Heavy-Ion Collisions, Phys. Rev. Lett. **74**, 4400 (1995)

[71] P. Bożek, Femtoscopy analysis of d-Au interactions at $\sqrt{s} =$ 200 GeV, Phys. Rev. C **90**, 064913 (2014).

[72] S. Baker and R. D. Cousins, Clarification of the use of CHI-quare and likelihood Ffunctions in fits to histograms, Nucl. Instrum. Methods **221**, 437 (1984).

[73] L. Ahle *et al.* (E-802 Collaboration), System, centrality, and transverse mass dependence of two-pion correlation radii in heavy ion collisions at 11.6A and 14.6A GeV/c, Phys. Rev. C **66**, 054906 (2002).

[74] F. James and M. Roos, Minuit: A system for function minimization and analysis of the parameter errors and correlations, Comput. Phys. Commun. **10**, 343 (1975).

[75] S. Pratt, Resolving the Hanbury Brown–Twiss Puzzle in Relativistic Heavy Ion Collision, Phys. Rev. Lett. **102**, 232301 (2009).

[76] ATLAS Collaboration, ATLAS Computing Acknowledgements 2016–2017, ATL-GEN-PUB-2016-002, 2016, https://cds.cern.ch/record/2202407

M. Aaboud,[136d] G. Aad,[87] B. Abbott,[114] J. Abdallah,[65] O. Abdinov,[12] B. Abeloos,[118] R. Aben,[108] O. S. AbouZeid,[138] N. L. Abraham,[152] H. Abramowicz,[156] H. Abreu,[155] R. Abreu,[117] Y. Abulaiti,[149a,149b] B. S. Acharya,[168a,168b,a] L. Adamczyk,[40a] D. L. Adams,[27] J. Adelman,[109] S. Adomeit,[101] T. Adye,[132] A. A. Affolder,[76] T. Agatonovic-Jovin,[14] J. Agricola,[56] J. A. Aguilar-Saavedra,[127a,127f] S. P. Ahlen,[24] F. Ahmadov,[67,b] G. Aielli,[134a,134b] H. Akerstedt,[149a,149b] T. P. A. Åkesson,[83] A. V. Akimov,[97] G. L. Alberghi,[22a,22b] J. Albert,[173] S. Albrand,[57] M. J. Alconada Verzini,[73] M. Aleksa,[32] I. N. Aleksandrov,[67] C. Alexa,[28b] G. Alexander,[156] T. Alexopoulos,[10] M. Alhroob,[114] B. Ali,[129] M. Aliev,[75a,75b] G. Alimonti,[93a] J. Alison,[33] S. P. Alkire,[37] B. M. M. Allbrooke,[152] B. W. Allen,[117] P. P. Allport,[19] A. Aloisio,[105a,105b] A. Alonso,[38] F. Alonso,[73] C. Alpigiani,[139] A. A. Alshehri,[55] M. Alstaty,[87] B. Alvarez Gonzalez,[32] D. Álvarez Piqueras,[171] M. G. Alviggi,[105a,105b] B. T. Amadio,[16] K. Amako,[68] Y. Amaral Coutinho,[26a] C. Amelung,[25] D. Amidei,[91] S. P. Amor Dos Santos,[127a,127c] A. Amorim,[127a,127b] S. Amoroso,[32] G. Amundsen,[25] C. Anastopoulos,[142] L. S. Ancu,[51] N. Andari,[19] T. Andeen,[11] C. F. Anders,[60b] G. Anders,[32] J. K. Anders,[76] K. J. Anderson,[33] A. Andreazza,[93a,93b] V. Andrei,[60a] S. Angelidakis,[9] I. Angelozzi,[108] P. Anger,[46] A. Angerami,[37] F. Anghinolfi,[32] A. V. Anisenkov,[110,c] N. Anjos,[13] A. Annovi,[125a,125b] C. Antel,[60a] M. Antonelli,[49] A. Antonov,[99,d] F. Anulli,[133a] M. Aoki,[68] L. Aperio Bella,[19] G. Arabidze,[92] Y. Arai,[68] J. P. Araque,[127a] A. T. H. Arce,[47] F. A. Arduh,[73] J-F. Arguin,[96] S. Argyropoulos,[65] M. Arik,[20a] A. J. Armbruster,[146] L. J. Armitage,[78] O. Arnaez,[32] H. Arnold,[50] M. Arratia,[30] O. Arslan,[23] A. Artamonov,[98] G. Artoni,[121] S. Artz,[85] S. Asai,[158] N. Asbah,[44] A. Ashkenazi,[156] B. Åsman,[149a,149b] L. Asquith,[152] K. Assamagan,[27] R. Astalos,[147a] M. Atkinson,[170] N. B. Atlay,[144] K. Augsten,[129] G. Avolio,[32] B. Axen,[16] M. K. Ayoub,[118] G. Azuelos,[96,e] M. A. Baak,[32] A. E. Baas,[60a] M. J. Baca,[19] H. Bachacou,[137] K. Bachas,[75a,75b] M. Backes,[121] M. Backhaus,[32] P. Bagiacchi,[133a,133b] P. Bagnaia,[133a,133b] Y. Bai,[35a] J. T. Baines,[132] O. K. Baker,[180] E. M. Baldin,[110,c] P. Balek,[176] T. Balestri,[151] F. Balli,[137] W. K. Balunas,[123] E. Banas,[41] Sw. Banerjee,[177,f] A. A. E. Bannoura,[179] L. Barak,[32] E. L. Barberio,[90] D. Barberis,[52a,52b] M. Barbero,[87] T. Barillari,[102] M-S Barisits,[32] T. Barklow,[146] N. Barlow,[30] S. L. Barnes,[86] B. M. Barnett,[132] R. M. Barnett,[16] Z. Barnovska-Blenessy,[5] A. Baroncelli,[135a] G. Barone,[25] A. J. Barr,[121] L. Barranco Navarro,[171] F. Barreiro,[84] J. Barreiro Guimarães da Costa,[35a] R. Bartoldus,[146] A. E. Barton,[74] P. Bartos,[147a] A. Basalaev,[124] A. Bassalat,[118,g] R. L. Bates,[55] S. J. Batista,[162] J. R. Batley,[30] M. Battaglia,[138] M. Bauce,[133a,133b] F. Bauer,[137] H. S. Bawa,[146,h] J. B. Beacham,[112] M. D. Beattie,[74] T. Beau,[82] P. H. Beauchemin,[166] P. Bechtle,[23] H. P. Beck,[18,i] K. Becker,[121] M. Becker,[85] M. Beckingham,[174] C. Becot,[111] A. J. Beddall,[20d] A. Beddall,[20b] V. A. Bednyakov,[67] M. Bedognetti,[108] C. P. Bee,[151] L. J. Beemster,[108] T. A. Beermann,[32] M. Begel,[27] J. K. Behr,[44] C. Belanger-Champagne,[89] A. S. Bell,[80] G. Bella,[156] L. Bellagamba,[22a] A. Bellerive,[31] M. Bellomo,[88] K. Belotskiy,[99] O. Beltramello,[32] N. L. Belyaev,[99] O. Benary,[156,d] D. Benchekroun,[136a] M. Bender,[101] K. Bendtz,[149a,149b] N. Benekos,[10] Y. Benhammou,[156] E. Benhar Noccioli,[180] J. Benitez,[65] D. P. Benjamin,[47] J. R. Bensinger,[25] S. Bentvelsen,[108] L. Beresford,[121] M. Beretta,[49] D. Berge,[108] E. Bergeaas Kuutmann,[169] N. Berger,[5] J. Beringer,[16] S. Berlendis,[57] N. R. Bernard,[88] C. Bernius,[111] F. U. Bernlochner,[23] T. Berry,[79] P. Berta,[130] C. Bertella,[85] G. Bertoli,[149a,149b] F. Bertolucci,[125a,125b] I. A. Bertram,[74] C. Bertsche,[44] D. Bertsche,[114] G. J. Besjes,[38] O. Bessidskaia Bylund,[149a,149b] M. Bessner,[44] N. Besson,[137] C. Betancourt,[50] A. Bethani,[57] S. Bethke,[102] A. J. Bevan,[78] R. M. Bianchi,[126] L. Bianchini,[25] M. Bianco,[32] O. Biebel,[101] D. Biedermann,[17] R. Bielski,[86] N. V. Biesuz,[125a,125b] M. Biglietti,[135a] J. Bilbao De Mendizabal,[51] T. R. V. Billoud,[96] H. Bilokon,[49] M. Bindi,[56] S. Binet,[118] A. Bingul,[20b] C. Bini,[133a,133b] S. Biondi,[22a,22b] T. Bisanz,[56] D. M. Bjergaard,[47] C. W. Black,[153] J. E. Black,[146] K. M. Black,[24] D. Blackburn,[139] R. E. Blair,[6] J.-B. Blanchard,[137] T. Blazek,[147a] I. Bloch,[44] C. Blocker,[25] A. Blue,[55] W. Blum,[85,d] U. Blumenschein,[56] S. Blunier,[34a] G. J. Bobbink,[108] V. S. Bobrovnikov,[110,c] S. S. Bocchetta,[83] A. Bocci,[47] C. Bock,[101] M. Boehler,[50] D. Boerner,[179] J. A. Bogaerts,[32] D. Bogavac,[14] A. G. Bogdanchikov,[110] C. Bohm,[149a] V. Boisvert,[79] P. Bokan,[14] T. Bold,[40a] A. S. Boldyrev,[168a,168c] M. Bomben,[82] M. Bona,[78] M. Boonekamp,[137] A. Borisov,[131] G. Borissov,[74] J. Bortfeldt,[32] D. Bortoletto,[121] V. Bortolotto,[62a,62b,62c] D. Boscherini,[22a]

M. Bosman,[13] J. D. Bossio Sola,[29] J. Boudreau,[126] J. Bouffard,[2] E. V. Bouhova-Thacker,[74] D. Boumediene,[36] C. Bourdarios,[118] S. K. Boutle,[55] A. Boveia,[32] J. Boyd,[32] I. R. Boyko,[67] J. Bracinik,[19] A. Brandt,[8] G. Brandt,[56] O. Brandt,[60a] U. Bratzler,[159] B. Brau,[88] J. E. Brau,[117] H. M. Braun,[179,d] W. D. Breaden Madden,[55] K. Brendlinger,[123] A. J. Brennan,[90] L. Brenner,[108] R. Brenner,[169] S. Bressler,[176] T. M. Bristow,[48] D. Britton,[55] D. Britzger,[44] F. M. Brochu,[30] I. Brock,[23] R. Brock,[92] G. Brooijmans,[37] T. Brooks,[79] W. K. Brooks,[34b] J. Brosamer,[16] E. Brost,[109] J. H Broughton,[19] P. A. Bruckman de Renstrom,[41] D. Bruncko,[147b] R. Bruneliere,[50] A. Bruni,[22a] G. Bruni,[22a] L. S. Bruni,[108] BH Brunt,[30] M. Bruschi,[22a] N. Bruscino,[23] P. Bryant,[33] L. Bryngemark,[83] T. Buanes,[15] Q. Buat,[145] P. Buchholz,[144] A. G. Buckley,[55] I. A. Budagov,[67] F. Buehrer,[50] M. K. Bugge,[120] O. Bulekov,[99] D. Bullock,[8] H. Burckhart,[32] S. Burdin,[76] C. D. Burgard,[50] B. Burghgrave,[109] K. Burka,[41] S. Burke,[132] I. Burmeister,[45] J. T. P. Burr,[121] E. Busato,[36] D. Büscher,[50] V. Büscher,[85] P. Bussey,[55] J. M. Butler,[24] C. M. Buttar,[55] J. M. Butterworth,[80] P. Butti,[108] W. Buttinger,[27] A. Buzatu,[55] A. R. Buzykaev,[110,c] S. Cabrera Urbán,[171] D. Caforio,[129] V. M. Cairo,[39a,39b] O. Cakir,[4a] N. Calace,[51] P. Calafiura,[16] A. Calandri,[87] G. Calderini,[82] P. Calfayan,[101] G. Callea,[39a,39b] L. P. Caloba,[26a] S. Calvente Lopez,[84] D. Calvet,[36] S. Calvet,[36] T. P. Calvet,[87] R. Camacho Toro,[33] S. Camarda,[32] P. Camarri,[134a,134b] D. Cameron,[120] R. Caminal Armadans,[170] C. Camincher,[57] S. Campana,[32] M. Campanelli,[80] A. Camplani,[93a,93b] A. Campoverde,[144] V. Canale,[105a,105b] A. Canepa,[164a] M. Cano Bret,[141] J. Cantero,[115] T. Cao,[42] M. D. M. Capeans Garrido,[32] I. Caprini,[28b] M. Caprini,[28b] M. Capua,[39a,39b] R. M. Carbone,[37] R. Cardarelli,[134a] F. Cardillo,[50] I. Carli,[130] T. Carli,[32] G. Carlino,[105a] L. Carminati,[93a,93b] S. Caron,[107] E. Carquin,[34b] G. D. Carrillo-Montoya,[32] J. R. Carter,[30] J. Carvalho,[127a,127c] D. Casadei,[19] M. P. Casado,[13,j] M. Casolino,[13] D. W. Casper,[167] E. Castaneda-Miranda,[148a] R. Castelijn,[108] A. Castelli,[108] V. Castillo Gimenez,[171] N. F. Castro,[127a,k] A. Catinaccio,[32] J. R. Catmore,[120] A. Cattai,[32] J. Caudron,[23] V. Cavaliere,[170] E. Cavallaro,[13] D. Cavalli,[93a] M. Cavalli-Sforza,[13] V. Cavasinni,[125a,125b] F. Ceradini,[135a,135b] L. Cerda Alberich,[171] B. C. Cerio,[47] A. S. Cerqueira,[26b] A. Cerri,[152] L. Cerrito,[134a,134b] F. Cerutti,[16] M. Cerv,[32] A. Cervelli,[18] S. A. Cetin,[20c] A. Chafaq,[136a] D. Chakraborty,[109] S. K. Chan,[58] Y. L. Chan,[62a] P. Chang,[170] J. D. Chapman,[30] D. G. Charlton,[19] A. Chatterjee,[51] C. C. Chau,[162] C. A. Chavez Barajas,[152] S. Che,[112] S. Cheatham,[168a,168c] A. Chegwidden,[92] S. Chekanov,[6] S. V. Chekulaev,[164a] G. A. Chelkov,[67,l] M. A. Chelstowska,[91] C. Chen,[66] H. Chen,[27] K. Chen,[151] S. Chen,[35b] S. Chen,[158] X. Chen,[35c,m] Y. Chen,[69] H. C. Cheng,[91] H. J. Cheng,[35a] Y. Cheng,[33] A. Cheplakov,[67] E. Cheremushkina,[131] R. Cherkaoui El Moursli,[136e] V. Chernyatin,[27,d] E. Cheu,[7] L. Chevalier,[137] V. Chiarella,[49] G. Chiarelli,[125a,125b] G. Chiodini,[75a] A. S. Chisholm,[32] A. Chitan,[28b] M. V. Chizhov,[67] K. Choi,[63] A. R. Chomont,[36] S. Chouridou,[9] B. K. B. Chow,[101] V. Christodoulou,[80] D. Chromek-Burckhart,[32] J. Chudoba,[128] A. J. Chuinard,[89] J. J. Chwastowski,[41] L. Chytka,[116] G. Ciapetti,[133a,133b] A. K. Ciftci,[4a] D. Cinca,[45] V. Cindro,[77] I. A. Cioara,[23] C. Ciocca,[22a,22b] A. Ciocio,[16] F. Cirotto,[105a,105b] Z. H. Citron,[176] M. Citterio,[93a] M. Ciubancan,[28b] A. Clark,[51] B. L. Clark,[58] M. R. Clark,[37] P. J. Clark,[48] R. N. Clarke,[16] C. Clement,[149a,149b] Y. Coadou,[87] M. Cobal,[168a,168c] A. Coccaro,[51] J. Cochran,[66] L. Colasurdo,[107] B. Cole,[37] A. P. Colijn,[108] J. Collot,[57] T. Colombo,[167] G. Compostella,[102] P. Conde Muiño,[127a,127b] E. Coniavitis,[50] S. H. Connell,[148b] I. A. Connelly,[79] V. Consorti,[50] S. Constantinescu,[28b] G. Conti,[32] F. Conventi,[105a,n] M. Cooke,[16] B. D. Cooper,[80] A. M. Cooper-Sarkar,[121] K. J. R. Cormier,[162] T. Cornelissen,[179] M. Corradi,[133a,133b] F. Corriveau,[89,o] A. Corso-Radu,[167] A. Cortes-Gonzalez,[32] G. Cortiana,[102] G. Costa,[93a] M. J. Costa,[171] D. Costanzo,[142] G. Cottin,[30] G. Cowan,[79] B. E. Cox,[86] K. Cranmer,[111] S. J. Crawley,[55] G. Cree,[31] S. Crépé-Renaudin,[57] F. Crescioli,[82] W. A. Cribbs,[149a,149b] M. Crispin Ortuzar,[121] M. Cristinziani,[23] V. Croft,[107] G. Crosetti,[39a,39b] A. Cueto,[84] T. Cuhadar Donszelmann,[142] J. Cummings,[180] M. Curatolo,[49] J. Cúth,[85] H. Czirr,[144] P. Czodrowski,[3] G. D'amen,[22a,22b] S. D'Auria,[55] M. D'Onofrio,[76] M. J. Da Cunha Sargedas De Sousa,[127a,127b] C. Da Via,[86] W. Dabrowski,[40a] T. Dado,[147a] T. Dai,[91] O. Dale,[15] F. Dallaire,[96] C. Dallapiccola,[88] M. Dam,[38] J. R. Dandoy,[33] N. P. Dang,[50] A. C. Daniells,[19] N. S. Dann,[86] M. Danninger,[172] M. Dano Hoffmann,[137] V. Dao,[50] G. Darbo,[52a] S. Darmora,[8] J. Dassoulas,[3] A. Dattagupta,[117] W. Davey,[23] C. David,[173] T. Davidek,[130] M. Davies,[156] P. Davison,[80] E. Dawe,[90] I. Dawson,[142] K. De,[8] R. de Asmundis,[105a] A. De Benedetti,[114] S. De Castro,[22a,22b] S. De Cecco,[82] N. De Groot,[107] P. de Jong,[108] H. De la Torre,[92] F. De Lorenzi,[66] A. De Maria,[56] D. De Pedis,[133a] A. De Salvo,[133a] U. De Sanctis,[152] A. De Santo,[152] J. B. De Vivie De Regie,[118] W. J. Dearnaley,[74] R. Debbe,[27] C. Debenedetti,[138] D. V. Dedovich,[67] N. Dehghanian,[3] I. Deigaard,[108] M. Del Gaudio,[39a,39b] J. Del Peso,[84] T. Del Prete,[125a,125b] D. Delgove,[118] F. Deliot,[137] C. M. Delitzsch,[51] A. Dell'Acqua,[32] L. Dell'Asta,[24] M. Dell'Orso,[125a,125b] M. Della Pietra,[105a,105b] D. della Volpe,[51] M. Delmastro,[5] P. A. Delsart,[57] D. A. DeMarco,[162] S. Demers,[180] M. Demichev,[67] A. Demilly,[82] S. P. Denisov,[131] D. Denysiuk,[137] D. Derendarz,[41] J. E. Derkaoui,[136d] F. Derue,[82] P. Dervan,[76] K. Desch,[23] C. Deterre,[44] K. Dette,[45] P. O. Deviveiros,[32] A. Dewhurst,[132] S. Dhaliwal,[25] A. Di Ciaccio,[134a,134b] L. Di Ciaccio,[5] W. K. Di Clemente,[123] C. Di Donato,[133a,133b] A. Di Girolamo,[32] B. Di Girolamo,[32] B. Di Micco,[135a,135b] R. Di Nardo,[32] A. Di Simone,[50] R. Di Sipio,[162] D. Di Valentino,[31] C. Diaconu,[87] M. Diamond,[162] F. A. Dias,[48] M. A. Diaz,[34a] E. B. Diehl,[91] J. Dietrich,[17] S. Díez Cornell,[44] A. Dimitrievska,[14] J. Dingfelder,[23] P. Dita,[28b] S. Dita,[28b] F. Dittus,[32] F. Djama,[87] T. Djobava,[53b] J. I. Djuvsland,[60a] M. A. B. do Vale,[26c] D. Dobos,[32] M. Dobre,[28b] C. Doglioni,[83] J. Dolejsi,[130] Z. Dolezal,[130] M. Donadelli,[26d] S. Donati,[125a,125b] P. Dondero,[122a,122b] J. Donini,[36] J. Dopke,[132] A. Doria,[105a] M. T. Dova,[73] A. T. Doyle,[55] E. Drechsler,[56] M. Dris,[10] Y. Du,[140] J. Duarte-Campderros,[156] E. Duchovni,[176] G. Duckeck,[101] O. A. Ducu,[96,p] D. Duda,[108] A. Dudarev,[32] A. Chr. Dudder,[85] E. M. Duffield,[16] L. Duflot,[118] M. Dührssen,[32] M. Dumancic,[176] M. Dunford,[60a] H. Duran Yildiz,[4a] M. Düren,[54] A. Durglishvili,[53b] D. Duschinger,[46] B. Dutta,[44] M. Dyndal,[44] C. Eckardt,[44] K. M. Ecker,[102] R. C. Edgar,[91] N. C. Edwards,[48] T. Eifert,[32] G. Eigen,[15] K. Einsweiler,[16] T. Ekelof,[169] M. El Kacimi,[136c] V. Ellajosyula,[87] M. Ellert,[169] S. Elles,[5] F. Ellinghaus,[179] A. A. Elliot,[173] N. Ellis,[32] J. Elmsheuser,[27] M. Elsing,[32] D. Emeliyanov,[132] Y. Enari,[158] O. C. Endner,[85] J. S. Ennis,[174] J. Erdmann,[45] A. Ereditato,[18] G. Ernis,[179] J. Ernst,[2] M. Ernst,[27] S. Errede,[170] E. Ertel,[85]

M. Escalier,[118] H. Esch,[45] C. Escobar,[126] B. Esposito,[49] A. I. Etienvre,[137] E. Etzion,[156] H. Evans,[63] A. Ezhilov,[124] F. Fabbri,[22a,22b] L. Fabbri,[22a,22b] G. Facini,[33] R. M. Fakhrutdinov,[131] S. Falciano,[133a] R. J. Falla,[80] J. Faltova,[32] Y. Fang,[35a] M. Fanti,[93a,93b] A. Farbin,[8] A. Farilla,[135a] C. Farina,[126] E. M. Farina,[122a,122b] T. Farooque,[13] S. Farrell,[16] S. M. Farrington,[174] P. Farthouat,[32] F. Fassi,[136e] P. Fassnacht,[32] D. Fassouliotis,[9] M. Faucci Giannelli,[79] A. Favareto,[52a,52b] W. J. Fawcett,[121] L. Fayard,[118] O. L. Fedin,[124,q] W. Fedorko,[172] S. Feigl,[120] L. Feligioni,[87] C. Feng,[140] E. J. Feng,[32] H. Feng,[91] A. B. Fenyuk,[131] L. Feremenga,[8] P. Fernandez Martinez,[171] S. Fernandez Perez,[13] J. Ferrando,[44] A. Ferrari,[169] P. Ferrari,[108] R. Ferrari,[122a] D. E. Ferreira de Lima,[60b] A. Ferrer,[171] D. Ferrere,[51] C. Ferretti,[91] A. Ferretto Parodi,[52a,52b] F. Fiedler,[85] A. Filipčič,[77] M. Filipuzzi,[44] F. Filthaut,[107] M. Fincke-Keeler,[173] K. D. Finelli,[153] M. C. N. Fiolhais,[127a,127c,r] L. Fiorini,[171] A. Firan,[42] A. Fischer,[2] C. Fischer,[13] J. Fischer,[179] W. C. Fisher,[92] N. Flaschel,[44] I. Fleck,[144] P. Fleischmann,[91] G. T. Fletcher,[142] R. R. M. Fletcher,[123] T. Flick,[179] A. Floderus,[83] L. R. Flores Castillo,[62a] M. J. Flowerdew,[102] G. T. Forcolin,[86] A. Formica,[137] A. Forti,[86] A. G. Foster,[19] D. Fournier,[118] H. Fox,[74] S. Fracchia,[13] P. Francavilla,[82] M. Franchini,[22a,22b] D. Francis,[32] L. Franconi,[120] M. Franklin,[58] M. Frate,[167] M. Fraternali,[122a,122b] D. Freeborn,[80] S. M. Fressard-Batraneanu,[32] F. Friedrich,[46] D. Froidevaux,[32] J. A. Frost,[121] C. Fukunaga,[159] E. Fullana Torregrosa,[85] T. Fusayasu,[103] J. Fuster,[171] C. Gabaldon,[57] O. Gabizon,[179] A. Gabrielli,[22a,22b] A. Gabrielli,[16] G. P. Gach,[40a] S. Gadatsch,[32] S. Gadomski,[79] G. Gagliardi,[52a,52b] L. G. Gagnon,[96] P. Gagnon,[63] C. Galea,[107] B. Galhardo,[127a,127c] E. J. Gallas,[121] B. J. Gallop,[132] P. Gallus,[129] G. Galster,[38] K. K. Gan,[112] J. Gao,[59] Y. Gao,[48] Y. S. Gao,[146,h] F. M. Garay Walls,[48] C. García,[171] J. E. García Navarro,[171] M. Garcia-Sciveres,[16] R. W. Gardner,[33] N. Garelli,[146] V. Garonne,[120] A. Gascon Bravo,[44] K. Gasnikova,[44] C. Gatti,[49] A. Gaudiello,[52a,52b] G. Gaudio,[122a] L. Gauthier,[96] I. L. Gavrilenko,[97] C. Gay,[172] G. Gaycken,[23] E. N. Gazis,[10] Z. Gecse,[172] C. N. P. Gee,[132] Ch. Geich-Gimbel,[23] M. Geisen,[85] M. P. Geisler,[60a] C. Gemme,[52a] M. H. Genest,[57] C. Geng,[59,s] S. Gentile,[133a,133b] C. Gentsos,[157] S. George,[79] D. Gerbaudo,[13] A. Gershon,[156] S. Ghasemi,[144] M. Ghneimat,[23] B. Giacobbe,[22a] S. Giagu,[133a,133b] P. Giannetti,[125a,125b] B. Gibbard,[27] S. M. Gibson,[79] M. Gignac,[172] M. Gilchriese,[16] T. P. S. Gillam,[30] D. Gillberg,[31] G. Gilles,[179] D. M. Gingrich,[3,e] N. Giokaris,[9,d] M. P. Giordani,[168a,168c] F. M. Giorgi,[22a] F. M. Giorgi,[17] P. F. Giraud,[137] P. Giromini,[58] D. Giugni,[93a] F. Giuli,[121] C. Giuliani,[102] M. Giulini,[60b] B. K. Gjelsten,[120] S. Gkaitatzis,[157] I. Gkialas,[9,t] E. L. Gkougkousis,[118] L. K. Gladilin,[100] C. Glasman,[84] J. Glatzer,[50] P. C. F. Glaysher,[48] A. Glazov,[44] M. Goblirsch-Kolb,[25] J. Godlewski,[41] S. Goldfarb,[90] T. Golling,[51] D. Golubkov,[131] A. Gomes,[127a,127b,127d] R. Gonçalo,[127a] J. Goncalves Pinto Firmino Da Costa,[137] G. Gonella,[50] L. Gonella,[19] A. Gongadze,[67] S. González de la Hoz,[171] G. Gonzalez Parra,[13] S. Gonzalez-Sevilla,[51] L. Goossens,[32] P. A. Gorbounov,[98] H. A. Gordon,[27] I. Gorelov,[106] B. Gorini,[32] E. Gorini,[75a,75b] A. Gorišek,[77] E. Gornicki,[41] A. T. Goshaw,[47] C. Gössling,[45] M. I. Gostkin,[67] C. R. Goudet,[118] D. Goujdami,[136c] A. G. Goussiou,[139] N. Govender,[148b,u] E. Gozani,[155] L. Graber,[56] I. Grabowska-Bold,[40a] P. O. J. Gradin,[57] P. Grafström,[22a,22b] J. Gramling,[51] E. Gramstad,[120] S. Grancagnolo,[17] V. Gratchev,[124] P. M. Gravila,[28e] H. M. Gray,[32] E. Graziani,[135a] Z. D. Greenwood,[81,v] C. Grefe,[23] K. Gregersen,[80] I. M. Gregor,[44] P. Grenier,[146] K. Grevtsov,[5] J. Griffiths,[8] A. A. Grillo,[138] K. Grimm,[74] S. Grinstein,[13,w] Ph. Gris,[36] J.-F. Grivaz,[118] S. Groh,[85] J. P. Grohs,[46] E. Gross,[176] J. Grosse-Knetter,[56] G. C. Grossi,[81] Z. J. Grout,[80] L. Guan,[91] W. Guan,[177] J. Guenther,[64] F. Guescini,[51] D. Guest,[167] O. Gueta,[156] E. Guido,[52a,52b] T. Guillemin,[5] S. Guindon,[2] U. Gul,[55] C. Gumpert,[32] J. Guo,[141] Y. Guo,[59,s] R. Gupta,[42] S. Gupta,[121] G. Gustavino,[133a,133b] P. Gutierrez,[114] N. G. Gutierrez Ortiz,[80] C. Gutschow,[46] C. Guyot,[137] C. Gwenlan,[121] C. B. Gwilliam,[76] A. Haas,[111] C. Haber,[16] H. K. Hadavand,[8] A. Hadef,[87] S. Hageböck,[23] Z. Hajduk,[41] H. Hakobyan,[181,d] M. Haleem,[44] J. Haley,[115] G. Halladjian,[92] G. D. Hallewell,[87] K. Hamacher,[179] P. Hamal,[116] K. Hamano,[173] A. Hamilton,[148a] G. N. Hamity,[142] P. G. Hamnett,[44] L. Han,[59] K. Hanagaki,[68,x] K. Hanawa,[158] M. Hance,[138] B. Haney,[123] P. Hanke,[60a] R. Hanna,[137] J. B. Hansen,[38] J. D. Hansen,[38] M. C. Hansen,[23] P. H. Hansen,[38] K. Hara,[165] A. S. Hard,[177] T. Harenberg,[179] F. Hariri,[118] S. Harkusha,[94] R. D. Harrington,[48] P. F. Harrison,[174] N. M. Hartmann,[101] M. Hasegawa,[69] Y. Hasegawa,[143] A. Hasib,[114] S. Hassani,[137] S. Haug,[18] R. Hauser,[92] L. Hauswald,[46] M. Havranek,[128] C. M. Hawkes,[19] R. J. Hawkings,[32] D. Hayakawa,[160] D. Hayden,[92] C. P. Hays,[121] J. M. Hays,[78] H. S. Hayward,[76] S. J. Haywood,[132] S. J. Head,[19] T. Heck,[85] V. Hedberg,[83] L. Heelan,[8] K. K. Heidegger,[50] S. Heim,[123] T. Heim,[16] B. Heinemann,[16] J. J. Heinrich,[101] L. Heinrich,[111] C. Heinz,[54] J. Hejbal,[128] L. Helary,[32] S. Hellman,[149a,149b] C. Helsens,[32] J. Henderson,[121] R. C. W. Henderson,[74] Y. Heng,[177] S. Henkelmann,[172] A. M. Henriques Correia,[32] S. Henrot-Versille,[118] G. H. Herbert,[17] H. Herde,[25] V. Herget,[178] Y. Hernández Jiménez,[171] G. Herten,[50] R. Hertenberger,[101] L. Hervas,[32] G. G. Hesketh,[80] N. P. Hessey,[108] J. W. Hetherly,[42] R. Hickling,[78] E. Higón-Rodriguez,[171] E. Hill,[173] J. C. Hill,[30] K. H. Hiller,[44] S. J. Hillier,[19] I. Hinchliffe,[16] E. Hines,[123] R. R. Hinman,[16] M. Hirose,[50] D. Hirschbuehl,[179] J. Hobbs,[151] N. Hod,[164a] M. C. Hodgkinson,[142] P. Hodgson,[142] A. Hoecker,[32] M. R. Hoeferkamp,[106] F. Hoenig,[101] D. Hohn,[23] T. R. Holmes,[16] M. Homann,[45] T. Honda,[68] T. M. Hong,[126] B. H. Hooberman,[170] W. H. Hopkins,[117] Y. Horii,[104] A. J. Horton,[145] J-Y. Hostachy,[57] S. Hou,[154] A. Hoummada,[136a] J. Howarth,[44] J. Hoya,[73] M. Hrabovsky,[116] I. Hristova,[17] J. Hrivnac,[118] T. Hryn'ova,[5] A. Hrynevich,[95] C. Hsu,[148c] P. J. Hsu,[154,y] S.-C. Hsu,[139] D. Hu,[37] Q. Hu,[59] S. Hu,[141] Y. Huang,[44] Z. Hubacek,[129] F. Hubaut,[87] F. Huegging,[23] T. B. Huffman,[121] E. W. Hughes,[37] G. Hughes,[74] M. Huhtinen,[32] P. Huo,[151] N. Huseynov,[67,b] J. Huston,[92] J. Huth,[58] G. Iacobucci,[51] G. Iakovidis,[27] I. Ibragimov,[144] L. Iconomidou-Fayard,[118] E. Ideal,[180] P. Iengo,[32] O. Igonkina,[108,z] T. Iizawa,[175] Y. Ikegami,[68] M. Ikeno,[68] Y. Ilchenko,[11,aa] D. Iliadis,[157] N. Ilic,[146] T. Ince,[102] G. Introzzi,[122a,122b] P. Ioannou,[9,d] M. Iodice,[135a] K. Iordanidou,[37] V. Ippolito,[58] N. Ishijima,[119] M. Ishino,[158] M. Ishitsuka,[160] R. Ishmukhametov,[112] C. Issever,[121] S. Istin,[20a] F. Ito,[165] J. M. Iturbe Ponce,[86] R. Iuppa,[163a,163b] W. Iwanski,[64] H. Iwasaki,[68] J. M. Izen,[43] V. Izzo,[105a] S. Jabbar,[3] B. Jackson,[123] P. Jackson,[1] V. Jain,[2] K. B. Jakobi,[85] K. Jakobs,[50] S. Jakobsen,[32] T. Jakoubek,[128] D. O. Jamin,[115] D. K. Jana,[81] R. Jansky,[64] J. Janssen,[23] M. Janus,[56] G. Jarlskog,[83] N. Javadov,[67,b] T. Javůrek,[50] M. Javurkova,[50] F. Jeanneau,[137]

L. Jeanty,[16] G.-Y. Jeng,[153] D. Jennens,[90] P. Jenni,[50,ab] C. Jeske,[174] S. Jézéquel,[5] H. Ji,[177] J. Jia,[151] H. Jiang,[66] Y. Jiang,[59] S. Jiggins,[80] J. Jimenez Pena,[171] S. Jin,[35a] A. Jinaru,[28b] O. Jinnouchi,[160] H. Jivan,[148c] P. Johansson,[142] K. A. Johns,[7] W. J. Johnson,[139] K. Jon-And,[149a,149b] G. Jones,[174] R. W. L. Jones,[74] S. Jones,[7] T. J. Jones,[76] J. Jongmanns,[60a] P. M. Jorge,[127a,127b] J. Jovicevic,[164a] X. Ju,[177] A. Juste Rozas,[13,w] M. K. Köhler,[176] A. Kaczmarska,[41] M. Kado,[118] H. Kagan,[112] M. Kagan,[146] S. J. Kahn,[87] T. Kaji,[175] E. Kajomovitz,[47] C. W. Kalderon,[121] A. Kaluza,[85] S. Kama,[42] A. Kamenshchikov,[131] N. Kanaya,[158] S. Kaneti,[30] L. Kanjir,[77] V. A. Kantserov,[99] J. Kanzaki,[68] B. Kaplan,[111] L. S. Kaplan,[177] A. Kapliy,[33] D. Kar,[148c] K. Karakostas,[10] A. Karamaoun,[3] N. Karastathis,[10] M. J. Kareem,[56] E. Karentzos,[10] M. Karnevskiy,[85] S. N. Karpov,[67] Z. M. Karpova,[67] K. Karthik,[111] V. Kartvelishvili,[74] A. N. Karyukhin,[131] K. Kasahara,[165] L. Kashif,[177] R. D. Kass,[112] A. Kastanas,[15] Y. Kataoka,[158] C. Kato,[158] A. Katre,[51] J. Katzy,[44] K. Kawade,[104] K. Kawagoe,[72] T. Kawamoto,[158] G. Kawamura,[56] V. F. Kazanin,[110,c] R. Keeler,[173] R. Kehoe,[42] J. S. Keller,[44] J. J. Kempster,[79] H. Keoshkerian,[162] O. Kepka,[128] B. P. Kerševan,[77] S. Kersten,[179] R. A. Keyes,[89] M. Khader,[170] F. Khalil-zada,[12] A. Khanov,[115] A. G. Kharlamov,[110,c] T. Kharlamova,[110,c] T. J. Khoo,[51] V. Khovanskiy,[98,d] E. Khramov,[67] J. Khubua,[53b,ac] S. Kido,[69] C. R. Kilby,[79] H. Y. Kim,[8] S. H. Kim,[165] Y. K. Kim,[33] N. Kimura,[157] O. M. Kind,[17] B. T. King,[76] M. King,[171] J. Kirk,[132] A. E. Kiryunin,[102] T. Kishimoto,[158] D. Kisielewska,[40a] F. Kiss,[50] K. Kiuchi,[165] O. Kivernyk,[137] E. Kladiva,[147b] M. H. Klein,[37] M. Klein,[76] U. Klein,[76] K. Kleinknecht,[85] P. Klimek,[109] A. Klimentov,[27] R. Klingenberg,[45] J. A. Klinger,[142] T. Klioutchnikova,[32] E.-E. Kluge,[60a] P. Kluit,[108] S. Kluth,[102] J. Knapik,[41] E. Kneringer,[64] E. B. F. G. Knoops,[87] A. Knue,[102] A. Kobayashi,[158] D. Kobayashi,[160] T. Kobayashi,[158] M. Kobel,[46] M. Kocian,[146] P. Kodys,[130] T. Koffas,[31] E. Koffeman,[108] N. M. Köhler,[102] T. Koi,[146] H. Kolanoski,[17] M. Kolb,[60b] I. Koletsou,[5] A. A. Komar,[97,d] Y. Komori,[158] T. Kondo,[68] N. Kondrashova,[44] K. Köneke,[50] A. C. König,[107] T. Kono,[68,ad] R. Konoplich,[111,ae] N. Konstantinidis,[80] R. Kopeliansky,[63] S. Koperny,[40a] L. Köpke,[85] A. K. Kopp,[50] K. Korcyl,[41] K. Kordas,[157] A. Korn,[80] A. A. Korol,[110,c] I. Korolkov,[13] E. V. Korolkova,[142] O. Kortner,[102] S. Kortner,[102] T. Kosek,[130] V. V. Kostyukhin,[23] A. Kotwal,[47] A. Kourkoumeli-Charalampidi,[122a,122b] C. Kourkoumelis,[9] V. Kouskoura,[27] A. B. Kowalewska,[41] R. Kowalewski,[173] T. Z. Kowalski,[40a] C. Kozakai,[158] W. Kozanecki,[137] A. S. Kozhin,[131] V. A. Kramarenko,[100] G. Kramberger,[77] D. Krasnopevtsev,[99] M. W. Krasny,[82] A. Krasznahorkay,[32] A. Kravchenko,[27] M. Kretz,[60c] J. Kretzschmar,[76] K. Kreutzfeldt,[54] P. Krieger,[162] K. Krizka,[33] K. Kroeninger,[45] H. Kroha,[102] J. Kroll,[123] J. Kroseberg,[23] J. Krstic,[14] U. Kruchonak,[67] H. Krüger,[23] N. Krumnack,[66] A. Kruse,[177] M. C. Kruse,[47] M. Kruskal,[24] T. Kubota,[90] H. Kucuk,[80] S. Kuday,[4b] J. T. Kuechler,[179] S. Kuehn,[50] A. Kugel,[60c] F. Kuger,[178] A. Kuhl,[138] T. Kuhl,[44] V. Kukhtin,[67] R. Kukla,[137] Y. Kulchitsky,[94] S. Kuleshov,[34b] M. Kuna,[133a,133b] T. Kunigo,[70] A. Kupco,[128] H. Kurashige,[69] Y. A. Kurochkin,[94] V. Kus,[128] E. S. Kuwertz,[173] M. Kuze,[160] J. Kvita,[116] T. Kwan,[173] D. Kyriazopoulos,[142] A. La Rosa,[102] J. L. La Rosa Navarro,[26d] L. La Rotonda,[39a,39b] C. Lacasta,[171] F. Lacava,[133a,133b] J. Lacey,[31] H. Lacker,[17] D. Lacour,[82] V. R. Lacuesta,[171] E. Ladygin,[67] R. Lafaye,[5] B. Laforge,[82] T. Lagouri,[180] S. Lai,[56] S. Lammers,[63] W. Lampl,[7] E. Lançon,[137] U. Landgraf,[50] M. P. J. Landon,[78] M. C. Lanfermann,[51] V. S. Lang,[60a] J. C. Lange,[13] A. J. Lankford,[167] F. Lanni,[27] K. Lantzsch,[23] A. Lanza,[122a] S. Laplace,[82] C. Lapoire,[32] J. F. Laporte,[137] T. Lari,[93a] F. Lasagni Manghi,[22a,22b] M. Lassnig,[32] P. Laurelli,[49] W. Lavrijsen,[16] A. T. Law,[138] P. Laycock,[76] T. Lazovich,[58] M. Lazzaroni,[93a,93b] B. Le,[90] O. Le Dortz,[82] E. Le Guirriec,[87] E. P. Le Quilleuc,[137] M. LeBlanc,[173] T. LeCompte,[6] F. Ledroit-Guillon,[57] C. A. Lee,[27] S. C. Lee,[154] L. Lee,[1] B. Lefebvre,[89] G. Lefebvre,[82] M. Lefebvre,[173] F. Legger,[101] C. Leggett,[16] A. Lehan,[76] G. Lehmann Miotto,[32] X. Lei,[7] W. A. Leight,[31] A. G. Leister,[180] M. A. L. Leite,[26d] R. Leitner,[130] D. Lellouch,[176] B. Lemmer,[56] K. J. C. Leney,[80] T. Lenz,[23] B. Lenzi,[32] R. Leone,[7] S. Leone,[125a,125b] C. Leonidopoulos,[48] S. Leontsinis,[10] G. Lerner,[152] C. Leroy,[96] A. A. J. Lesage,[137] C. G. Lester,[30] M. Levchenko,[124] J. Levêque,[5] D. Levin,[91] L. J. Levinson,[176] M. Levy,[19] D. Lewis,[78] A. M. Leyko,[23] B. Li,[59,s] Changqiao Li,[59] H. Li,[151] H. L. Li,[33] L. Li,[47] L. Li,[141] Q. Li,[35a] S. Li,[47] X. Li,[86] Y. Li,[144] Z. Liang,[35a] B. Liberti,[134a] A. Liblong,[162] P. Lichard,[32] K. Lie,[170] J. Liebal,[23] W. Liebig,[15] A. Limosani,[153] S. C. Lin,[154,af] T. H. Lin,[85] B. E. Lindquist,[151] A. E. Lionti,[51] E. Lipeles,[123] A. Lipniacka,[15] M. Lisovyi,[60b] T. M. Liss,[170,ag] A. Lister,[172] A. M. Litke,[138] B. Liu,[154,ah] D. Liu,[154] H. Liu,[91] H. Liu,[27] J. Liu,[87] J. B. Liu,[59] K. Liu,[87] L. Liu,[170] M. Liu,[47] M. Liu,[59] Y. L. Liu,[59] Y. Liu,[59] M. Livan,[122a,122b] A. Lleres,[57] J. Llorente Merino,[35a] S. L. Lloyd,[78] F. Lo Sterzo,[154] E. M. Lobodzinska,[44] P. Loch,[7] W. S. Lockman,[138] F. K. Loebinger,[86] A. E. Loevschall-Jensen,[38] K. M. Loew,[25] A. Loginov,[180,d] T. Lohse,[17] K. Lohwasser,[44] M. Lokajicek,[128] B. A. Long,[24] J. D. Long,[170] R. E. Long,[74] L. Longo,[75a,75b] K. A. Looper,[112] D. Lopez Mateos,[58] B. Lopez Paredes,[142] I. Lopez Paz,[13] A. Lopez Solis,[82] J. Lorenz,[101] N. Lorenzo Martinez,[63] M. Losada,[21] P. J. Lösel,[101] X. Lou,[35a] A. Lounis,[118] J. Love,[6] P. A. Love,[74] H. Lu,[62a] N. Lu,[91] H. J. Lubatti,[139] C. Luci,[133a,133b] A. Lucotte,[57] C. Luedtke,[50] F. Luehring,[63] W. Lukas,[64] L. Luminari,[133a] O. Lundberg,[149a,149b] B. Lund-Jensen,[150] P. M. Luzi,[82] D. Lynn,[27] R. Lysak,[128] E. Lytken,[83] V. Lyubushkin,[67] H. Ma,[27] L. L. Ma,[140] Y. Ma,[140] G. Maccarrone,[49] A. Macchiolo,[102] C. M. Macdonald,[142] B. Maček,[77] J. Machado Miguens,[123,127b] D. Madaffari,[87] R. Madar,[36] H. J. Maddocks,[169] W. F. Mader,[46] A. Madsen,[44] J. Maeda,[69] S. Maeland,[15] T. Maeno,[27] A. S. Maevskiy,[100] E. Magradze,[56] J. Mahlstedt,[108] C. Maiani,[118] C. Maidantchik,[26a] A. A. Maier,[102] T. Maier,[101] A. Maio,[127a,127b,127d] S. Majewski,[117] Y. Makida,[68] N. Makovec,[118] B. Malaescu,[82] Pa. Malecki,[41] V. P. Maleev,[124] F. Malek,[57] U. Mallik,[65] D. Malon,[6] C. Malone,[146] C. Malone,[30] S. Maltezos,[10] S. Malyukov,[32] J. Mamuzic,[171] G. Mancini,[49] L. Mandelli,[93a] I. Mandić,[77] J. Maneira,[127a,127b] L. Manhaes de Andrade Filho,[26b] J. Manjarres Ramos,[164b] A. Mann,[101] A. Manousos,[32] B. Mansoulie,[137] J. D. Mansour,[35a] R. Mantifel,[89] M. Mantoani,[56] S. Manzoni,[93a,93b] L. Mapelli,[32] G. Marceca,[29] L. March,[51] G. Marchiori,[82] M. Marcisovsky,[128] M. Marjanovic,[14] D. E. Marley,[91] F. Marroquim,[26a] S. P. Marsden,[86] Z. Marshall,[16] S. Marti-Garcia,[171] B. Martin,[92] T. A. Martin,[174] V. J. Martin,[48] B. Martin dit Latour,[15] M. Martinez,[13,w] V. I. Martinez Outschoorn,[170] S. Martin-Haugh,[132] V. S. Martoiu,[28b] A. C. Martyniuk,[80] M. Marx,[139]

A. Marzin,[32] L. Masetti,[85] T. Mashimo,[158] R. Mashinistov,[97] J. Masik,[86] A. L. Maslennikov,[110,c] I. Massa,[22a,22b] L. Massa,[22a,22b] P. Mastrandrea,[5] A. Mastroberardino,[39a,39b] T. Masubuchi,[158] P. Mättig,[179] J. Mattmann,[85] J. Maurer,[28b] S. J. Maxfield,[76] D. A. Maximov,[110,c] R. Mazini,[154] S. M. Mazza,[93a,93b] N. C. Mc Fadden,[106] G. Mc Goldrick,[162] S. P. Mc Kee,[91] A. McCarn,[91] R. L. McCarthy,[151] T. G. McCarthy,[102] L. I. McClymont,[80] E. F. McDonald,[90] J. A. Mcfayden,[80] G. Mchedlidze,[56] S. J. McMahon,[132] R. A. McPherson,[173,o] M. Medinnis,[44] S. Meehan,[139] S. Mehlhase,[101] A. Mehta,[76] K. Meier,[60a] C. Meineck,[101] B. Meirose,[43] D. Melini,[171,ai] B. R. Mellado Garcia,[148c] M. Melo,[147a] F. Meloni,[18] X. T. Meng,[91] A. Mengarelli,[22a,22b] S. Menke,[102] E. Meoni,[166] S. Mergelmeyer,[17] P. Mermod,[51] L. Merola,[105a,105b] C. Meroni,[93a] F. S. Merritt,[33] A. Messina,[133a,133b] J. Metcalfe,[6] A. S. Mete,[167] C. Meyer,[85] C. Meyer,[123] J-P. Meyer,[137] J. Meyer,[108] H. Meyer Zu Theenhausen,[60a] F. Miano,[152] R. P. Middleton,[132] S. Miglioranzi,[52a,52b] L. Mijović,[48] G. Mikenberg,[176] M. Mikestikova,[128] M. Mikuž,[77] M. Milesi,[90] A. Milic,[64] D. W. Miller,[33] C. Mills,[48] A. Milov,[176] D. A. Milstead,[149a,149b] A. A. Minaenko,[131] Y. Minami,[158] I. A. Minashvili,[67] A. I. Mincer,[111] B. Mindur,[40a] M. Mineev,[67] Y. Minegishi,[158] Y. Ming,[177] L. M. Mir,[13] K. P. Mistry,[123] T. Mitani,[175] J. Mitrevski,[101] V. A. Mitsou,[171] A. Miucci,[18] P. S. Miyagawa,[142] J. U. Mjörnmark,[83] T. Moa,[149a,149b] K. Mochizuki,[96] S. Mohapatra,[37] S. Molander,[149a,149b] R. Moles-Valls,[23] R. Monden,[70] M. C. Mondragon,[92] K. Mönig,[44] J. Monk,[38] E. Monnier,[87] A. Montalbano,[151] J. Montejo Berlingen,[32] F. Monticelli,[73] S. Monzani,[93a,93b] R. W. Moore,[3] N. Morange,[118] D. Moreno,[21] M. Moreno Llácer,[56] P. Morettini,[52a] S. Morgenstern,[32] D. Mori,[145] T. Mori,[158] M. Morii,[58] M. Morinaga,[158] V. Morisbak,[120] S. Moritz,[85] A. K. Morley,[153] G. Mornacchi,[32] J. D. Morris,[78] L. Morvaj,[151] M. Mosidze,[53b] J. Moss,[146,aj] K. Motohashi,[160] R. Mount,[146] E. Mountricha,[27] E. J. W. Moyse,[88] S. Muanza,[87] R. D. Mudd,[19] F. Mueller,[102] J. Mueller,[126] R. S. P. Mueller,[101] T. Mueller,[30] D. Muenstermann,[74] P. Mullen,[55] G. A. Mullier,[18] F. J. Munoz Sanchez,[86] J. A. Murillo Quijada,[19] W. J. Murray,[174,132] H. Musheghyan,[56] M. Muškinja,[77] A. G. Myagkov,[131,ak] M. Myska,[129] B. P. Nachman,[146] O. Nackenhorst,[51] K. Nagai,[121] R. Nagai,[68,ad] K. Nagano,[68] Y. Nagasaka,[61] K. Nagata,[165] M. Nagel,[50] E. Nagy,[87] A. M. Nairz,[32] Y. Nakahama,[104] K. Nakamura,[68] T. Nakamura,[158] I. Nakano,[113] H. Namasivayam,[43] R. F. Naranjo Garcia,[44] R. Narayan,[11] D. I. Narrias Villar,[60a] I. Naryshkin,[124] T. Naumann,[44] G. Navarro,[21] R. Nayyar,[7] H. A. Neal,[91] P. Yu. Nechaeva,[97] T. J. Neep,[86] A. Negri,[122a,122b] M. Negrini,[22a] S. Nektarijevic,[107] C. Nellist,[118] A. Nelson,[167] S. Nemecek,[128] P. Nemethy,[111] A. A. Nepomuceno,[26a] M. Nessi,[32,al] M. S. Neubauer,[170] M. Neumann,[179] R. M. Neves,[111] P. Nevski,[27] P. R. Newman,[19] D. H. Nguyen,[6] T. Nguyen Manh,[96] R. B. Nickerson,[121] R. Nicolaidou,[137] J. Nielsen,[138] A. Nikiforov,[17] V. Nikolaenko,[131,ak] I. Nikolic-Audit,[82] K. Nikolopoulos,[19] J. K. Nilsen,[120] P. Nilsson,[27] Y. Ninomiya,[158] A. Nisati,[133a] R. Nisius,[102] T. Nobe,[158] M. Nomachi,[119] I. Nomidis,[31] T. Nooney,[78] S. Norberg,[114] M. Nordberg,[32] N. Norjoharuddeen,[121] O. Novgorodova,[46] S. Nowak,[102] M. Nozaki,[68] L. Nozka,[116] K. Ntekas,[167] E. Nurse,[80] F. Nuti,[90] F. O'grady,[7] D. C. O'Neil,[145] A. A. O'Rourke,[44] V. O'Shea,[55] F. G. Oakham,[31,e] H. Oberlack,[102] T. Obermann,[23] J. Ocariz,[82] A. Ochi,[69] I. Ochoa,[37] J. P. Ochoa-Ricoux,[34a] S. Oda,[72] S. Odaka,[68] H. Ogren,[63] A. Oh,[86] S. H. Oh,[47] C. C. Ohm,[16] H. Ohman,[169] H. Oide,[32] H. Okawa,[165] Y. Okumura,[158] T. Okuyama,[68] A. Olariu,[28b] L. F. Oleiro Seabra,[127a] S. A. Olivares Pino,[48] D. Oliveira Damazio,[27] A. Olszewski,[41] J. Olszowska,[41] A. Onofre,[127a,127e] K. Onogi,[104] P. U. E. Onyisi,[11,aa] M. J. Oreglia,[33] Y. Oren,[156] D. Orestano,[135a,135b] N. Orlando,[62b] R. S. Orr,[162] B. Osculati,[52a,52b,d] R. Ospanov,[86] G. Otero y Garzon,[29] H. Otono,[72] M. Ouchrif,[136d] F. Ould-Saada,[120] A. Ouraou,[137] K. P. Oussoren,[108] Q. Ouyang,[35a] M. Owen,[55] R. E. Owen,[19] V. E. Ozcan,[20a] N. Ozturk,[8] K. Pachal,[145] A. Pacheco Pages,[13] L. Pacheco Rodriguez,[137] C. Padilla Aranda,[13] S. Pagan Griso,[16] F. Paige,[27] P. Pais,[88] K. Pajchel,[120] G. Palacino,[164b] S. Palazzo,[39a,39b] S. Palestini,[32] M. Palka,[40b] D. Pallin,[36] E. St. Panagiotopoulou,[10] C. E. Pandini,[82] J. G. Panduro Vazquez,[79] P. Pani,[149a,149b] S. Panitkin,[27] D. Pantea,[28b] L. Paolozzi,[51] Th. D. Papadopoulou,[10] K. Papageorgiou,[9,t] A. Paramonov,[6] D. Paredes Hernandez,[180] A. J. Parker,[74] M. A. Parker,[30] K. A. Parker,[142] F. Parodi,[52a,52b] J. A. Parsons,[37] U. Parzefall,[50] V. R. Pascuzzi,[162] E. Pasqualucci,[133a] S. Passaggio,[52a] Fr. Pastore,[79] G. Pásztor,[31,am] S. Pataraia,[179] J. R. Pater,[86] T. Pauly,[32] J. Pearce,[173] B. Pearson,[114] L. E. Pedersen,[38] S. Pedraza Lopez,[171] R. Pedro,[127a,127b] S. V. Peleganchuk,[110,c] O. Penc,[128] C. Peng,[35a] H. Peng,[59] J. Penwell,[63] B. S. Peralva,[26b] M. M. Perego,[137] D. V. Perepelitsa,[27] E. Perez Codina,[164a] L. Perini,[93a,93b] H. Pernegger,[32] S. Perrella,[105a,105b] R. Peschke,[44] V. D. Peshekhonov,[67] K. Peters,[44] R. F. Y. Peters,[86] B. A. Petersen,[32] T. C. Petersen,[38] E. Petit,[57] A. Petridis,[1] C. Petridou,[157] P. Petroff,[118] E. Petrolo,[133a] M. Petrov,[121] F. Petrucci,[135a,135b] N. E. Pettersson,[88] A. Peyaud,[137] R. Pezoa,[34b] P. W. Phillips,[132] G. Piacquadio,[146,an] E. Pianori,[174] A. Picazio,[88] E. Piccaro,[78] M. Piccinini,[22a,22b] M. A. Pickering,[121] R. Piegaia,[29] J. E. Pilcher,[33] A. D. Pilkington,[86] A. W. J. Pin,[86] M. Pinamonti,[168a,168c,ao] J. L. Pinfold,[3] A. Pingel,[38] S. Pires,[82] H. Pirumov,[44] M. Pitt,[176] L. Plazak,[147a] M.-A. Pleier,[27] V. Pleskot,[85] E. Plotnikova,[67] P. Plucinski,[92] D. Pluth,[66] R. Poettgen,[149a,149b] L. Poggioli,[118] D. Pohl,[23] G. Polesello,[122a] A. Poley,[44] A. Policicchio,[39a,39b] R. Polifka,[162] A. Polini,[22a] C. S. Pollard,[55] V. Polychronakos,[27] K. Pommès,[32] L. Pontecorvo,[133a] B. G. Pope,[92] G. A. Popeneciu,[28c] A. Poppleton,[32] S. Pospisil,[129] K. Potamianos,[16] I. N. Potrap,[67] C. J. Potter,[30] C. T. Potter,[117] G. Poulard,[32] J. Poveda,[32] V. Pozdnyakov,[67] M. E. Pozo Astigarraga,[32] P. Pralavorio,[87] A. Pranko,[16] S. Prell,[66] D. Price,[86] L. E. Price,[6] M. Primavera,[75a] S. Prince,[89] K. Prokofiev,[62c] F. Prokoshin,[34b] S. Protopopescu,[27] J. Proudfoot,[6] M. Przybycien,[40a] D. Puddu,[135a,135b] M. Purohit,[27,ap] P. Puzo,[118] J. Qian,[91] G. Qin,[55] Y. Qin,[86] A. Quadt,[56] W. B. Quayle,[168a,168b] M. Queitsch-Maitland,[86] D. Quilty,[55] S. Raddum,[120] V. Radeka,[27] V. Radescu,[121] S. K. Radhakrishnan,[151] P. Radloff,[117] P. Rados,[90] F. Ragusa,[93a,93b] G. Rahal,[182] J. A. Raine,[86] S. Rajagopalan,[27] M. Rammensee,[32] C. Rangel-Smith,[169] M. G. Ratti,[93a,93b] F. Rauscher,[101] S. Rave,[85] T. Ravenscroft,[55] I. Ravinovich,[176] M. Raymond,[32] A. L. Read,[120] N. P. Readioff,[76] M. Reale,[75a,75b] D. M. Rebuzzi,[122a,122b] A. Redelbach,[178] G. Redlinger,[27] R. Reece,[138] K. Reeves,[43] L. Rehnisch,[17] J. Reichert,[123] C. Rembser,[32] H. Ren,[35a] M. Rescigno,[133a] S. Resconi,[93a] O. L. Rezanova,[110,c] P. Reznicek,[130]

R. Rezvani,[96] R. Richter,[102] S. Richter,[80] E. Richter-Was,[40b] O. Ricken,[23] M. Ridel,[82] P. Rieck,[17] C. J. Riegel,[179] J. Rieger,[56] O. Rifki,[114] M. Rijssenbeek,[151] A. Rimoldi,[122a,122b] M. Rimoldi,[18] L. Rinaldi,[22a] B. Ristić,[51] E. Ritsch,[32] I. Riu,[13] F. Rizatdinova,[115] E. Rizvi,[78] C. Rizzi,[13] S. H. Robertson,[89,o] A. Robichaud-Veronneau,[89] D. Robinson,[30] J. E. M. Robinson,[44] A. Robson,[55] C. Roda,[125a,125b] Y. Rodina,[87,aq] A. Rodriguez Perez,[13] D. Rodriguez Rodriguez,[171] S. Roe,[32] C. S. Rogan,[58] O. Røhne,[120] A. Romaniouk,[99] M. Romano,[22a,22b] S. M. Romano Saez,[36] E. Romero Adam,[171] N. Rompotis,[139] M. Ronzani,[50] L. Roos,[82] E. Ros,[171] S. Rosati,[133a] K. Rosbach,[50] P. Rose,[138] N.-A. Rosien,[56] V. Rossetti,[149a,149b] E. Rossi,[105a,105b] L. P. Rossi,[52a] J. H. N. Rosten,[30] R. Rosten,[139] M. Rotaru,[28b] I. Roth,[176] J. Rothberg,[139] D. Rousseau,[118] A. Rozanov,[87] Y. Rozen,[155] X. Ruan,[148c] F. Rubbo,[146] M. S. Rudolph,[162] F. Rühr,[50] A. Ruiz-Martinez,[31] Z. Rurikova,[50] N. A. Rusakovich,[67] A. Ruschke,[101] H. L. Russell,[139] J. P. Rutherfoord,[7] N. Ruthmann,[32] Y. F. Ryabov,[124] M. Rybar,[170] G. Rybkin,[118] S. Ryu,[6] A. Ryzhov,[131] G. F. Rzehorz,[56] A. F. Saavedra,[153] G. Sabato,[108] S. Sacerdoti,[29] H. F-W. Sadrozinski,[138] R. Sadykov,[67] F. Safai Tehrani,[133a] P. Saha,[109] M. Sahinsoy,[60a] M. Saimpert,[137] T. Saito,[158] H. Sakamoto,[158] Y. Sakurai,[175] G. Salamanna,[135a,135b] A. Salamon,[134a,134b] J. E. Salazar Loyola,[34b] D. Salek,[108] P. H. Sales De Bruin,[139] D. Salihagic,[102] A. Salnikov,[146] J. Salt,[171] D. Salvatore,[39a,39b] F. Salvatore,[152] A. Salvucci,[62a] A. Salzburger,[32] D. Sammel,[50] D. Sampsonidis,[157] J. Sánchez,[171] V. Sanchez Martinez,[171] A. Sanchez Pineda,[105a,105b] H. Sandaker,[120] R. L. Sandbach,[78] H. G. Sander,[85] M. Sandhoff,[179] C. Sandoval,[21] D. P. C. Sankey,[132] M. Sannino,[52a,52b] A. Sansoni,[49] C. Santoni,[36] R. Santonico,[134a,134b] H. Santos,[127a] I. Santoyo Castillo,[152] K. Sapp,[126] A. Sapronov,[67] J. G. Saraiva,[127a,127d] B. Sarrazin,[23] O. Sasaki,[68] K. Sato,[165] E. Sauvan,[5] G. Savage,[79] P. Savard,[162,e] N. Savic,[102] C. Sawyer,[132] L. Sawyer,[81,v] J. Saxon,[33] C. Sbarra,[22a] A. Sbrizzi,[22a,22b] T. Scanlon,[80] D. A. Scannicchio,[167] M. Scarcella,[153] V. Scarfone,[39a,39b] J. Schaarschmidt,[176] P. Schacht,[102] B. M. Schachtner,[101] D. Schaefer,[32] L. Schaefer,[123] R. Schaefer,[44] J. Schaeffer,[85] S. Schaepe,[23] S. Schaetzel,[60b] U. Schäfer,[85] A. C. Schaffer,[118] D. Schaile,[101] R. D. Schamberger,[151] V. Scharf,[60a] V. A. Schegelsky,[124] D. Scheirich,[130] M. Schernau,[167] C. Schiavi,[52a,52b] S. Schier,[138] C. Schillo,[50] M. Schioppa,[39a,39b] S. Schlenker,[32] K. R. Schmidt-Sommerfeld,[102] K. Schmieden,[32] C. Schmitt,[85] S. Schmitt,[44] S. Schmitz,[85] B. Schneider,[164a] U. Schnoor,[50] L. Schoeffel,[137] A. Schoening,[60b] B. D. Schoenrock,[92] E. Schopf,[23] M. Schott,[85] J. F. P. Schouwenberg,[107] J. Schovancova,[8] S. Schramm,[51] M. Schreyer,[178] N. Schuh,[85] A. Schulte,[85] M. J. Schultens,[23] H.-C. Schultz-Coulon,[60a] H. Schulz,[17] M. Schumacher,[50] B. A. Schumm,[138] Ph. Schune,[137] A. Schwartzman,[146] T. A. Schwarz,[91] H. Schweiger,[86] Ph. Schwemling,[137] R. Schwienhorst,[92] J. Schwindling,[137] T. Schwindt,[23] G. Sciolla,[25] F. Scuri,[125a,125b] F. Scutti,[90] J. Searcy,[91] P. Seema,[23] S. C. Seidel,[106] A. Seiden,[138] F. Seifert,[129] J. M. Seixas,[26a] G. Sekhniaidze,[105a] K. Sekhon,[91] S. J. Sekula,[42] D. M. Seliverstov,[124,d] N. Semprini-Cesari,[22a,22b] C. Serfon,[120] L. Serin,[118] L. Serkin,[168a,168b] M. Sessa,[135a,135b] R. Seuster,[173] H. Severini,[114] T. Sfiligoj,[77] F. Sforza,[32] A. Sfyrla,[51] E. Shabalina,[56] N. W. Shaikh,[149a,149b] L. Y. Shan,[35a] R. Shang,[170] J. T. Shank,[24] M. Shapiro,[16] P. B. Shatalov,[98] K. Shaw,[168a,168b] S. M. Shaw,[86] A. Shcherbakova,[149a,149b] C. Y. Shehu,[152] P. Sherwood,[80] L. Shi,[154,ar] S. Shimizu,[69] C. O. Shimmin,[167] M. Shimojima,[103] M. Shiyakova,[67,as] A. Shmeleva,[97] D. Shoaleh Saadi,[96] M. J. Shochet,[33] S. Shojaii,[93a] D. R. Shope,[114] S. Shrestha,[112] E. Shulga,[99] M. A. Shupe,[7] P. Sicho,[128] A. M. Sickles,[170] P. E. Sidebo,[150] O. Sidiropoulou,[178] D. Sidorov,[115] A. Sidoti,[22a,22b] F. Siegert,[46] Dj. Sijacki,[14] J. Silva,[127a,127d] S. B. Silverstein,[149a] V. Simak,[129] Lj. Simic,[14] S. Simion,[118] E. Simioni,[85] B. Simmons,[80] D. Simon,[36] M. Simon,[85] P. Sinervo,[162] N. B. Sinev,[117] M. Sioli,[22a,22b] G. Siragusa,[178] S. Yu. Sivoklokov,[100] J. Sjölin,[149a,149b] M. B. Skinner,[74] H. P. Skottowe,[58] P. Skubic,[114] M. Slater,[19] T. Slavicek,[129] M. Slawinska,[108] K. Sliwa,[166] R. Slovak,[130] V. Smakhtin,[176] B. H. Smart,[5] L. Smestad,[15] J. Smiesko,[147a] S. Yu. Smirnov,[99] Y. Smirnov,[99] L. N. Smirnova,[100,at] O. Smirnova,[83] M. N. K. Smith,[37] R. W. Smith,[37] M. Smizanska,[74] K. Smolek,[129] A. A. Snesarev,[97] S. Snyder,[27] R. Sobie,[173,o] F. Socher,[46] A. Soffer,[156] D. A. Soh,[154] G. Sokhrannyi,[77] C. A. Solans Sanchez,[32] M. Solar,[129] E. Yu. Soldatov,[99] U. Soldevila,[171] A. A. Solodkov,[131] A. Soloshenko,[67] O. V. Solovyanov,[131] V. Solovyev,[124] P. Sommer,[50] H. Son,[166] H. Y. Song,[59,au] A. Sood,[16] A. Sopczak,[129] V. Sopko,[129] V. Sorin,[13] D. Sosa,[60b] C. L. Sotiropoulou,[125a,125b] R. Soualah,[168a,168c] A. M. Soukharev,[110,c] D. South,[44] B. C. Sowden,[79] S. Spagnolo,[75a,75b] M. Spalla,[125a,125b] M. Spangenberg,[174] F. Spanò,[79] D. Sperlich,[17] F. Spettel,[102] R. Spighi,[22a] G. Spigo,[32] L. A. Spiller,[90] M. Spousta,[130] R. D. St. Denis,[55,d] A. Stabile,[93a] R. Stamen,[60a] S. Stamm,[17] E. Stanecka,[41] R. W. Stanek,[6] C. Stanescu,[135a] M. Stanescu-Bellu,[44] M. M. Stanitzki,[44] S. Stapnes,[120] E. A. Starchenko,[131] G. H. Stark,[33] J. Stark,[57] S. H Stark,[38] P. Staroba,[128] P. Starovoitov,[60a] S. Stärz,[32] R. Staszewski,[41] P. Steinberg,[27] B. Stelzer,[145] H. J. Stelzer,[32] O. Stelzer-Chilton,[164a] H. Stenzel,[54] G. A. Stewart,[55] J. A. Stillings,[23] M. C. Stockton,[89] M. Stoebe,[89] G. Stoicea,[28b] P. Stolte,[56] S. Stonjek,[102] A. R. Stradling,[8] A. Straessner,[46] M. E. Stramaglia,[18] J. Strandberg,[150] S. Strandberg,[149a,149b] A. Strandlie,[120] M. Strauss,[114] P. Strizenec,[147b] R. Ströhmer,[178] D. M. Strom,[117] R. Stroynowski,[42] A. Strubig,[107] S. A. Stucci,[27] B. Stugu,[15] N. A. Styles,[44] D. Su,[146] J. Su,[126] S. Suchek,[60a] Y. Sugaya,[119] M. Suk,[129] V. V. Sulin,[97] S. Sultansoy,[4c] T. Sumida,[70] S. Sun,[58] X. Sun,[35a] J. E. Sundermann,[50] K. Suruliz,[152] G. Susinno,[39a,39b] M. R. Sutton,[152] S. Suzuki,[68] M. Svatos,[128] M. Swiatlowski,[33] I. Sykora,[147a] T. Sykora,[130] D. Ta,[50] C. Taccini,[135a,135b] K. Tackmann,[44] J. Taenzer,[162] A. Taffard,[167] R. Tafirout,[164a] N. Taiblum,[156] H. Takai,[27] R. Takashima,[71] T. Takeshita,[143] Y. Takubo,[68] M. Talby,[87] A. A. Talyshev,[110,c] K. G. Tan,[90] J. Tanaka,[158] M. Tanaka,[160] R. Tanaka,[118] S. Tanaka,[68] R. Tanioka,[69] B. B. Tannenwald,[112] S. Tapia Araya,[34b] S. Tapprogge,[85] S. Tarem,[155] G. F. Tartarelli,[93a] P. Tas,[130] M. Tasevsky,[128] T. Tashiro,[70] E. Tassi,[39a,39b] A. Tavares Delgado,[127a,127b] Y. Tayalati,[136e] A. C. Taylor,[106] G. N. Taylor,[90] P. T. E. Taylor,[90] W. Taylor,[164b] F. A. Teischinger,[32] P. Teixeira-Dias,[79] D. Temple,[145] H. Ten Kate,[32] P. K. Teng,[154] J. J. Teoh,[119] F. Tepel,[179] S. Terada,[68] K. Terashi,[158] J. Terron,[84] S. Terzo,[13] M. Testa,[49] R. J. Teuscher,[162,o] T. Theveneaux-Pelzer,[87] J. P. Thomas,[19] J. Thomas-Wilsker,[79] E. N. Thompson,[37] P. D. Thompson,[19] A. S. Thompson,[55] L. A. Thomsen,[180] E. Thomson,[123] M. Thomson,[30] M. J. Tibbetts,[16] R. E. Ticse Torres,[87]

V. O. Tikhomirov,[97,av] Yu. A. Tikhonov,[110,c] S. Timoshenko,[99] P. Tipton,[180] S. Tisserant,[87] K. Todome,[160] T. Todorov,[5,d] S. Todorova-Nova,[130] J. Tojo,[72] S. Tokár,[147a] K. Tokushuku,[68] E. Tolley,[58] L. Tomlinson,[86] M. Tomoto,[104] L. Tompkins,[146,aw] K. Toms,[106] B. Tong,[58] E. Torrence,[117] H. Torres,[145] E. Torró Pastor,[139] J. Toth,[87,ax] F. Touchard,[87] D. R. Tovey,[142] T. Trefzger,[178] A. Tricoli,[27] I. M. Trigger,[164a] S. Trincaz-Duvoid,[82] M. F. Tripiana,[13] W. Trischuk,[162] B. Trocmé,[57] A. Trofymov,[44] C. Troncon,[93a] M. Trottier-McDonald,[16] M. Trovatelli,[173] L. Truong,[168a,168c] M. Trzebinski,[41] A. Trzupek,[41] J. C-L. Tseng,[121] P. V. Tsiareshka,[94] G. Tsipolitis,[10] N. Tsirintanis,[9] S. Tsiskaridze,[13] V. Tsiskaridze,[50] E. G. Tskhadadze,[53a] K. M. Tsui,[62a] I. I. Tsukerman,[98] V. Tsulaia,[16] S. Tsuno,[68] D. Tsybychev,[151] Y. Tu,[62b] A. Tudorache,[28b] V. Tudorache,[28b] A. N. Tuna,[58] S. A. Tupputi,[22a,22b] S. Turchikhin,[67] D. Turecek,[129] D. Turgeman,[176] R. Turra,[93a] A. J. Turvey,[42] P. M. Tuts,[37] M. Tyndel,[132] G. Ucchielli,[22a,22b] I. Ueda,[158] M. Ughetto,[149a,149b] F. Ukegawa,[165] G. Unal,[32] A. Undrus,[27] G. Unel,[167] F. C. Ungaro,[90] Y. Unno,[68] C. Unverdorben,[101] J. Urban,[147b] P. Urquijo,[90] P. Urrejola,[85] G. Usai,[8] L. Vacavant,[87] V. Vacek,[129] B. Vachon,[89] C. Valderanis,[101] E. Valdes Santurio,[149a,149b] N. Valencic,[108] S. Valentinetti,[22a,22b] A. Valero,[171] L. Valéry,[13] S. Valkar,[130] J. A. Valls Ferrer,[171] W. Van Den Wollenberg,[108] P. C. Van Der Deijl,[108] H. van der Graaf,[108] N. van Eldik,[155] P. van Gemmeren,[6] J. Van Nieuwkoop,[145] I. van Vulpen,[108] M. C. van Woerden,[32] M. Vanadia,[133a,133b] W. Vandelli,[32] R. Vanguri,[123] A. Vaniachine,[161] P. Vankov,[108] G. Vardanyan,[181] R. Vari,[133a] E. W. Varnes,[7] T. Varol,[42] D. Varouchas,[82] A. Vartapetian,[8] K. E. Varvell,[153] J. G. Vasquez,[180] G. A. Vasquez,[34b] F. Vazeille,[36] T. Vazquez Schroeder,[89] J. Veatch,[56] V. Veeraraghavan,[7] L. M. Veloce,[162] F. Veloso,[127a,127c] S. Veneziano,[133a] A. Ventura,[75a,75b] M. Venturi,[173] N. Venturi,[162] A. Venturini,[25] V. Vercesi,[122a] M. Verducci,[133a,133b] W. Verkerke,[108] J. C. Vermeulen,[108] A. Vest,[46,ay] M. C. Vetterli,[145,e] O. Viazlo,[83] I. Vichou,[170,d] T. Vickey,[142] O. E. Vickey Boeriu,[142] G. H. A. Viehhauser,[121] S. Viel,[16] L. Vigani,[121] M. Villa,[22a,22b] M. Villaplana Perez,[93a,93b] E. Vilucchi,[49] M. G. Vincter,[31] V. B. Vinogradov,[67] C. Vittori,[22a,22b] I. Vivarelli,[152] S. Vlachos,[10] M. Vlasak,[129] M. Vogel,[179] P. Vokac,[129] G. Volpi,[125a,125b] M. Volpi,[90] H. von der Schmitt,[102] E. von Toerne,[23] V. Vorobel,[130] K. Vorobev,[99] M. Vos,[171] R. Voss,[32] J. H. Vossebeld,[76] N. Vranjes,[14] M. Vranjes Milosavljevic,[14] V. Vrba,[128] M. Vreeswijk,[108] R. Vuillermet,[32] I. Vukotic,[33] Z. Vykydal,[129] P. Wagner,[23] W. Wagner,[179] H. Wahlberg,[73] S. Wahrmund,[46] J. Wakabayashi,[104] J. Walder,[74] R. Walker,[101] W. Walkowiak,[144] V. Wallangen,[149a,149b] C. Wang,[35b] C. Wang,[140,az] F. Wang,[177] H. Wang,[16] H. Wang,[42] J. Wang,[44] J. Wang,[153] K. Wang,[89] R. Wang,[6] S. M. Wang,[154] T. Wang,[23] T. Wang,[37] W. Wang,[59] X. Wang,[180] C. Wanotayaroj,[117] A. Warburton,[89] C. P. Ward,[30] D. R. Wardrope,[80] A. Washbrook,[48] P. M. Watkins,[19] A. T. Watson,[19] M. F. Watson,[19] G. Watts,[139] S. Watts,[86] B. M. Waugh,[80] S. Webb,[85] M. S. Weber,[18] S. W. Weber,[178] J. S. Webster,[6] A. R. Weidberg,[121] B. Weinert,[63] J. Weingarten,[56] C. Weiser,[50] H. Weits,[108] P. S. Wells,[32] T. Wenaus,[27] T. Wengler,[32] S. Wenig,[32] N. Wermes,[23] M. Werner,[50] M. D. Werner,[66] P. Werner,[32] M. Wessels,[60a] J. Wetter,[166] K. Whalen,[117] N. L. Whallon,[139] A. M. Wharton,[74] A. White,[8] M. J. White,[1] R. White,[34b] D. Whiteson,[167] F. J. Wickens,[132] W. Wiedenmann,[177] M. Wielers,[132] C. Wiglesworth,[38] L. A. M. Wiik-Fuchs,[23] A. Wildauer,[102] F. Wilk,[86] H. G. Wilkens,[32] H. H. Williams,[123] S. Williams,[108] C. Willis,[92] S. Willocq,[88] J. A. Wilson,[19] I. Wingerter-Seez,[5] F. Winklmeier,[117] O. J. Winston,[152] B. T. Winter,[23] M. Wittgen,[146] J. Wittkowski,[101] T. M. H. Wolf,[108] M. W. Wolter,[41] H. Wolters,[127a,127c] S. D. Worm,[132] B. K. Wosiek,[41] J. Wotschack,[32] M. J. Woudstra,[86] K. W. Wozniak,[41] M. Wu,[57] M. Wu,[33] S. L. Wu,[177] X. Wu,[51] Y. Wu,[91] T. R. Wyatt,[86] B. M. Wynne,[48] S. Xella,[38] D. Xu,[35a] L. Xu,[27] B. Yabsley,[153] S. Yacoob,[148a] D. Yamaguchi,[160] Y. Yamaguchi,[119] A. Yamamoto,[68] S. Yamamoto,[158] T. Yamanaka,[158] K. Yamauchi,[104] Y. Yamazaki,[69] Z. Yan,[24] H. Yang,[141,bc] H. Yang,[177] Y. Yang,[154] Z. Yang,[15] W-M. Yao,[16] Y. C. Yap,[82] Y. Yasu,[68] E. Yatsenko,[5] K. H. Yau Wong,[23] J. Ye,[42] S. Ye,[27] I. Yeletskikh,[67] A. L. Yen,[58] E. Yildirim,[85] K. Yorita,[175] R. Yoshida,[6] K. Yoshihara,[123] C. Young,[146] C. J. S. Young,[32] S. Youssef,[24] D. R. Yu,[16] J. Yu,[8] J. M. Yu,[91] J. Yu,[66] L. Yuan,[69] S. P. Y. Yuen,[23] I. Yusuff,[30,ba] B. Zabinski,[41] R. Zaidan,[65] A. M. Zaitsev,[131,ak] N. Zakharchuk,[44] J. Zalieckas,[15] A. Zaman,[151] S. Zambito,[58] L. Zanello,[133a,133b] D. Zanzi,[90] C. Zeitnitz,[179] M. Zeman,[129] A. Zemla,[40a] J. C. Zeng,[170] Q. Zeng,[146] K. Zengel,[25] O. Zenin,[131] T. Ženiš,[147a] D. Zerwas,[118] D. Zhang,[91] F. Zhang,[177] G. Zhang,[59,au] H. Zhang,[35b] J. Zhang,[6] L. Zhang,[50] R. Zhang,[23] R. Zhang,[59,az] X. Zhang,[140] Z. Zhang,[118] X. Zhao,[42] Y. Zhao,[140,bb] Z. Zhao,[59] A. Zhemchugov,[67] J. Zhong,[121] B. Zhou,[91] C. Zhou,[47] L. Zhou,[37] L. Zhou,[42] M. Zhou,[151] N. Zhou,[35c] C. G. Zhu,[140] H. Zhu,[35a] J. Zhu,[91] Y. Zhu,[59] X. Zhuang,[35a] K. Zhukov,[97] A. Zibell,[178] D. Zieminska,[63] N. I. Zimine,[67] C. Zimmermann,[85] S. Zimmermann,[50] Z. Zinonos,[56] M. Zinser,[85] M. Ziolkowski,[144] L. Živković,[14] G. Zobernig,[177] A. Zoccoli,[22a,22b] M. zur Nedden,[17] and L. Zwalinski[32]

(ATLAS Collaboration)

[1]*Department of Physics, University of Adelaide, Adelaide, Australia*
[2]*Physics Department, SUNY Albany, Albany, New York, USA*
[3]*Department of Physics, University of Alberta, Edmonton, Alberta, Canada*
[4a]*Department of Physics, Ankara University, Ankara, Turkey*
[4b]*Istanbul Aydin University, Istanbul, Turkey*
[4c]*Division of Physics, TOBB University of Economics and Technology, Ankara, Turkey*
[5]*LAPP, CNRS/IN2P3 and Université Savoie Mont Blanc, Annecy-le-Vieux, France*
[6]*High Energy Physics Division, Argonne National Laboratory, Argonne, Illinois, USA*
[7]*Department of Physics, University of Arizona, Tucson, Arizona, USA*
[8]*Department of Physics, The University of Texas at Arlington, Arlington, Texas, USA*

[9]Physics Department, National and Kapodistrian University of Athens, Athens, Greece
[10]Physics Department, National Technical University of Athens, Zografou, Greece
[11]Department of Physics, The University of Texas at Austin, Austin, Texas, USA
[12]Institute of Physics, Azerbaijan Academy of Sciences, Baku, Azerbaijan
[13]Institut de Física d'Altes Energies (IFAE), The Barcelona Institute of Science and Technology, Barcelona, Spain
[14]Institute of Physics, University of Belgrade, Belgrade, Serbia
[15]Department for Physics and Technology, University of Bergen, Bergen, Norway
[16]Physics Division, Lawrence Berkeley National Laboratory and University of California, Berkeley, California, USA
[17]Department of Physics, Humboldt University, Berlin, Germany
[18]Albert Einstein Center for Fundamental Physics and Laboratory for High Energy Physics, University of Bern, Bern, Switzerland
[19]School of Physics and Astronomy, University of Birmingham, Birmingham, United Kingdom
[20a]Department of Physics, Bogazici University, Istanbul, Turkey
[20b]Department of Physics Engineering, Gaziantep University, Gaziantep, Turkey
[20c]Istanbul Bilgi University, Faculty of Engineering and Natural Sciences, Istanbul, Turkey
[20d]Bahcesehir University, Faculty of Engineering and Natural Sciences, Istanbul, Turkey
[21]Centro de Investigaciones, Universidad Antonio Narino, Bogota, Colombia
[22a]INFN Sezione di Bologna, Bologna, Italy
[22b]Dipartimento di Fisica e Astronomia, Università di Bologna, Bologna, Italy
[23]Physikalisches Institut, University of Bonn, Bonn, Germany
[24]Department of Physics, Boston University, Boston, Massachusetts, USA
[25]Department of Physics, Brandeis University, Waltham, Massachusetts, USA
[26a]Universidade Federal do Rio De Janeiro COPPE/EE/IF, Rio de Janeiro, Brazil
[26b]Electrical Circuits Department, Federal University of Juiz de Fora (UFJF), Juiz de Fora, Brazil
[26c]Federal University of Sao Joao del Rei (UFSJ), Sao Joao del Rei, Brazil
[26d]Instituto de Fisica, Universidade de Sao Paulo, Sao Paulo, Brazil
[27]Physics Department, Brookhaven National Laboratory, Upton, New York, USA
[28a]Transilvania University of Brasov, Brasov, Romania
[28b]Horia Hulubei National Institute of Physics and Nuclear Engineering, Bucharest, Romania
[28c]National Institute for Research and Development of Isotopic and Molecular Technologies, Physics Department, Cluj Napoca, Romania
[28d]University Politehnica Bucharest, Bucharest, Romania
[28e]West University in Timisoara, Timisoara, Romania
[29]Departamento de Física, Universidad de Buenos Aires, Buenos Aires, Argentina
[30]Cavendish Laboratory, University of Cambridge, Cambridge, United Kingdom
[31]Department of Physics, Carleton University, Ottawa, Ontario, Canada
[32]CERN, Geneva, Switzerland
[33]Enrico Fermi Institute, University of Chicago, Chicago, Illinois, USA
[34a]Departamento de Física, Pontificia Universidad Católica de Chile, Santiago, Chile
[34b]Departamento de Física, Universidad Técnica Federico Santa María, Valparaíso, Chile
[35a]Institute of High Energy Physics, Chinese Academy of Sciences, Beijing, China
[35b]Department of Physics, Nanjing University, Jiangsu, China
[35c]Physics Department, Tsinghua University, Beijing 100084, China
[36]Université Clermont Auvergne, CNRS/IN2P3, LPC, Clermont-Ferrand, France
[37]Nevis Laboratory, Columbia University, Irvington, New York, USA
[38]Niels Bohr Institute, University of Copenhagen, Kobenhavn, Denmark
[39a]INFN Gruppo Collegato di Cosenza, Laboratori Nazionali di Frascati, Rende, Italy
[39b]Dipartimento di Fisica, Università della Calabria, Rende, Italy
[40a]AGH University of Science and Technology, Faculty of Physics and Applied Computer Science, Krakow, Poland
[40b]Marian Smoluchowski Institute of Physics, Jagiellonian University, Krakow, Poland
[41]Institute of Nuclear Physics Polish Academy of Sciences, Krakow, Poland
[42]Physics Department, Southern Methodist University, Dallas, Texas, USA
[43]Physics Department, University of Texas at Dallas, Richardson, Texas, USA
[44]DESY, Hamburg and Zeuthen, Germany
[45]Lehrstuhl für Experimentelle Physik IV, Technische Universität Dortmund, Dortmund, Germany
[46]Institut für Kern- und Teilchenphysik, Technische Universität Dresden, Dresden, Germany
[47]Department of Physics, Duke University, Durham, North Carolina, USA
[48]SUPA - School of Physics and Astronomy, University of Edinburgh, Edinburgh, United Kingdom
[49]INFN e Laboratori Nazionali di Frascati, Frascati, Italy
[50]Fakultät für Mathematik und Physik, Albert-Ludwigs-Universität, Freiburg, Germany
[51]Departement de Physique Nucleaire et Corpusculaire, Université de Genève, Geneva, Switzerland

[52a]*INFN Sezione di Genova, Genova, Italy*
[52b]*Dipartimento di Fisica, Università di Genova, Genova, Italy*
[53a]*E. Andronikashvili Institute of Physics, Iv. Javakhishvili Tbilisi State University, Tbilisi, Georgia*
[53b]*High Energy Physics Institute, Tbilisi State University, Tbilisi, Georgia*
[54]*II Physikalisches Institut, Justus-Liebig-Universität Giessen, Giessen, Germany*
[55]*SUPA - School of Physics and Astronomy, University of Glasgow, Glasgow, United Kingdom*
[56]*II Physikalisches Institut, Georg-August-Universität, Göttingen, Germany*
[57]*Laboratoire de Physique Subatomique et de Cosmologie, Université Grenoble-Alpes, CNRS/IN2P3, Grenoble, France*
[58]*Laboratory for Particle Physics and Cosmology, Harvard University, Cambridge, Massachusetts, USA*
[59]*Department of Modern Physics and State Key Laboratory of Particle Detection and Electronics, University of Science and Technology of China, Anhui, China*
[60a]*Kirchhoff-Institut für Physik, Ruprecht-Karls-Universität Heidelberg, Heidelberg, Germany*
[60b]*Physikalisches Institut, Ruprecht-Karls-Universität Heidelberg, Heidelberg, Germany*
[60c]*ZITI Institut für technische Informatik, Ruprecht-Karls-Universität Heidelberg, Mannheim, Germany*
[61]*Faculty of Applied Information Science, Hiroshima Institute of Technology, Hiroshima, Japan*
[62a]*Department of Physics, The Chinese University of Hong Kong, Shatin, N.T., Hong Kong, China*
[62b]*Department of Physics, The University of Hong Kong, Hong Kong, China*
[62c]*Department of Physics and Institute for Advanced Study, The Hong Kong University of Science and Technology, Clear Water Bay, Kowloon, Hong Kong, China*
[63]*Department of Physics, Indiana University, Bloomington, Indiana, USA*
[64]*Institut für Astro- und Teilchenphysik, Leopold-Franzens-Universität, Innsbruck, Austria*
[65]*University of Iowa, Iowa City, Iowa, USA*
[66]*Department of Physics and Astronomy, Iowa State University, Ames, Iowa, USA*
[67]*Joint Institute for Nuclear Research, JINR Dubna, Dubna, Russia*
[68]*KEK, High Energy Accelerator Research Organization, Tsukuba, Japan*
[69]*Graduate School of Science, Kobe University, Kobe, Japan*
[70]*Faculty of Science, Kyoto University, Kyoto, Japan*
[71]*Kyoto University of Education, Kyoto, Japan*
[72]*Research Center for Advanced Particle Physics and Department of Physics, Kyushu University, Fukuoka, Japan*
[73]*Instituto de Física La Plata, Universidad Nacional de La Plata and CONICET, La Plata, Argentina*
[74]*Physics Department, Lancaster University, Lancaster, United Kingdom*
[75a]*INFN Sezione di Lecce, Lecce, Italy*
[75b]*Dipartimento di Matematica e Fisica, Università del Salento, Lecce, Italy*
[76]*Oliver Lodge Laboratory, University of Liverpool, Liverpool, United Kingdom*
[77]*Department of Experimental Particle Physics, Jožef Stefan Institute and Department of Physics, University of Ljubljana, Ljubljana, Slovenia*
[78]*School of Physics and Astronomy, Queen Mary University of London, London, United Kingdom*
[79]*Department of Physics, Royal Holloway University of London, Surrey, United Kingdom*
[80]*Department of Physics and Astronomy, University College London, London, United Kingdom*
[81]*Louisiana Tech University, Ruston, Louisiana, USA*
[82]*Laboratoire de Physique Nucléaire et de Hautes Energies, UPMC and Université Paris-Diderot and CNRS/IN2P3, Paris, France*
[83]*Fysiska institutionen, Lunds universitet, Lund, Sweden*
[84]*Departamento de Fisica Teorica C-15, Universidad Autonoma de Madrid, Madrid, Spain*
[85]*Institut für Physik, Universität Mainz, Mainz, Germany*
[86]*School of Physics and Astronomy, University of Manchester, Manchester, United Kingdom*
[87]*CPPM, Aix-Marseille Université and CNRS/IN2P3, Marseille, France*
[88]*Department of Physics, University of Massachusetts, Amherst, Massachusetts, USA*
[89]*Department of Physics, McGill University, Montreal, Quebec, Canada*
[90]*School of Physics, University of Melbourne, Victoria, Australia*
[91]*Department of Physics, The University of Michigan, Ann Arbor, Michigan, USA*
[92]*Department of Physics and Astronomy, Michigan State University, East Lansing, Michigan, USA*
[93a]*INFN Sezione di Milano, Milano, Italy*
[93b]*Dipartimento di Fisica, Università di Milano, Milano, Italy*
[94]*B. I. Stepanov Institute of Physics, National Academy of Sciences of Belarus, Minsk, Republic of Belarus*
[95]*Research Institute for Nuclear Problems of Byelorussian State University, Minsk, Republic of Belarus*
[96]*Group of Particle Physics, University of Montreal, Montreal, Quebec, Canada*
[97]*P. N. Lebedev Physical Institute of the Russian Academy of Sciences, Moscow, Russia*
[98]*Institute for Theoretical and Experimental Physics (ITEP), Moscow, Russia*
[99]*National Research Nuclear University MEPhI, Moscow, Russia*
[100]*D. V. Skobeltsyn Institute of Nuclear Physics, M.V. Lomonosov Moscow State University, Moscow, Russia*

[101]Fakultät für Physik, Ludwig-Maximilians-Universität München, München, Germany
[102]Max-Planck-Institut für Physik (Werner-Heisenberg-Institut), München, Germany
[103]Nagasaki Institute of Applied Science, Nagasaki, Japan
[104]Graduate School of Science and Kobayashi-Maskawa Institute, Nagoya University, Nagoya, Japan
[105a]INFN Sezione di Napoli, Napoli, Italy
[105b]Dipartimento di Fisica, Università di Napoli, Napoli, Italy
[106]Department of Physics and Astronomy, University of New Mexico, Albuquerque, New Mexico, USA
[107]Institute for Mathematics, Astrophysics and Particle Physics, Radboud University Nijmegen/Nikhef, Nijmegen, Netherlands
[108]Nikhef National Institute for Subatomic Physics and University of Amsterdam, Amsterdam, Netherlands
[109]Department of Physics, Northern Illinois University, DeKalb, Illinois, USA
[110]Budker Institute of Nuclear Physics, SB RAS, Novosibirsk, Russia
[111]Department of Physics, New York University, New York, New York, USA
[112]Ohio State University, Columbus, Ohio, USA
[113]Faculty of Science, Okayama University, Okayama, Japan
[114]Homer L. Dodge Department of Physics and Astronomy, University of Oklahoma, Norman, Oklahoma, USA
[115]Department of Physics, Oklahoma State University, Stillwater, Oklahoma, USA
[116]Palacký University, RCPTM, Olomouc, Czech Republic
[117]Center for High Energy Physics, University of Oregon, Eugene, Oregon, USA
[118]LAL, Univ. Paris-Sud, CNRS/IN2P3, Université Paris-Saclay, Orsay, France
[119]Graduate School of Science, Osaka University, Osaka, Japan
[120]Department of Physics, University of Oslo, Oslo, Norway
[121]Department of Physics, Oxford University, Oxford, United Kingdom
[122a]INFN Sezione di Pavia, Pavia, Italy
[122b]Dipartimento di Fisica, Università di Pavia, Pavia, Italy
[123]Department of Physics, University of Pennsylvania, Philadelphia, Pennsylvania, USA
[124]National Research Centre "Kurchatov Institute" B.P.Konstantinov Petersburg Nuclear Physics Institute, St. Petersburg, Russia
[125a]INFN Sezione di Pisa, Pisa, Italy
[125b]Dipartimento di Fisica E. Fermi, Università di Pisa, Pisa, Italy
[126]Department of Physics and Astronomy, University of Pittsburgh, Pittsburgh, Pennsylvania, USA
[127a]Laboratório de Instrumentação e Física Experimental de Partículas - LIP, Lisboa, Portugal
[127b]Faculdade de Ciências, Universidade de Lisboa, Lisboa, Portugal
[127c]Department of Physics, University of Coimbra, Coimbra, Portugal
[127d]Centro de Física Nuclear da Universidade de Lisboa, Lisboa, Portugal
[127e]Departamento de Fisica, Universidade do Minho, Braga, Portugal
[127f]Departamento de Fisica Teorica y del Cosmos and CAFPE, Universidad de Granada, Granada, Portugal
[127g]Dep Fisica and CEFITEC of Faculdade de Ciencias e Tecnologia, Universidade Nova de Lisboa, Caparica, Portugal
[128]Institute of Physics, Academy of Sciences of the Czech Republic, Praha, Czech Republic
[129]Czech Technical University in Prague, Praha, Czech Republic
[130]Charles University, Faculty of Mathematics and Physics, Prague, Czech Republic
[131]State Research Center Institute for High Energy Physics (Protvino), NRC KI, Protvino Russia
[132]Particle Physics Department, Rutherford Appleton Laboratory, Didcot, United Kingdom
[133a]INFN Sezione di Roma, Roma, Italy
[133b]Dipartimento di Fisica, Sapienza Università di Roma, Roma, Italy
[134a]INFN Sezione di Roma Tor Vergata, Roma, Italy
[134b]Dipartimento di Fisica, Università di Roma Tor Vergata, Roma, Italy
[135a]INFN Sezione di Roma Tre, Roma, Italy
[135b]Dipartimento di Matematica e Fisica, Università Roma Tre, Roma, Italy
[136a]Faculté des Sciences Ain Chock, Réseau Universitaire de Physique des Hautes Energies - Université Hassan II, Casablanca, Morocco
[136b]Centre National de l'Energie des Sciences Techniques Nucleaires, Rabat, Morocco
[136c]Faculté des Sciences Semlalia, Université Cadi Ayyad, LPHEA-Marrakech, Morocco
[136d]Faculté des Sciences, Université Mohamed Premier and LPTPM, Oujda, Morocco
[136e]Faculté des sciences, Université Mohammed V, Rabat, Morocco
[137]DSM/IRFU (Institut de Recherches sur les Lois Fondamentales de l'Univers), CEA Saclay (Commissariat à l'Energie Atomique et aux Energies Alternatives), Gif-sur-Yvette, France
[138]Santa Cruz Institute for Particle Physics, University of California Santa Cruz, Santa Cruz, California, USA
[139]Department of Physics, University of Washington, Seattle, Washington, USA
[140]School of Physics, Shandong University, Shandong, China
[141]Department of Physics and Astronomy, Key Laboratory for Particle Physics, Astrophysics and Cosmology, Ministry of Education; Shanghai Key Laboratory for Particle Physics and Cosmology, Shanghai Jiao Tong University, Shanghai, China

[142]*Department of Physics and Astronomy, University of Sheffield, Sheffield, United Kingdom*
[143]*Department of Physics, Shinshu University, Nagano, Japan*
[144]*Department Physik, Universität Siegen, Siegen, Germany*
[145]*Department of Physics, Simon Fraser University, Burnaby, British Columbia, Canada*
[146]*SLAC National Accelerator Laboratory, Stanford, California, USA*
[147a]*Faculty of Mathematics, Physics & Informatics, Comenius University, Bratislava, Slovak Republic*
[147b]*Department of Subnuclear Physics, Institute of Experimental Physics of the Slovak Academy of Sciences, Kosice, Slovak Republic*
[148a]*Department of Physics, University of Cape Town, Cape Town, South Africa*
[148b]*Department of Physics, University of Johannesburg, Johannesburg, South Africa*
[148c]*School of Physics, University of the Witwatersrand, Johannesburg, South Africa*
[149a]*Department of Physics, Stockholm University, Stockholm, Sweden*
[149b]*The Oskar Klein Centre, Stockholm, Sweden*
[150]*Physics Department, Royal Institute of Technology, Stockholm, Sweden*
[151]*Departments of Physics & Astronomy and Chemistry, Stony Brook University, Stony Brook, New York, USA*
[152]*Department of Physics and Astronomy, University of Sussex, Brighton, United Kingdom*
[153]*School of Physics, University of Sydney, Sydney, Australia*
[154]*Institute of Physics, Academia Sinica, Taipei, Taiwan*
[155]*Department of Physics, Technion: Israel Institute of Technology, Haifa, Israel*
[156]*Raymond and Beverly Sackler School of Physics and Astronomy, Tel Aviv University, Tel Aviv, Israel*
[157]*Department of Physics, Aristotle University of Thessaloniki, Thessaloniki, Greece*
[158]*International Center for Elementary Particle Physics and Department of Physics, The University of Tokyo, Tokyo, Japan*
[159]*Graduate School of Science and Technology, Tokyo Metropolitan University, Tokyo, Japan*
[160]*Department of Physics, Tokyo Institute of Technology, Tokyo, Japan*
[161]*Tomsk State University, Tomsk, Russia*
[162]*Department of Physics, University of Toronto, Toronto, Ontaria, Canada*
[163a]*INFN-TIFPA, Trento, Italy*
[163b]*University of Trento, Trento, Italy*
[164a]*TRIUMF, Vancouver BC, Ontario, Canada*
[164b]*Department of Physics and Astronomy, York University, Toronto, Ontario, Canada*
[165]*Faculty of Pure and Applied Sciences, and Center for Integrated Research in Fundamental Science and Engineering, University of Tsukuba, Tsukuba, Japan*
[166]*Department of Physics and Astronomy, Tufts University, Medford, Massachusetts, USA*
[167]*Department of Physics and Astronomy, University of California Irvine, Irvine, California, USA*
[168a]*INFN Gruppo Collegato di Udine, Sezione di Trieste, Udine, Italy*
[168b]*ICTP, Trieste, Italy*
[168c]*Dipartimento di Chimica, Fisica e Ambiente, Università di Udine, Udine, Italy*
[169]*Department of Physics and Astronomy, University of Uppsala, Uppsala, Sweden*
[170]*Department of Physics, University of Illinois, Urbana, Illinois, USA*
[171]*Instituto de Fisica Corpuscular (IFIC), Centro Mixto Universidad de Valencia - CSIC, Valencia, Spain*
[172]*Department of Physics, University of British Columbia, Vancouver, British Columbia, Canada*
[173]*Department of Physics and Astronomy, University of Victoria, Victoria, British Columbia, Canada*
[174]*Department of Physics, University of Warwick, Coventry, United Kingdom*
[175]*Waseda University, Tokyo, Japan*
[176]*Department of Particle Physics, The Weizmann Institute of Science, Rehovot, Israel*
[177]*Department of Physics, University of Wisconsin, Madison, Wisconsin, USA*
[178]*Fakultät für Physik und Astronomie, Julius-Maximilians-Universität, Würzburg, Germany*
[179]*Fakultät für Mathematik und Naturwissenschaften, Fachgruppe Physik, Bergische Universität Wuppertal, Wuppertal, Germany*
[180]*Department of Physics, Yale University, New Haven, Connecticut, USA*
[181]*Yerevan Physics Institute, Yerevan, Armenia*
[182]*Centre de Calcul de l'Institut National de Physique Nucléaire et de Physique des Particules (IN2P3), Villeurbanne, France*

[a]Also at Department of Physics, King's College London, London, United Kingdom.
[b]Also at Institute of Physics, Azerbaijan Academy of Sciences, Baku, Azerbaijan.
[c]Also at Novosibirsk State University, Novosibirsk, Russia.
[d]Deceased.
[e]Also at TRIUMF, Vancouver, British Columbia, Canada.
[f]Also at Department of Physics & Astronomy, University of Louisville, Louisville, Kentucky, USA.
[g]Also at Physics Department, An-Najah National University, Nablus, Palestinian Authority.
[h]Also at Department of Physics, California State University, Fresno, California, USA.

[i]Also at Department of Physics, University of Fribourg, Fribourg, Switzerland.
[j]Also at Departament de Fisica de la Universitat Autonoma de Barcelona, Barcelona, Spain.
[k]Also at Departamento de Fisica e Astronomia, Faculdade de Ciencias, Universidade do Porto, Portugal.
[l]Also at Tomsk State University, Tomsk, Russia.
[m]Also at The Collaborative Innovation Center of Quantum Matter (CICQM), Beijing, China.
[n]Also at Universita di Napoli Parthenope, Napoli, Italy.
[o]Also at Institute of Particle Physics (IPP), Canada.
[p]Also at Horia Hulubei National Institute of Physics and Nuclear Engineering, Bucharest, Romania.
[q]Also at Department of Physics, St. Petersburg State Polytechnical University, St. Petersburg, Russia.
[r]Also at Borough of Manhattan Community College, City University of New York, New York City, New York, USA.
[s]Also at Department of Physics, The University of Michigan, Ann Arbor, Michigan, USA.
[t]Also at Department of Financial and Management Engineering, University of the Aegean, Chios, Greece.
[u]Also at Centre for High Performance Computing, CSIR Campus, Rosebank, Cape Town, South Africa.
[v]Also at Louisiana Tech University, Ruston, Louisiana, USA.
[w]Also at Institucio Catalana de Recerca i Estudis Avancats, ICREA, Barcelona, Spain.
[x]Also at Graduate School of Science, Osaka University, Osaka, Japan.
[y]Also at Department of Physics, National Tsing Hua University, Hsinchu City, Taiwan.
[z]Also at Institute for Mathematics, Astrophysics and Particle Physics, Radboud University Nijmegen/Nikhef, Nijmegen, Netherlands.
[aa]Also at Department of Physics, The University of Texas at Austin, Austin, Texas, USA.
[ab]Also at CERN, Geneva, Switzerland.
[ac]Also at Georgian Technical University (GTU), Tbilisi, Georgia.
[ad]Also at Ochadai Academic Production, Ochanomizu University, Tokyo, Japan.
[ae]Also at Manhattan College, New York, New York, USA.
[af]Also at Academia Sinica Grid Computing, Institute of Physics, Academia Sinica, Taipei, Taiwan.
[ag]Also at The City College of New York, New York, New York, USA.
[ah]Also at School of Physics, Shandong University, Shandong, China.
[ai]Also at Departamento de Fisica Teorica y del Cosmos and CAFPE, Universidad de Granada, Granada, Portugal.
[aj]Also at Department of Physics, California State University, Sacramento, California, USA.
[ak]Also at Moscow Institute of Physics and Technology State University, Dolgoprudny, Russia.
[al]Also at Departement de Physique Nucleaire et Corpusculaire, Université de Genève, Geneva, Switzerland.
[am]Also at Eotvos Lorand University, Budapest, Hungary.
[an]Also at Departments of Physics & Astronomy and Chemistry, Stony Brook University, Stony Brook, New York, USA.
[ao]Also at International School for Advanced Studies (SISSA), Trieste, Italy.
[ap]Also at Department of Physics and Astronomy, University of South Carolina, Columbia, South Carolina, USA.
[aq]Also at Institut de Física d'Altes Energies (IFAE), The Barcelona Institute of Science and Technology, Barcelona, Spain.
[ar]Also at School of Physics, Sun Yat-sen University, Guangzhou, China.
[as]Also at Institute for Nuclear Research and Nuclear Energy (INRNE) of the Bulgarian Academy of Sciences, Sofia, Bulgaria.
[at]Also at Faculty of Physics, M.V.Lomonosov Moscow State University, Moscow, Russia.
[au]Also at Institute of Physics, Academia Sinica, Taipei, Taiwan.
[av]Also at National Research Nuclear University MEPhI, Moscow, Russia.
[aw]Also at Department of Physics, Stanford University, Stanford, California, USA.
[ax]Also at Institute for Particle and Nuclear Physics, Wigner Research Centre for Physics, Budapest, Hungary.
[ay]Also at Flensburg University of Applied Sciences, Flensburg, Germany.
[az]Also at CPPM, Aix-Marseille Université and CNRS/IN2P3, Marseille, France.
[ba]Also at University of Malaya, Department of Physics, Kuala Lumpur, Malaysia.
[bb]Also at LAL, Univ. Paris-Sud, CNRS/IN2P3, Université Paris-Saclay, Orsay, France.
[bc]Also at PKU-CHEP.